An Intrinsic and Geometric Framework for the Synthesis and Analysis of Distributed Compliant Mechanisms

by

Girish Krishnan

A dissertation submitted in partial fulfillment
of the requirements for the degree of
Doctor of Philosophy
(Mechanical Engineering)
in The University of Michigan
2011

Doctoral Committee:

Assistant Professor Charles J. Kim, Co-Chair
Professor Sridhar Kota, Co-Chair
Associate Professor Jerome P. Lynch
Assistant Professor Shorya Awtar

To my wife Ramya, and my parents.

ACKNOWLEDGEMENTS

I especially wish to express my gratitude to my advisors, Professor Charles Kim and Professor Sridhar Kota. In today's world, I believe success has more to do with inspiration than its allotted 10%. I got all the inspiration that I asked for from my advisors. From the beginning, Professor Kim was a constant source of encouragement. I sincerely thank him for all the discussions we had, all the ideas we exchanged, and all the articles we wrote. When my ideas were half-baked, it was these discussions that crystallized them and provided direction to my thinking. Furthermore, I owe some important parts of my thesis to the strong foundation laid by him.

It is a great honor for me to be Professor Sridhar Kota's student. When I got the opportunity to work under him for my doctoral degree, it was a dream come true. His motivation was unique. It encouraged free thinking in me by breaking the barriers of convention. He always encouraged me towards solving some of the toughest problems. Though both Professor Kota and Professor Kim were physically away from my location of work, the entire three and a half years of research seemed very smooth. This speaks more about their advising skills than my research acumen. And If I had any research acumen to begin with, the credit goes to Prof. G. K. Ananthasuresh at the Indian Institute of Science, who introduced me to the field of compliant mechanisms.

I have also immensely benefited from the interaction with my committee members Professor Jerome Lynch and Professor Shorya Awtar. I sincerely thank them for reviewing my work. I have had significant interactions with Professor Shorya Awtar

on my thesis. His deep sense of understanding of the subject, the suggestions he provided, and continues to provide has greatly shaped my work. I would also like to thank Professor Victor Li for being present for my oral defense.

Being a part of the Compliant Systems Design Laboratory, I consider myself very fortunate to have interacted with a number of my colleagues. I would like to thank Brian Trease, Christine Vehar-Jutte, Froukje Euwe, Youngseok Oh, Mike Cherry, and Joshua Bishop-Moser. My initial interaction with Youngseok Oh and Mike Cherry greatly shaped my work. My interaction towards the later half with Joshua Bishop-Moser was of immense help. The rate at which he generates ideas is truly remarkable. Furthermore, I would like to thank him for helping me proofread the dissertation and helping me make prototypes.

Finally, I would like to thank my family for supporting me unconditionally throughout my tenure as a graduate student. I would like to thank my wife Ramya for being my friend, companion and support. My experiences of Ann Arbor with her are some of my most cherished memories. My parents, Girija Krishnan and Mr. K. R. Krishnan have always supported me. It was their grooming, all the lessons that they taught while I was young that made me what I am today. I see this doctorate as a seed they sowed years ago. I would also like to thank my second parents and a sister obtained through marriage. Their constant support and prayers have helped me throughout.

TABLE OF CONTENTS

LIST OF FIGURES

Figure

ABSTRACT

An Intrinsic and Geometric Framework for the Synthesis of Distributed Compliant Mechanisms

by

Girish Krishnan

Co-Chairs: Charles J. Kim and Sridhar Kota

Traditional engineering designs associate strength with rigidity. As a result, most engineering systems that involve mechanical motion typically consist of rigid links connected with joints or interfaces. In contrast, nature achieves motion by flexibility or compliance through elastic deformation. It maintains strength by distributing compliance throughout its geometry rather than localizing it. Incorporating distributed compliance in engineering designs yield monolithic systems that are cost-effective, lightweight, having reduced peak stress, and zero friction and wear. The principles of mechanics accurately predict the behavior of these compliant mechanisms, but yield little insight into their systematic synthesis. This thesis proposes a mathematical framework to represent problem specifications and the mechanism behavior in terms of geometrically intuitive quantities that enable analysis and synthesis. Compliance representation is proposed for (i) single port mechanisms with a unique point of interest in terms of geometric quantities such as ellipses and vectors, and (ii) multiple port mechanisms with transmission of load and motion between distinct input(s) and output(s) is captured in terms of load flow. This geometric representation provides

a direct mapping between the mechanism geometry and their behavior, and is used to characterize simple deformable members that form a library of building blocks. The design space spanned by the building block library guides the decomposition of a given problem specification into tractable sub-problems that can be each solved from an entry in the library. The effectiveness of this geometric representation aids user insight in design, and enables discovery of trends and guidelines to obtain practical conceptual designs. Furthermore, the thesis proposes an optimization technique for dimensional synthesis of conceptual designs to uniformly distribute stresses throughout its constituent members, thereby reducing peak stresses that lead to failure. The resulting metric used for refinement enables an objective comparison and global ranking of various mechanism geometries and their actuation schemes based on their ability to store energy, or perform work before failure.

The geometrically insightful conceptual synthesis methodology, optimization technique and global comparison of resulting designs furnish a pragmatic methodology for the synthesis of distributed compliant mechanisms. This methodology is successfully applied to obtain solutions for some practical applications.

CHAPTER I

Literature Review: Compliant Mechanisms and their Design Methodologies

This chapter reviews evolution of compliant mechanisms in literature and their design methodologies. The next section focuses on early compliant designs involving lumped flexures, followed by distributed compliance inspired by examples in nature. The following section introduces a functional classification of compliant mechanisms into single port and multi port mechanisms. Compliance representation for these two types of mechanisms are reviewed. Then, an overview of design methodologies of compliant mechanisms is presented, highlighting their merits and demerits. This leads to identifying the gaps in literature and defining the scope of the thesis. The chapter concludes with the organization of the thesis.

1.1 Introduction

Compliance by definition implies the ability of a body to deform due to load applied on it, while rigidity implies its ability to retain its original shape and form. In principle there are no perfectly rigid bodies, as they all deform albeit minutely towards applied loads. Thus compliance is a property that can be found in every object in universe.

However, the usefulness of this property depends upon the ability of the body to store and retrieve energy thereby deforming in a prescribed manner or performing output work. Designs in nature and engineering use compliance to their benefit, as seen below.

1.1.1 Compliance in Nature

Nature presents number of examples where motion is achieved through compliance alone. Books on conceptual engineering designs by *French* (1988) and extensive comparison of designs in engineering and biology by Steven Vogel (*Vogel* (1988), *Vogel* (1998), *Vogel* (2003)) have articulated compliance as a preferred mode of deformation in nature and possibly in design. Invertebrates that lack a stiff backbone comprise 95% of the animal species. An example of compliance in insect locomotion can be seen in spiders, which extends its flexible legs due to pressurized fluids.

Nature exemplifies compliance as it faces significant constraints in design; in the limited choice of materials and manufacturing techniques. This leads nature to optimize its geometry to increase strength and thus handle large loads before failure. An example of this is the tapered and elliptical cross-section of tree branches. Though trees and other plants act as structures, whose functions are to stay fixed, nature's constraints are unable to incorporate sufficient rigidity to withstand large wind loads. However, by significantly flexing to wind loads they align themselves aerodynamically thereby reducing drag forces and uprooting moments. Thus nature effectively uses compliance to increase strength. In contrast, strength has always been synonymous with rigidity in traditional engineering designs. A historical perspective of how compliance has evolved in engineering artifacts is presented below.

1.1.2 Historical perspective of compliant mechanisms in human history

In prehistoric times, flexible strings were used as bows to store strain energy in them through deformation, and retrieving it as kinetic energy imparted to the arrow. These early historical artifacts are mentioned in a number of articles cited by *Howell* (2001). A number of historical sightings of spring based devices were reported in the ancient Greek and Roman civilizations by historians (Associated Springs *Corporation* (1964)). However, the first coiled spring was not fabricated until early 15th century (*Dohrn-van Rossum* (1997)) and found its use in clocks and later in the industrial revolution. Ever since, springs have become one of the most fundamental building blocks of mechanical design.

The above historical examples and springs can also be classified under mechanisms, as they transform energy or force (*Erdman et al.* (2001)) (Eg. springs transform strain energy to kinetic energy). Mechanisms that transform motion, on the other hand historically were made of rigid bodies with joints in between them. When both forces and motion specifications were involved, functional decoupling was advocated. Rigid links were used to obtain required motion, and springs to store the prescribed energy. For example, a number of consumer devices like staplers, pens, crimping devices, automobile clutches etc. consist of springs and rigid links.

It was towards the later half of the twentieth century that mechanisms with compliance in them started to appear. These were devices that had a deterministic direction of motion as well as stored strain energy in them. Coupling of function naturally led to coupling of form resulting in the monolithic nature of these mechanisms. Flexures were the earliest examples of this coupling, being used in precision instruments since the 18th century (*Smith* (2000)). Mechanisms made of flexures were adapted from rigid link mechanisms by using them to replace joints. These mechanisms are classified under lumped compliant mechanisms.

1.1.3 Lumped Compliant Mechanisms: Flexural Hinges

Flexural hinges are demonstrated in Fig. 1.1a and b. The deformation of flexures resemble rigid links with joints. This is because the narrow hinges in flexures are located at the joints. *Paros and Weisbord* (1965) were the first to locate the optimal locations of flexure placement at the links. The strain energy stored due to deformation is entirely concentrated in this region. Hence the name lumped compliance. The similarity between rigid links and flexure behavior make it easy to design them from rigid link kinematic approaches. Furthermore, they are easy to fabricate due to their monolithic nature, lack of friction and wear thus being ideally suited towards obtaining precise motion (*Slocum* (1992)). Furthermore, flexures act as near ideal elastic constraints (*Blanding* (1999)) as they seem to deform about the hinge, without considerable deflection in any other direction. Detailed analysis of different types of flexures are presented in books by *Smith* (2000) and *Lobontiu* (2003). A number of flexure based grippers, pliers and scissors have been introduced by *Howell* (2001). Even to this day a number of flexure based positioning devices have been built at various length scales with integrated controls for obtaining motion that has nanometer precision (*Ryu et al.* (1997), *Li and Xu* (2010),*Liaw and Shirinzadeh* (2010)). Apart from precision instruments flexures are also used in a number of consumer products like living hinges in cap openings fabricated using injected molding.

Despite their advantages, flexures have certain operational limitations. Flexures undergo large stresses at the lumped joints. This limits their capability to provide large deformations and transmit loads simultaneously. These limitations led researchers to distribute stresses evenly throughout the mechanism geometry so that stresses are not localized at the joints. These are explained in the section below.

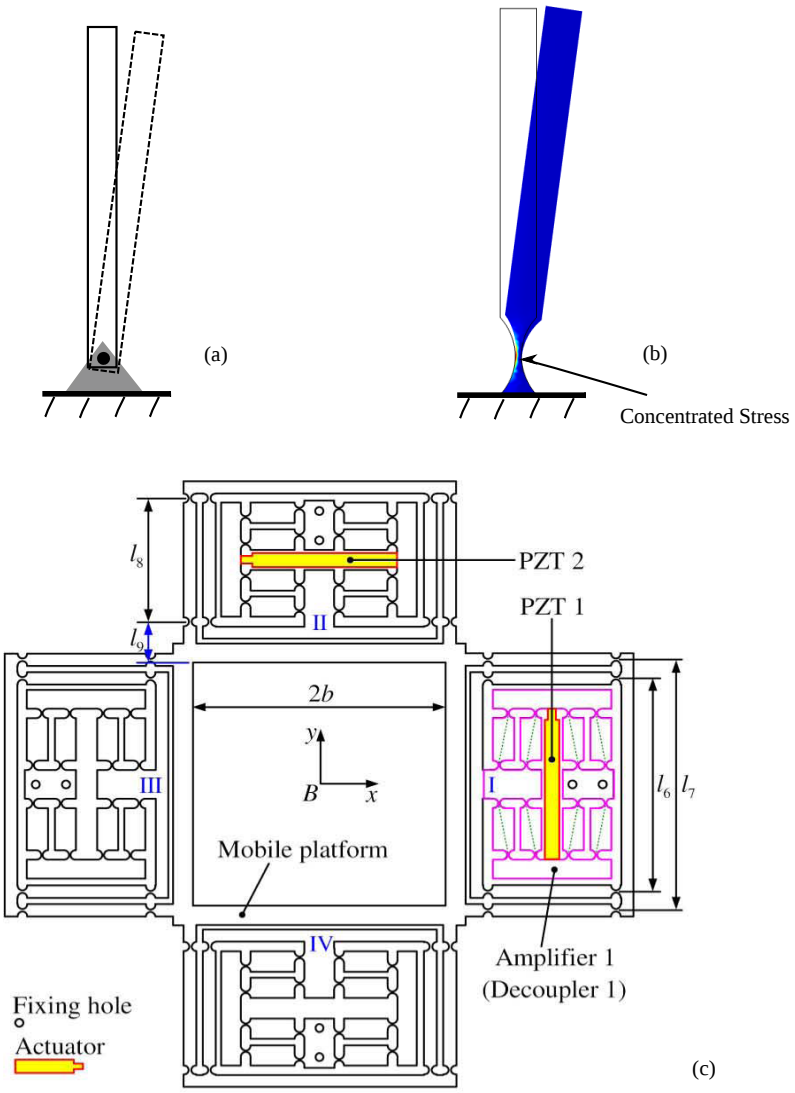

Figure 1.1: Flexures are inspired from rigid link with joints (a) A rigid link with a revolute joint (b) A rigid link with a flexure and its deformation (c) A decoupled XY Stage using flexures for nanopositioning (*Li and Xu* (2010))

1.1.4 Distributed Compliant Mechanisms

Figure 1.2a shows a tree branch with a tapering cross section. For a load acting on the tip of a beam with tapered cross section shown in 1.2b, the stress is evenly distributed throughout the mechanism. In literature, distributed compliant mechanisms are referred to the presence of slender beams without any lumped flexures. An example of distributed compliance is a leaf spring. Leaf springs were used since early 15th century and even to this day in automobiles as suspensions.

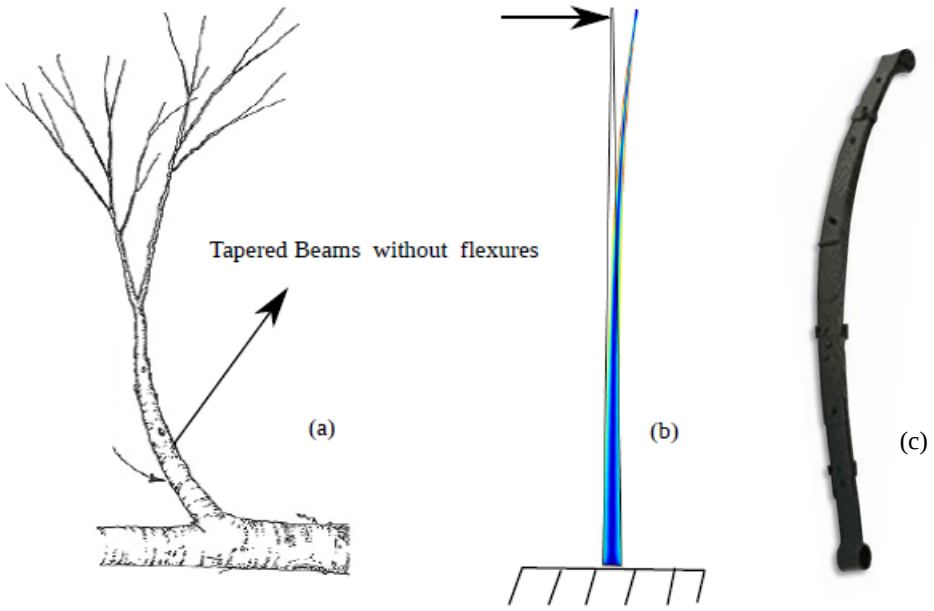

Figure 1.2: Distributed compliance is inspired by observing nature's designs (a) tapering branches of trees (b) stress in tapered beams are evenly distributed all along its length (c) leaf springs are examples of distributed compliant mechanisms

A number of engineering marvels have been accomplished by utilizing designs with distributed compliance. Some of them are enlisted below

1. Aircraft wings that adapt to the surrounding weather and flight conditions by changing their geometries have been designed and tested (see Fig.1.3a) by Flexsys inc. (*http://www.flxsys.com*). These wings have within it a monolithic compliant mechanism that is strong enough to withstand external loads, but will

deform towards a predetermined shape when actuated. The monolithic nature of the mechanism and the seamless wing profiles decrease the overall weight of the wing, and increase fuel efficiency. The design of these mechanisms for shape changing applications were researched extensively by *Lu and Kota* (2005).

2. The advantages of compliant mechanisms and its ease of manufacturing in the MEMS scale have resulted in number of designs. One such design involved the concept of displacement amplification to match the large force and small displacement of electrostatic actuators to a large displacement needs of the output (*Hetrick and Kota* (2003)). Such a design involving distributed compliance is shown in Fig. 1.3b.

3. Though flexures are popular for obtaining precision motion, *Awtar* (2004) demonstrated the design of a X-Y motion stage with nanometer precision using a symmetric arrangement of distributed beams as shown in Fig. 1.3c using the concept of elastic averaging.

4. Low cost force sensors for micro-manipulation involves flexible suspensions made of materials like PDMS as shown in Fig. 1.3d. The deformation of the suspensions is tracked using a microscope and the force is evaluated by inverse elasticity as proposed by *Cappelleri* (2008).

5. Distributed compliant leaf springs made of carbon fiber reinforced composites have been used as passive elements in an orthotic exoskeleton to aid in running (see Fig. 1.3e) by *Cherry* (2009). These springs are designed to take in excess kinetic energy of the foot during heel strike and release the energy as a boost during toe-off. The exoskeleton complements the action of muscles and the spring like tendons during running.

6. A compliant one-piece wiper blade (*Kota and Hetrick* (2008)) shown in Fig. 1.3f

demonstrates the effectiveness of compliant mechanisms to reduce the number of parts needed for assembly.

7. A large range of motion translational and revolute joints were designed by *Trease et al.* (2005) to match the precision of flexures without any localized stresses. The designs shown in Fig. 1.3g consist of optimum number of beams in parallel aligned such that one degree of freedom is permitted.

The examples shown so far have exemplified different advantages of compliant mechanisms. Successful realization of the above examples is only an indication of their increased use in the future. However, there are some limitations and challenges. Some of these are intrinsic to the use of compliance, while others can be overcome by better design. They are detailed in the section below.

1.1.5 Advantages and Limitations of Compliant Mechanisms

Most of the advantages of compliant mechanisms are due to its monolithic structure. The combination of energy storage and motion generation within a monolithic device have interested engineers and researchers alike. The advantages are listed below.

1. Reduced costs and easy to manufacture: This results from the reduced need to assemble different parts. As devices get smaller, assembly requires more skill and care. This is even more pronounced at the micron levels while fabricating using silicon based semiconductor technology, where making moving parts compliant and monolithic is the only solution.

2. Precision: Monolithic elastic mechanisms such as beams and flexures do not experience friction at joints as there are no siding elements. Furthermore, there is no backlash in these mechanisms leading to increasing accuracy and repeatability. However, for cyclic loading hysteresis has often been reported.

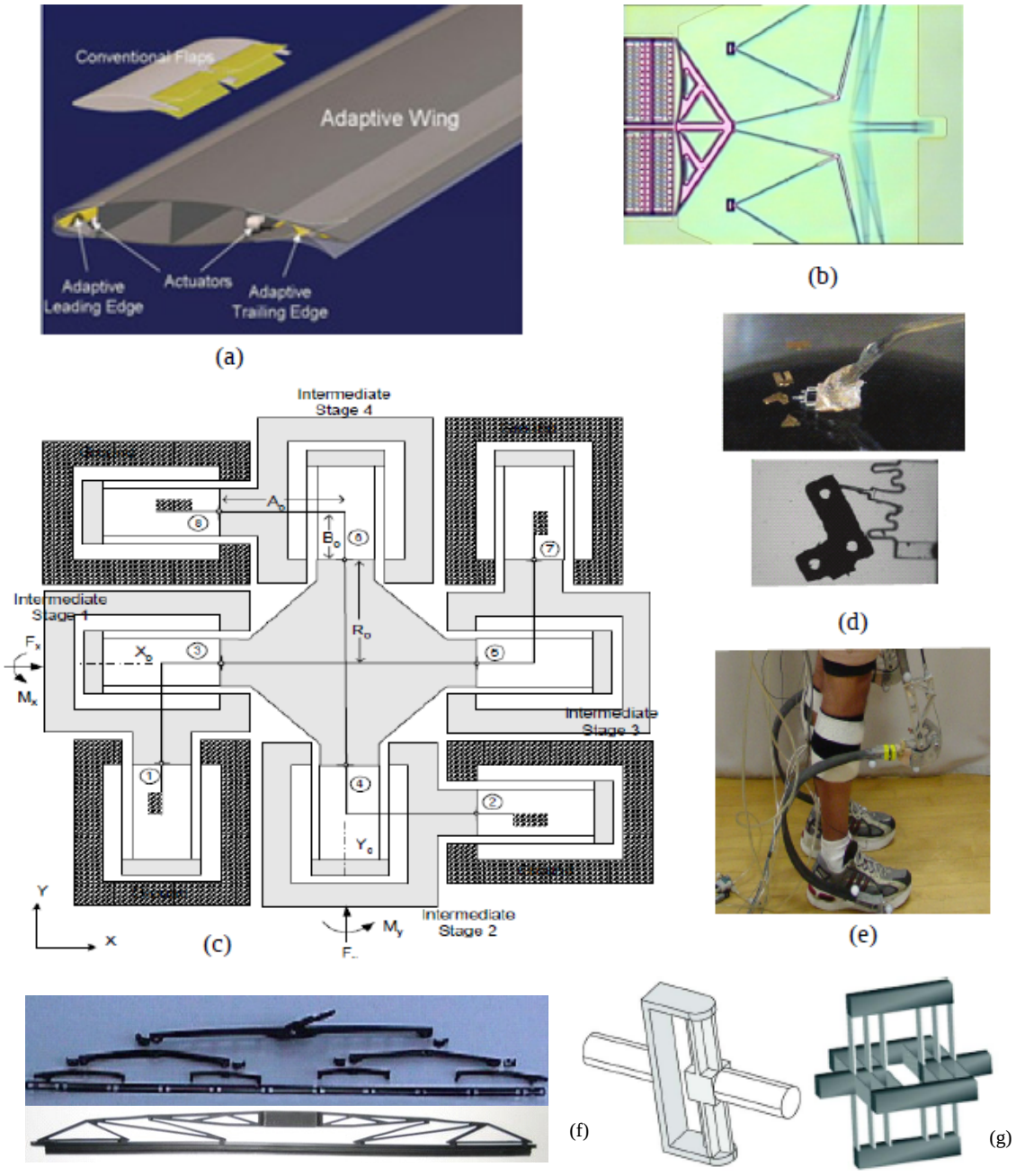

Figure 1.3: Distributed compliance in engineered designs (a) a mission adaptive aircraft wing that changes its profile based on flight conditions, (b) a MEMS displacement amplifier (*Hetrick and Kota* (2003)) (c) a nanometer precision X-Y stage with distributed compliant beams (d) a PDMS compliant suspension as a vision-based force sensor, (e) a compliant spring used for a passive knee orthosis exoskeleton, (f) a compliant one-piece wind shield wiper (*Kota and Hetrick* (2008)) showing above it the numerous parts of a traditional wipers, and (g) a large displacement translational and revolute joint.

3. Maintenance free: Compliant mechanisms are maintenance free as there is very little wear. This is again due to absence of sliding elements. However, for longevity they have to be operating within the permissible stress. Mechanisms made in the macro scale suffer from fatigue due to cyclic loads, but in the micro-scale where there is a better control of micro-structure during fabrication, they have been found to last a billion cycles without failure.

4. Functional Coupling: Compliant mechanisms can store energy as well as transmit motion. Thus it couples kinematics and kinetics which is very useful in some applications.

Some of the disadvantages of compliant mechanisms are

1. Range of Motion: Material stresses limit the range of motion and load carrying ability of compliant mechanisms. With distributed compliance, range of motion can be increased and failure stress decreased but this is in no comparison with the rigid link mechanisms. Furthermore, continuous rotation motion can never be achieved with compliant mechanisms.

2. Fatigue and Crepe: Compliant mechanisms made of polymers and plastics experience significant crepe when continuously stressed. Furthermore, cyclic loading induces fatigue in designs with lumped compliance thus limiting their life.

3. Design Challenges: While conventional rigid link mechanisms are analyzed and designed using kinematics and geometry alone, complaint mechanisms involve an intricate coupling between motion and the forces that cause motion. For large deformation ranges, this relationship is nonlinear. Though this nonlinearity provides significant design freedom in obtaining a wide range of force deflection and energy storage curves, their analysis involves large computational models.

Though the above disadvantages cannot be mitigated, their effects can be minimized by better design. For example, distributed compliant mechanisms in literature have

better stress distribution characteristics than lumped flexures. However most of them do not strictly distribute material evenly. Effective material distribution is one of the foremost design challenges for compliant mechanisms.

The chapter henceforth focuses on design methodologies for compliant mechanisms. Towards this a functional classification is proposed in the section below.

1.1.6 Functional Classification of Compliant Mechanisms

Focus of compliant mechanisms in this thesis will be limited to monolithic elastic mechanisms that have prescribed motion and force transformation characteristics. As a consequence of this, there are two functional requirements that are important

1. Ability to selectively constrain motion in different directions. This requires the mechanism to deform selectively to forces in different directions at a single point of interest.The $X-Y$ stage shown in Fig. 1.3c and a compliant suspension based force sensor shown in Fig. 1.3d are examples of this mechanism as they have a selected deformation response to applied forces. This usually requires them to be stiff in one direction and compliant in the other. Furthermore, the force deflection relationship can be nonlinear at that particular point of interest. Together, these mechanisms are termed *single port compliant mechanisms* as the focus is on the force deflection relationship at a single point of interest.

2. Ability to transmit forces and motion from one point (input) to another. Transmission implicitly involves relative interactions between two unique locations. The shape morphing examples of Fig. 1.3a and the displacement amplifier of Fig. 1.3b are examples of transmission problems. They are required to match the load characteristics of an actuator to the deformation requirement at the output. As the focus is on more than one point of interest, they are termed as *multi-port compliant mechanisms* with a special case being the two port single-input single-output mechanism. Multi-port mechanisms also involve design of

multiple single port mechanisms at various points to provide directionality.

The functional classification introduced above has important implications on the methodology involved in design. Design is an iterative approach between analysis and synthesis, which require a model or a mathematical representation of the mechanism behavior. For single port mechanisms, this representation must capture the relationship between applied force and obtained displacement at a single point. For multi-port mechanisms, this representation must capture the relationship between applied force at one point and obtained displacement at the other. The design methodologies for compliant mechanisms are detailed below.

1.2 Design Methodologies of Compliant Mechanisms

This section reviews design methodologies of complaint mechanisms based on the functional classifications, namely for single port and multi-port mechanisms. It details the advantages and shortcomings of the methodologies that sets the stage for the scope of the thesis.

1.2.1 Single Port Compliant Mechanisms

Single port compliance involves the characterization of the force displacement relationship at a single point of interest. This relationship is expressed in terms of compliance or stiffness matrix given by

$$\begin{aligned} \mathbf{u} &= \mathbf{C}\mathbf{f} \\ \mathbf{f} &= \mathbf{K}\mathbf{u} \end{aligned} \tag{1.1}$$

where $\mathbf{C}$ and $\mathbf{K}$ represent the compliance and stiffness matrices respectively, while $\mathbf{f}$ and $\mathbf{u}$ represent the force vector displacement vector respectively. In three dimensional space the stiffness and compliance matrices are 6×6 positive definite matrices,

while the force and displacement vectors are 6×1 vectors signifying three translations and three rotational degrees of freedom. The degrees of freedom can also be represented as screws and pitches.

Compliance at a single port has received attention in the design for robotic grippers. The end effectors of the grippers are required to have an appropriate remote center of compliance (RCC) that enables generation of a corrective moment to accurately align parts that are prone to positional errors as described by *Nevins and Whitney* (1985) (see Fig. 1.4a). The corrective moments re-orient the angle of the shaft so that it accurately fits into the hole. This is accomplished only when the elastic nature of the gripper enables the corrective moments to produce pure rotation at the end of the shaft, without any translation. This decoupling of translations and rotations have been the focus of researchers since the 70's. Decoupling of translational and rotational compliance was first mentioned in a textbook on structural mechanics by *Parcel and Moorman* (1955). They called this point as the elastic center. *Loncaric* (1985) proposed a formulation to maximally decouple the 6×6 compliance and stiffness matrices that result from the three dimensional linear elastic modeling of compliance at a point. Patterson and Lipkin (*H. Lipkin* (1992a), *H. Lipkin* (1992b), *Lipkin and Patterson* (1992)) proposed a formulation of decoupling that lead to the definition of geometric point known as the center of elasticity. At the center of elasticity any force produces pure translation, while any rotation produces a pure reaction moment. However, such a point does not physically exist for all geometries. *Ciblak and Lipkin* (1996) reviewed RCC devices and their realization using beam based topologies. Recently *Kim* (2008) proved the existence and the uniqueness of the center of elasticity for 2-D planar geometries where it coincides with the elastic center, remote center and the center of stiffness.

While the above efforts focus on simplifying the representation of compliance from a general 6×6 positive definite matrix to enable design, they do not propose a

systematic synthesis methodology to obtain any required compliance behavior.

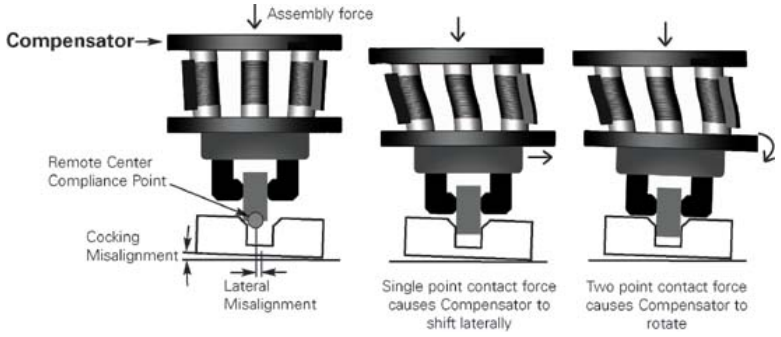

Figure 1.4: Remote Center of Compliance (RCC) Devices, where the compliance in the end effector adjusts for any misalignment in the mating parts

Realization of Arbitrary Stiffness Matrix in 3D space

While the representation of compliance at a single point was motivated by applications involving decoupling of translations and rotations, various researchers have independently tried to design systems that can attain any given three dimensional compliance using springs. Huang and Schimmels (*Huang and Schimmels* (1998a), *Huang and Schimmels* (1998b), *Roberts* (1999), *Huang and Schimmels* (2000), *Huang and Schimmels* (2001)) have defined a screw spring shown in Fig. 1.5a as a fundamental building block to generate any given compliance requirement. However, difficulty in the physical realization of screw springs have motivated the need for the use of compliant building blocks to achieve the same. Furthermore, though the characterization proposed is mathematically robust, it does not give an insight into the behavior of the mechanism that they represent. This precludes user insight in systematic synthesis.

Principles of constraint based design are not directly based on the stiffness or the compliance matrix, but provide a geometric insight into their behavior and enable easier conceptual synthesis.

A Constraint based Design using Screw Theory Formulation

Researchers in constraint based design have characterized flexures based on its most compliant and most stiff directions as freedom and constraints respectively. The guidelines for constraint based synthesis is illustrated in *Blanding* (1999). More recent work by Hopkins and Culpepper (*Hopkins and Culpepper* (2010a), *Hopkins and Culpepper* (2010b)), and *Su et al.* (2009) represent constraints and freedom in three dimensions as wrenches and twists respectively. For a given motion requirement this method focuses on generating constraint and freedom spaces. Principles of reciprocity are used to generate constraint space from a given freedom space. The constraint lines can be used to orient a flexure along that direction. Figure 1.5 b shows how each constraint wrench corresponds to the axis of orientation of a flexure. This method of generating conceptual solutions provides user insight as the representations of constraint wrenches directly correspond to the flexure geometry. However, constraints and freedoms are subjective quantities in compliant mechanisms depending on the ratio of stiffness between two directions. Thus, this representation and the design methodology do not take into account the holistic compliance behavior. Awtar and his group (*Awtar et al.* (2007), *Awtar and Slocum* (2007)) have analytically quantified the behavior of beam flexures by evaluating cross-axis stiffness and parasitic errors to provide an objective estimation of constraint and freedom. These characterizations provide insight into better designs.

A Geometric Representation for Two-Dimensional Compliance Characterization

Kim et al. (2008) and *Kim* (2005) proposed a geometrically insightful characterization of simple two dimensional complaint building blocks. The dimensionally reduced from of Eq. 1.1 consisted of two translational degrees of freedom and two rotational degrees of freedom. To overcome the dimensional mismatch between translational and

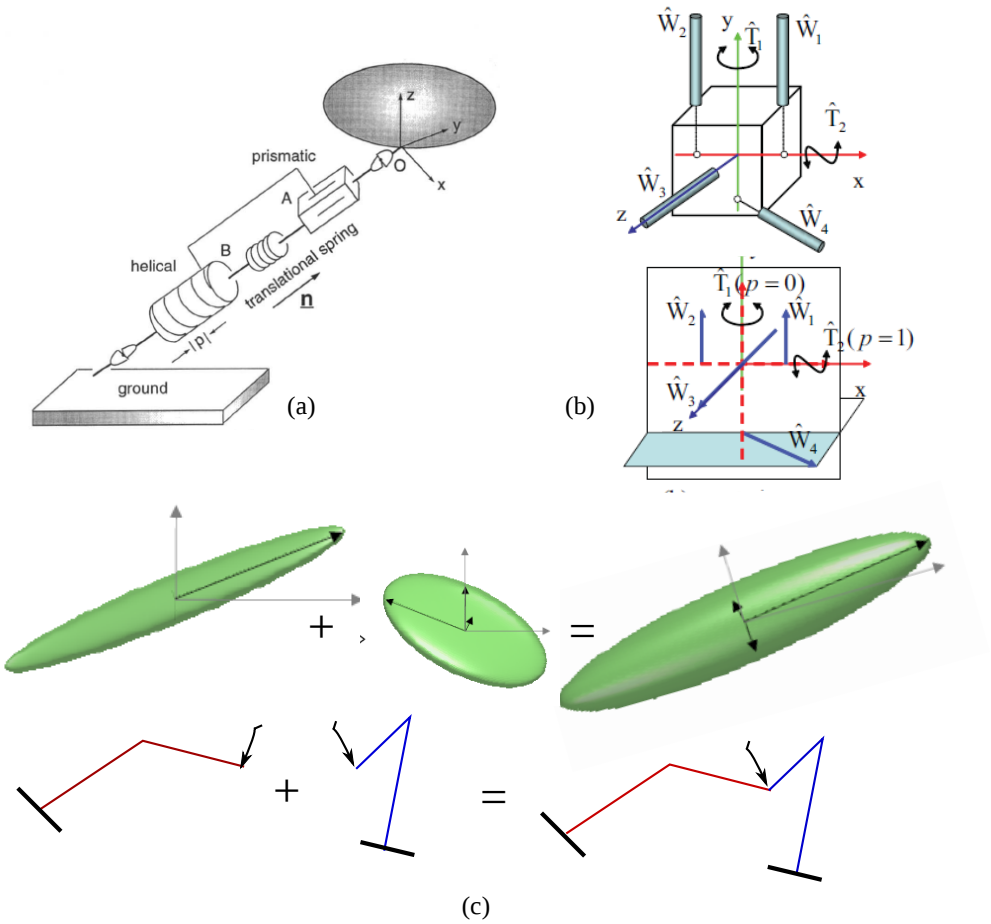

Figure 1.5: Single port compliance design (a) using screw springs (b) constraint based screw theory (c) geometric compliance ellipsoid approach.

rotational quantities, normalizing length was used to convert rotations to translations and moments to forces as shown below

$$\mathbf{C}_n = \begin{bmatrix} 1 & 0 & 0 \\ 0 & 1 & 0 \\ 0 & 0 & l_1 \end{bmatrix} \begin{bmatrix} C_{11} & C_{12} & C_{13} \\ C_{12} & C_{22} & C_{23} \\ C_{13} & C_{23} & C_{33} \end{bmatrix} \begin{bmatrix} 1 & 0 & 0 \\ 0 & 1 & 0 \\ 0 & 0 & l_2 \end{bmatrix} \tag{1.2}$$

However, there was no physical relevance to these normalizing lengths l_1 and l_2. This enabled an overall representation of compliance as an ellipsoid, with its semi-major axis representing a principal direction of compliance. Apart from rendering a geometric interpretation of the behavior of a mechanism, it enables a graphical representation of series combination of two or more mechanisms as captured in Fig. 1.5c. This enables a systematic building blocks based methodology as detailed in the section below.

1.3 Building Block based Design Methodology

Design of complex systems such as an automobile, aircraft and electronic gadgets are always broken down into simpler subsystems that can be easily designed. For example, an automobile consists of the combustion, transmission, electrical subsystems all working together. These subsystems are designed and fabricated separately and integrated during assembly. A similar building block approach was proposed for mechanism design by *Kota and Chiou* (1992) for conventional rigid link mechanism synthesis. Figure 1.6 shows how a complex mechanism such as a sewing machine can be decomposed into a number of simple submechanisms each having its own kinematic function. In a building block based design approach, the required kinematic specification was broken down into a number of simple, yet fundamental motion specifications. They used a building block library to solve subproblem specifications and combined them to obtain the entire mechanism.

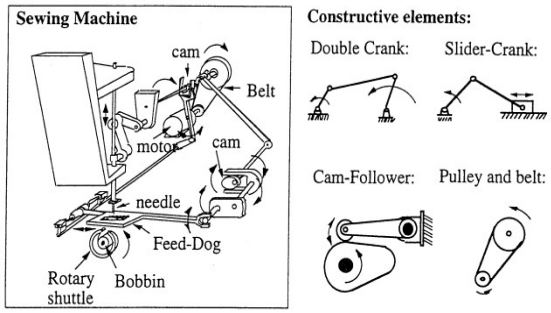

Figure 1.6: A sewing machine and its constituents adapted from *Chiou and Kota* (1999)

Kim et al. (2008) proposed a building block method for the design of single port mechanisms shown in fig. 1.7. The required stiffness specification is represented as a target ellipse. A number of simple deformable members like beams and dyads (series combination of two beams) are characterized in terms of its ellipsoid parameters to form a database of building blocks. First, a search is conducted to see if there is a candidate building block to meet the problem specifications. If not the ellipsoid is decomposed into two simpler ellipsoids, and the database is searched again to see if there is a solution the subproblems. If a solution is found, the subproblems are assembled to obtain the net mechanism. If no solution is found a different decomposition is tried.

Though this method provided user insight in synthesis, it suffered from some drawbacks. For example, ellipsoid representation was cumbersome and difficult to visualize. Furthermore, there was no direct mapping possible between the topology of a building block and the compliance ellipsoid. This was due to the physically non-intuitive normalizing lengths that were needed to evaluate the ellipsoid parameters. Furthermore, as required by early robotics applications, there was no natural decoupling of translational and rotational parameters. The effectiveness of the synthesis methodology depended on the right decomposition and population of the building

block library, both of which cannot be determined apriori. These shortcomings motivate a characterization that is more intrinsic to the topology of the building block, and the need for guidelines for determining the topology from the problem specifications.

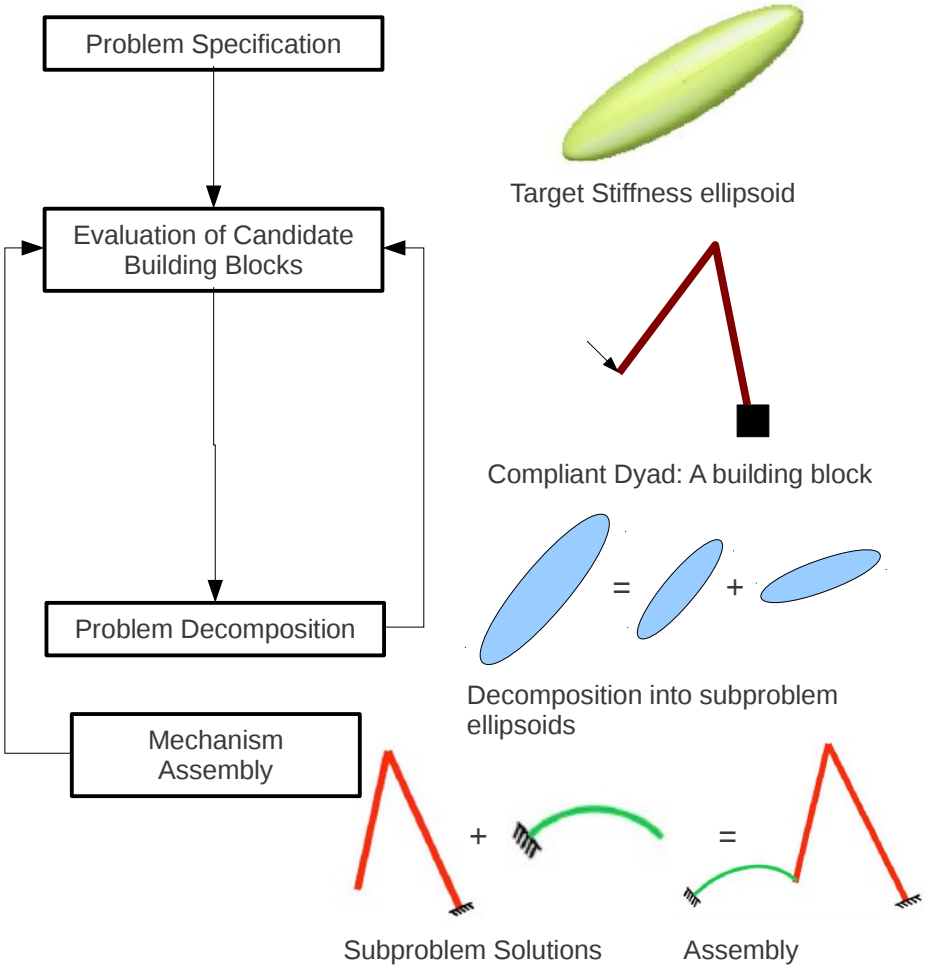

Figure 1.7: Building block method for the design of compliant mechanisms adapted from *Kim et al.* (2008).

1.3.1 Single Port Synthesis for Large Deformations

Apart from the design for linear Compliance, *Vehar-Jutte* (2008) proposed a methodology for the design of nonlinear springs for a given force deflection profile or energy profile as seen in Fig. 1.8a. This methodology uses an interconnected

framework of cubic splines and a genetic algorithm to determine the optimum geometry and cross-section dimensions that meet the required specifications. *Oh* (2008) proposed a robust design for bistable compliant mechanisms, and a systematic combination of bistable elements to obtain multistable mechanisms (see Fig. 1.8b and c).

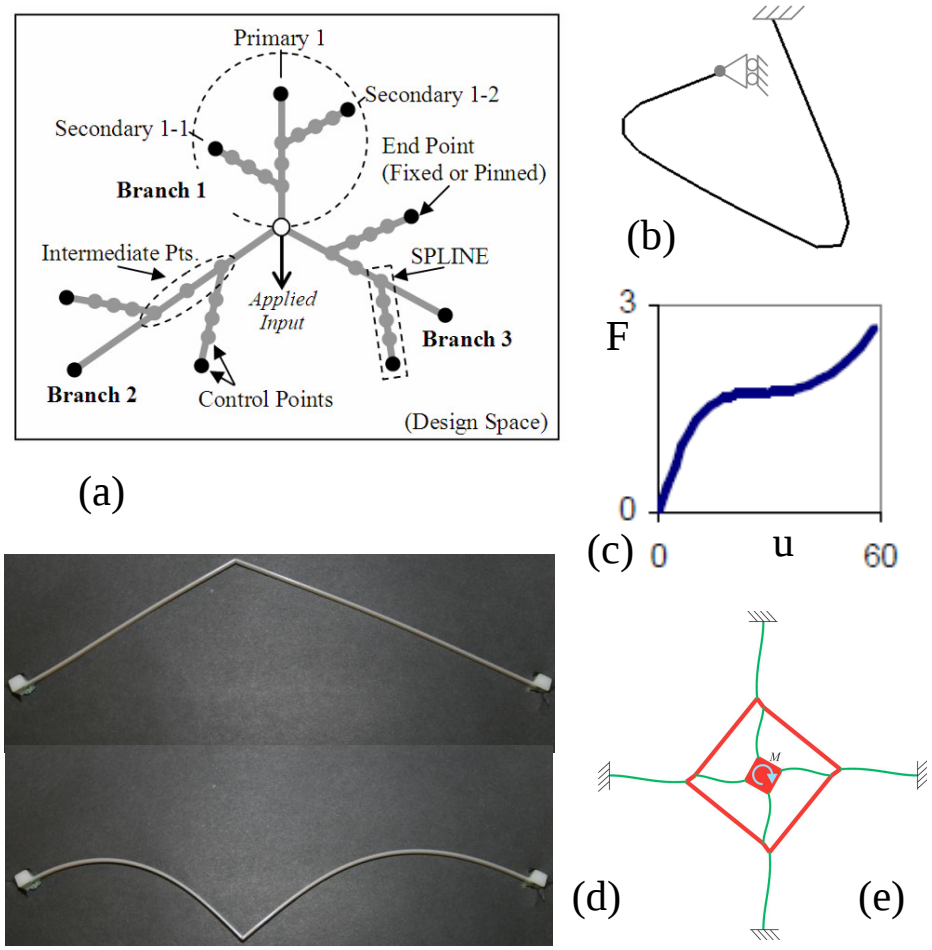

Figure 1.8: Synthesis of compliant mechanisms involving large deformations (a) A cubic spline based network for optimization based generation of (b) spring topologies with (c) nonlinear force displacement behavior (adapted from *Vehar-Jutte* (2008)) (d) a robust bistable mechanism with a living hinge and (e) a rotational bistable mechanism having multiple equilibrium configurations (adapted from *Oh* (2008))

1.4 Multi-Port Compliant Mechanisms

Multi-Port compliant mechanisms involve transmission of applied input energy to drive output loads. An example is a piezo-electric amplifier, where a large input force and small input displacement is delivered to the output as a large displacement driving against a moderate load. Some other examples mentioned earlier are grippers, and shape morphing mechanisms where a mechanism changes the shape of a surface or contour through a handful number of actuators. Design of these compliant mechanisms are influenced by the two stage process of designing conventional mechanisms as professed by *Erdman et al.* (2001).

1. Topology or Conceptual design

2. Shape-Geometry refinement

In this first stage a skeleton topology that approximately satisfies the kinematic requirements is conceptualized, while in the second stage practical dimensions are associated with it to more accurately match the footprint and motion specifications. It must be noted that while separation of the above two stages is accurate for rigid link mechanism synthesis, the intricate coupling between the topology and the actual associated dimensions for compliance makes the synthesis methodology inaccurate.

1.4.1 Topology or Conceptual Design

There are different methodologies to guide conceptual topology design of multi-port compliant mechanisms. Each of these methodologies involve a different representation of compliance to suit the design methodology. These are discussed below.

1.4.1.1 Kinematics based Design Methodologies

These are the earliest design methodologies for multi-port compliant mechanisms. In order to use conventional rigid link topologies for a compliant mechanism design,

certain approximations have to be made to the link lengths and joint stiffness. Howell and Midha (*Howell et al.* (1996), *Midha et al.* (2000), *Howell* (2001), *Howell and Midha* (1996)) devised a unique modeling technique known as pseudo-rigid body modeling where the deformation of a compliant mechanism is modeled based on the kinematics of an equivalent linkage and the force displacement relationship is captured by torsional springs of appropriate stiffness at the joints as shown in Fig. 1.9. The value of the spring stiffness and the link lengths are established by empirical approximations on the beams that make up the compliant mechanism. While this modeling technique is used to explain the behavior of compliant mechanisms, synthesis involves conceptualization of a rigid link mechanism with torsional springs at the joints. The dimensions of the link lengths and its cross section are determined by the values of torsional spring stiffness.

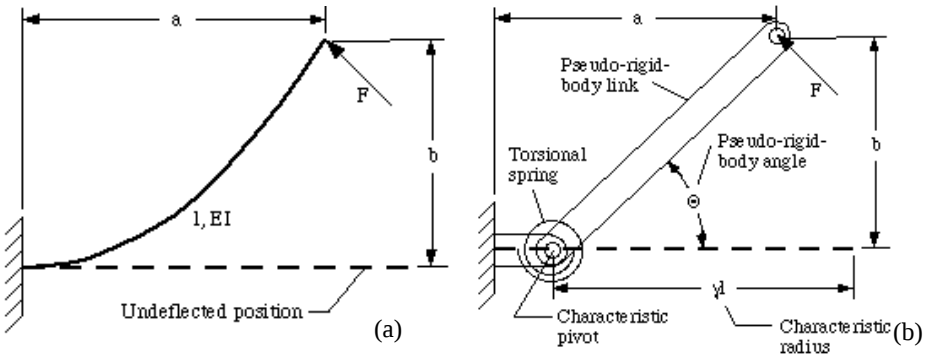

Figure 1.9: Pseudo-rigid body modelling of a (a) cantilever beam (b) equivalent link and torsional spring that models the deformation behavior of the cantilever beams (adapted from *Howell* (2001))

The effectiveness of this method is the simplistic representation of large deformation, and the availability of a large body of literature in the area of rigid link kinematics. However, various empirical approximations coupled with lumping compliance as a torsional spring at the joints limits the accuracy of the model. For example, the design method cannot account for off-axis and parasitic motion and thus is not holistic in nature (*Awtar and Sen* (2010)).

1.4.1.2 Optimum Search Based Methods

Topology can be defined in context of compliant mechanisms as an interconnected set of deformable members that connects the input to the output and the fixed ports. These connections can be direct or through a complex network of members. An optimum topology is one which meets the kinematic specifications and all the stiffness and stress specifications. The optimum search based methods require

- (a) *A Ground Structure*: This is a network of all possible interconnections there can be among the input, output and the fixed points and contains as many intermediate points as possible. These connections can be made of beam elements or continuum plane stress or plane strain elements as shown in Fig. 1.10.

- (b) *functional Metric*: Any performance requirement, such as kinematic relation between the input and output, maximum attainable stress, stiffness requirements, and volume must be expressed as functionals or as a metric that is a function of all the geometric and size variables that make up the topology.

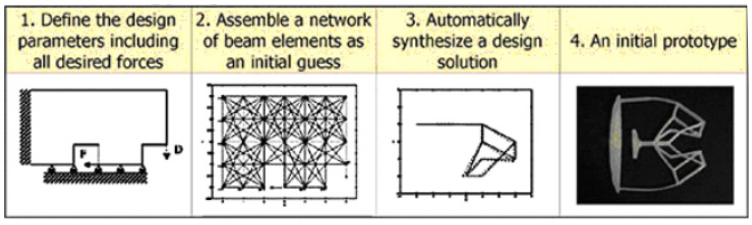

Figure 1.10: Steps in topology optimization of a compliant gripper adapted from *Joo* (2001)

The basic philosophy behind this method is that an optimum solution is attainable if it is contained within the network of members in the ground structure. An optimization algorithm minimizes (or maximizes) a primary functional known as the objective function subjected to satisfying some secondary functionals known as the constraints. The variables used for the optimization are the widths or thickness of

the members in the network as described in the paper on homogenization by *Bendsoe and Kikuchi* (1988). If the algorithm yields widths that are numerically insignificant, that member will be deleted from the optimum topology. The first attempt at using topology optimization on continuum elements was by *Ananthasuresh* (1994). The functional used to guide this optimization is a weighted average of strain energy to make the input stiff, and mutual potential energy to enable a large displacement at the output. However, these methods yielded lumped flexures at the joints. To obtain better distributed compliance *Frecker et al.* (1997) used a frame based ground structure. *Hetrick and Kota* (1999) used frame based ground structure with varying node locations to capture more of the design space. Ever since, a number of researchers (*Saxena and Ananthasuresh* (2006), *Frecker and Canfield* (2000)) have used the frame based ground structure with an output spring as an external load. Additional criteria towards obtaining distributed compliance was proposed by *Luzhong Yin* (2003). This output spring was necessary to provide connected designs. *Wang* (2009) developed a kineto-elastic formulation where the intrinsic mechanism stiffness is optimized to obtain connected designs. Some of the functionals used in the generation of these designs include ratio of the input and output displacements, energy efficiency and spring efficiency. These objective functions were compared by *Deepak et al.* (2009). While topology optimization yielded satisfactory designs for certain benchmark problems, there were a number of disadvantages.

1. Optimization did not yield practical or readily manufacturable designs requiring post processing of grey areas in continuum elements and unconnected or floating areas in frame based elements in ground structure.

2. These algorithms do not provide user with any intuition on how optimum topologies are reached.

3. Adding constraints of manufacturability or stress makes the problem complex

and computationally intensive.

Lu and Kota (2005) and *Lu and Kota* (2006) developed the load path representation to ensure connection between the input, grounded points, the output and some user-defined intermediate points. A number of interconnections between them are explored by a genetic algorithm and the best mechanism that minimizes the objective function projected by the algorithm. The complexity of the topology depends on the number of intermediate points between input, ground and the output that the user chooses. Choosing more points increases the computation time, but the algorithm may choose not to use any of them based on the optimum design. The optimization algorithm is evolutionary in nature coupled with graph search techniques. Apart from determining the connectivity the algorithm optimizes the cross-section of the beams that model the connections. Stress constraints were further imposed in order to obtain practical designs. While the designs that originate from this method are connected and feasible, there is still a lack of user intuition as to why a certain connection is preferred over the others. Furthermore there are no guidelines for the number of intermediate points to be chosen. An attempt towards answering these questions are undertaken in the building block method explained below.

1.4.1.3 Building Block Approach

Building block methods were developed by *Kim* (2005) to overcome the disadvantages of topology optimization and develop a tractable learning curve towards the design of compliant mechanisms. These methods were developed primarily for the design of single port mechanisms, and were extended to cover single input single output mechanisms (*Kim et al.* (2008)) and dual input single output mechanisms (*Kim* (2009)). A given two port problem was decomposed into three single port problems, namely the input constraint, the output constraint and an intermediate transmission member as shown in Fig. 1.12. Solutions for these single port problems were solved using a

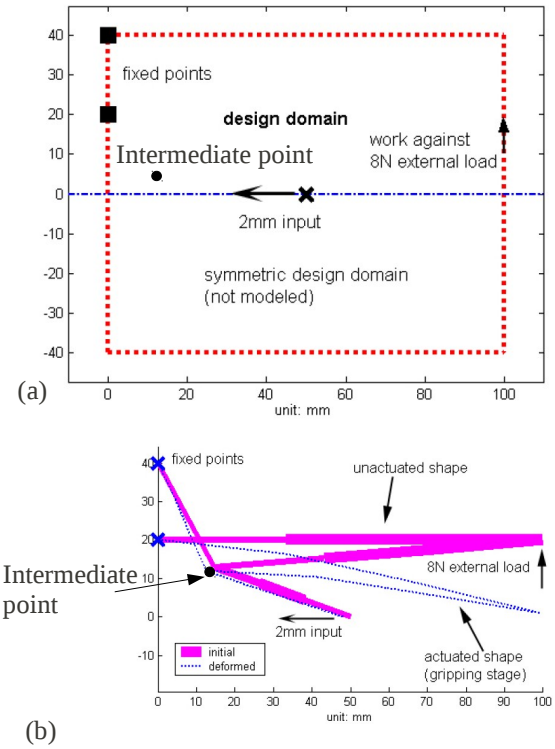

Figure 1.11: Formulation of a problem based on the load path method adapted from *Lu* (2004): (a) design domain initialization, and (b) optimal topology for the problem specification.

parallel combination of dyad building blocks as detailed in the single port section.

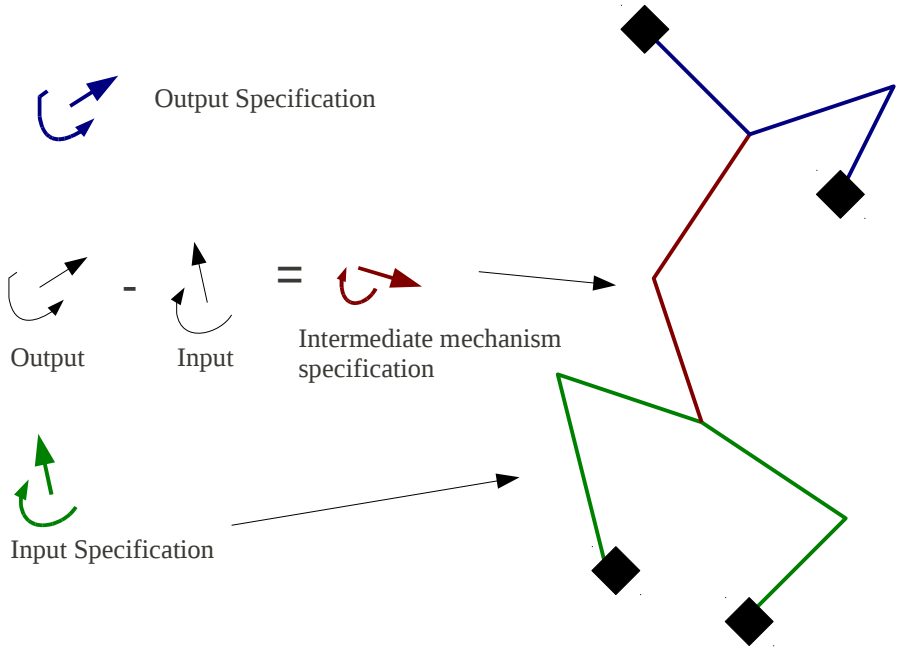

Figure 1.12: A building block method for the design of two port compliant mechanisms adapted from *Kim et al.* (2008).

There are a number of inaccuracies involved in this method of decomposition. For example, the kinematic behavior of building blocks change due to the coupling effects that arise from series combination of input constraint to the transmitter. This means that though the subproblem specifications are exactly met by the corresponding building blocks, the behavior of the assembled mechanism would be different from the target specifications. This requires a holistic characterization of multi-port compliance to capture the coupling between compliant building blocks when they are combined. *Kim et al.* (2006) also attempted to capture approximate kinematic relationship between two ports in terms of instant centers. The premise of this method is that the planar displacement of each point in the mechanism can be captured by an instant center of rotation. For example, pure translation can be represented as rotation about an axis at infinity. The relationship between the deformation of two different points in a compliant mechanism can be represented by rotation about a

common instant center. The distance between the instant center and the respective input and output ports determines the kinematics (geometric or mechanical amplification) of the mechanism (see Fig. 1.13. Though this technique is simple and intuitive, it does not capture the coupling terms when two building blocks are combined.

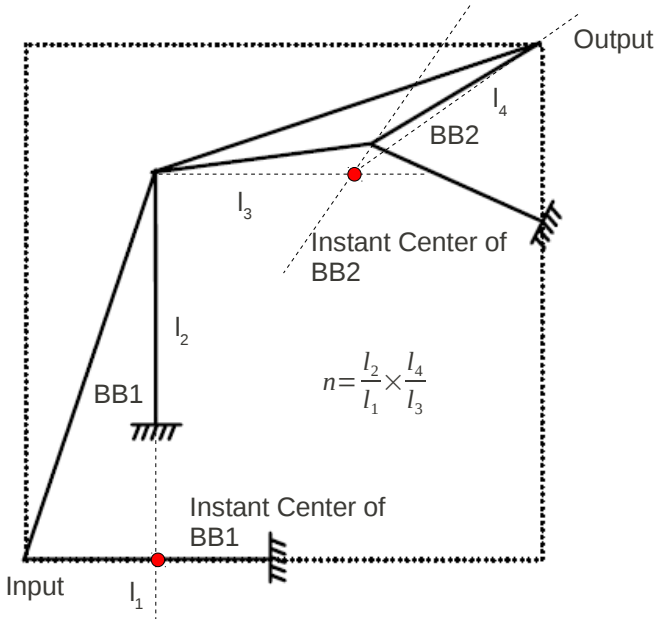

Figure 1.13: Instant center based design of two port mechanisms (*Kim et al.* (2006)).

1.4.1.4 Selection Based Approach

With almost two decades of research on design methodologies for compliant mechanisms, there is a growing literature of mechanism topologies for a number of applications. Almost any new problem specification can be solved by looking at existing mechanisms. Towards this end, it is useful to have a database of existing mechanisms. Furthermore since the behavior of mechanisms are not only dependent on their topology but also the length scales,and dimensions associated with the cross-sections. In order to enable an objective comparison of different topologies based on their stiffness and kinematics, Krishnan and Ananthasuresh (*Krishnan and Ananthasuresh* (2008), *Krishnan* (2006)) developed a lumped spring-lever model shown in fig. 1.14a. The model completely captures the input and output stiffness as lumped springs and the

kinematic relationship between them as a lever. *Hegde and Ananthasuresh* (2010) used selection based maps to compare a number of topologies and systematically select the best topology for the application. The map is a three-dimensional space spanned by feasible values of the lumped parameters. The given problem specification is expressed as a subset of this map. Then, a topology made of beams having a certain uniform cross-section is taken, and its input stiffness, output stiffness and the magnification factor is plotted in the map. A uniform increase or decrease in the cross-section dimensions changes the lumped parameters. This is captured as a path traversed by the mechanism on the map as shown in Fig. 1.14b. A similar path can be drawn by uniformly changing the length scales of the mechanism. If any of these path intersect the region defined by the problem specifications, then that mechanism is taken as the potential solution. If no mechanism in the database meets the specification set forth by the application, then a mechanism is synthesized afresh.

Though these charts provide insight into design, a three dimensional space is quite nonintuitive to visualize. Furthermore, the lumped model can accurately represent a unidirectional mechanism, but not its holistic behavior. Furthermore stresses are not taken into account within the maps, and they are dealt with separately.

1.4.2 Size and Geometry refinement

The design methodologies reviewed in the previous section generates only a skeletal or conceptual topology. Embodiment of the topology with practical dimensions to meet given specification is the next step. In some design methodologies load path method, topology and size are simultaneously designed. However, most conceptual topologies need to undergo size and geometry refinement as the number of variables to be optimized is lower when compared to topology generation. This speeds up the computational time and enables handling of a number of constraints like stress and manufacturability. Shape and geometry optimization were proposed by Hetrick and

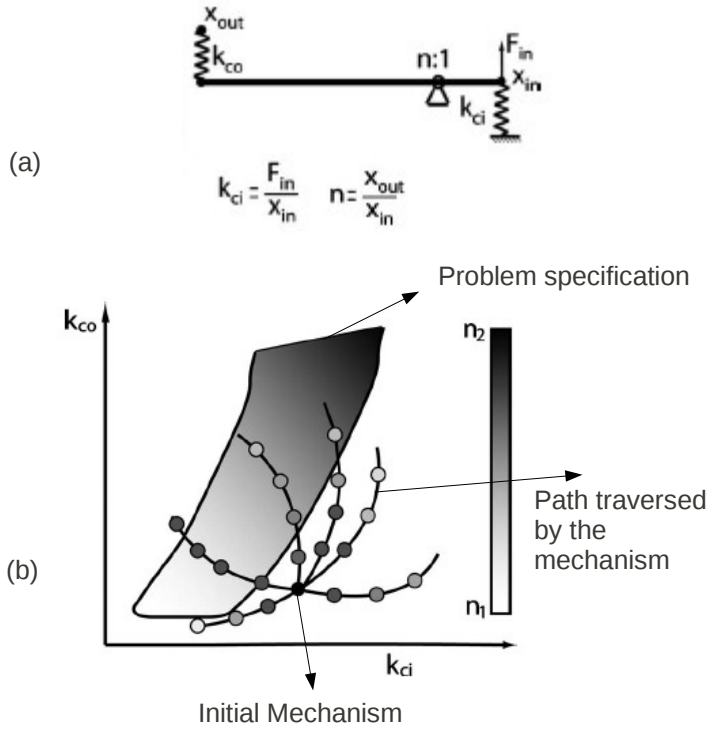

Figure 1.14: A map based selection technique for compliant mechanisms: (a) spring-lever model that captures the mechanism's lumped behavior, and (b) the map spanned by the lumped quantities (adapted from *Hegde and Ananthasuresh* (2010)).

Kota (*Hetrick and Kota* (1999), *Kota et al.* (1999)) where energy efficiency defined by the ratio of the output work done on an external load to the input work supplied was maximized with respect to stress constraints. The geometric locations of each node and the thickness of each element were allowed to vary within a given limit. This design process is shown in fig. 1.15. The authors state that using just the objective functions without imposing any stress constraints yield designs with lumped compliance. This indicates that lumped designs are more efficient due to their proximity in behavior with rigid link mechanisms. Imposing stress constraints enables a more distributed design. However the tendency towards lumped flexures remain. There is a need to distribute stresses evenly in this stage of the design process.

Apart from the above techniques *Xu and Ananthasuresh* (2003) developed a method to treat each member that makes up the topology as a bezier curve and optimize the control polygon of the curves to attain a kinematic objective with stress constraints. Special constraints are imposed to prevent self intersection of each curve. However, apart from limiting the maximum stress, these techniques donot enforce uniform stress distribution.

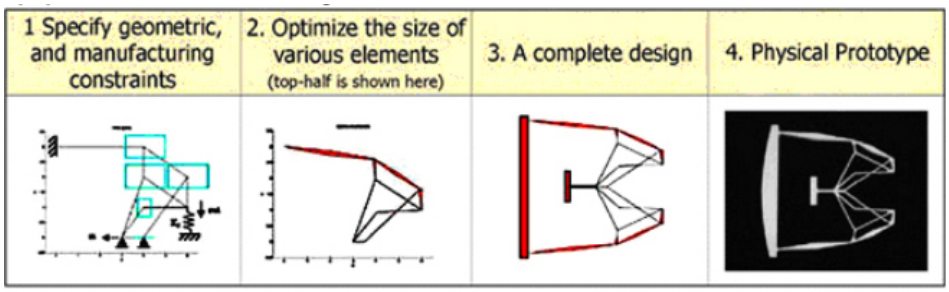

Figure 1.15: Steps in shape and geometry refinement of a compliant gripper adapted from *Joo* (2001)

1.5 Identifying Gaps in Literature

Compliant mechanism design is dependent on the representation of compliance. Some representations are mathematically robust, while others provide user insight without

any basis from the fundamental principles of mechanics. every representation has its limitations. For example the compliance ellipsoids represent the holistic nature of the compliance, but is limited to small deformations and the physical relevance of normalizing lengths. In contrast, pseudo-rigid body model is inaccurate in capturing compliance holistically, but retains its accuracy over a large range of motion. For topology optimization, the challenge lies in formulating the right functional that not only captures compliance accurately, but guides the algorithm towards desired results. The metrics proposed so far yield designs that tend towards lumped flexures far from the vision of evenly distributing stress. Furthermore, computationally intensive methods lack user intuition and require significant post-processing to obtain practical designs. Thus there is a need for a representation that not only captures compliance holistically and accurately, but also favors topology synthesis with user insight.

Apart from conceptual or topology synthesis, dimensional synthesis using size and geometry refinement suffers from designs that tend towards lumped flexures. Application of stress constrains lead to practical but sub-optimal designs. These designs do not maximally utilize the material by evenly distributing stresses. Size and geometry optimization thus requires a metric that can guide the optimizer algorithm towards designs that distribute stress. In short, there are three wide areas where gap in literature is identified

1. A mathematically robust representation of compliance that also enables user insight in synthesis: while there is prior literature that attempts at such a representation for single port compliance, there is no prior attempt for multi-port compliance.

2. A synthesis procedure involving user insight: Computationally intensive automated synthesis process may provide a practical solution, but does not yield insight on why a certain topology was achieved, why a certain specification was achieved, or not achieved. If specifications are not met, it does not yield a

plausible explanation. The user needs to make intelligent guesses on whether it could be the domain initialization, choice of algorithm or unachievable specification. In other words, there is no determinism in synthesis. Thus there need to provide all this knowledge to the designer.

3. Moving away from lumped flexures: Every single optimization technique, both conceptual topology generation as well as refinement of conceptual designs have yielded thin regions at the joints or fixed ends. These emulate the behavior of lumped flexures. Flexures fail when large loads are applied and thus are not optimal. The metrics used for optimization have been based on efficiency and other kinematic considerations, with stress imposed as constraints. There is a need to propose a better metric that takes the strength considerations into account.

1.6 Scope of the Thesis

The main goal of the thesis is to develop an accurate representation for single-port and multi-port compliance that favours a systematic building block based methodology for topology synthesis. Such a methodology requires the representation to be intrinsic to the mechanism geometry in order to permit a parametric characterization of simple deformable members known as building blocks. Furthermore, it must enable problem subdivision into tractable sub-problems that can be solved by the existing library of building blocks. All formulations in this thesis will be limited to capturing small deformation and linear elastic material behavior of the mechanisms. Though the formulation is general its definition and application in the design methodology will be limited to two dimensional planar problems alone. All representations will be evaluated from linear finite element stiffness matrices using beam elements. This is because most compliant mechanisms in literature consist of slender elements well ap-

proximated by Euler-Bernoulli beams. However, the generality of the representation does not preclude evaluation by other experimental and analytical methods. This formulation will thus be based entirely on the principle of mechanics without any approximations other than the ones mentioned above.

Apart from the building block methodology, this thesis seeks to formulate a metric to evaluate the performance of mechanisms based on topology, relative dimensions and actuation scheme. The objective of this metric is to objectively explain the effectiveness of designs in nature in terms of even stress distribution as opposed to engineered designs that tend towards lumped compliance. Optimizing conceptual topologies using this metric must yield designs that emulate the distributed compliance of nature. Apart from dimensional synthesis, the metric must objectively compare various topologies and their actuation schemes. Single-port, single-input single-output and distributed-input single-output mechanisms must be compared under the same scale in terms of its effectiveness in performing work and ability to evenly distribute stresses. The resulting comparison must set the trend for future research on compliant mechanisms.

1.7 Organization of the Dissertation

The thesis introduces a new representation of compliance from the fundamentals of mechanics. While single port compliance is well articulated in literature, the thesis aims to adapt the eigen-twist and eigen-wrench characterization within the framework of the building block methodology. This includes providing graphical insight into series and parallel combination of planar mechanisms. Chapter 2 presents these insights along with practical guidelines for planar single point design. A compliant suspension for vision-based force sensing in the micromanipulation of cells is designed using the methodology.

Chapter 3 presents a unique characterization of multi-port compliance using the

concept of load flow in structures. The physical interpretation of load flow is discussed and evaluated in terms of transferred forces. Fundamental building blocks that are responsible for load flow are isolated and their geometric embodiments are analyzed. A framework for load flow visualization in compliant mechanisms is presented with a number of practical examples from literature. Chapter 4 uses this characterization of multi-port compliance to propose guidelines for a building block based synthesis methodology. Some benchmark examples such as single-input single-output mechanisms, and shape morphing applications are designed to illustrate the effectiveness of the method.

While the above chapters focused on conceptual topology synthesis for compliant mechanisms, Chapter 5 introduces a novel performance metric for dimensional synthesis by size and geometry optimization of conceptual compliant mechanism designs. This metric is obtained by evaluating nature's designs for the amount of work done before failure. Optimization using this metric yields deigns with better performance. Benchmark problems are illustrated to confirm that the metric distributes stress evenly within the topology. The conceptual topologies synthesized in the previous chapters are optimized to evenly distribute stresses in them. Furthermore, this metric is used to compare various topologies with different actuation schemes. The effectiveness of distributed actuation is highlighted to motivate a new class of mechanisms actuated with pressurized fluids. Conclusions, summary of the contributions and future work are detailed in Chapter 6.

CHAPTER II

An Intrinsic Geometric Framework for the Building Block Synthesis of Single Port Compliant Mechanisms

In this chapter a characterization based on eigen-twists and eigen-wrenches is implemented for the synthesis of a compliant mechanism at a given point. For 2-D mechanisms, this involves characterizing the compliance matrix at a unique point called the center of elasticity, where translational and rotational compliances are decoupled.Furthermore the translational compliance may be represented graphically as an ellipse and the coupling between the translational and rotational components as vectors. These representations facilitate geometric insight into the operations of serial and parallel concatenation. Parametric trends are ascertained for the compliant dyad building block and are utilized in example problems involving serial concatenation of building blocks. The synthesis technique is also extended to combination of series and parallel concatenation to achieve any compliance requirements.

2.1 Introduction

For a compliant mechanisms where the point of application of load and measurement of displacement are the same, the compliance matrix captures the load-displacement relationship. Mechanism geometry is intricately embedded within this matrix, making it difficult to obtain meaningful mapping between geometry and function. There is a need to characterize the compliance matrix with parameters independent of orientationto enable a general representation of the compliance matrix. One such approach involves the eigen-values and eigen-vectors of a modified compliance matrix, while representing it graphically as a 3-D ellipsoid (*Kim* (2005), *Kim et al.* (2008)).

The compliance matrix has terms involving both translational and rotational compliance. These terms are coupled within the matrix. The coupling prevents taking direct eigen-values of the compliance matrix, which except under very special cases yields a combination of the translational and rotational parameters. The eigenvectors of the compliance matrix are dimensionally inconsistent, non-intuitive, and unsuitable for characterization. The rotational and the translational compliance must be characterized separately. This can be effectively accomplished by shifting the point of interest to a location where any force applied yields pure translation and any moment applied yields pure rotation. This was defined by Lipkin and Patterson (*H. Lipkin* (1992a), *H. Lipkin* (1992b)) for a general 3-D elastic body with six degrees of freedom as the Center of elasticity. At the CoE in 3-D, translations and rotations are not necessarily decoupled, but in 2-D this decoupling is always guaranteed. (*Kim* (2008)). In this case, this point is equivalent to the commonly used *center of stiffness* (*Hale* (1999)), or the *Remote Center of Compliance* (RCC) in robotics (*Nevins and Whitney* (1985)), or the *elastic center* which diagonalizes the compliance matrix (*Ciblak and Lipkin* (1996)). Though the center of elasticity need not be a material point, it can be accessed through a rigid body attached from this point to the input

of the mechanism.

The main objective of the chapter is to apply the eigen-twist and eigen-wrench characterization to 2-D compliant building blocks and decouple compliance terms associated with translation and rotation. This characterization enables graphical representation of series and parallel combination of building blocks. Guidelines are proposed to enable synthesis of a mechanism topology for any given compliance requirements.

The following section reviews the eigen-twist and eigen-wrench characterization of the compliance matrix. These quantities decouple the effect of translations and rotations and effectively characterize building blocks without the introduction of a normalizing lengths. In Section 3, the parametric behavior of a common building block, the compliant dyad, is described in terms of the eigen characterization. This enables us to quantify its limitations and propose the need for combination of building blocks. The effect of series combination are studied in Section 4. Based on this understanding, the limits of series combination of building blocks are understood. In Section 5, two examples to demonstrate the effectiveness of the characterization are solved.

2.2 Building Block Characterization

This section reviews the mathematics involved in characterizing the compliance matrix at a given point of interest. *Kim et al.* (2008) utilized compliance ellipsoids to characterize the primary kinematic behavior of compliant building blocks. The drawback of this approach is the introduction of a normalizing length to resolve units of length and rotation (and force and moment). The present characterization is adapted from the screw-theory based representation of 3-D compliance wherein the rotational and translational components of the compliance matrix are decoupled without the introduction of normalizing lengths. The approach is mathematically robust and is

invariant to coordinate transformations and changes in length scale. Stiffness and compliance *coupling vectors*, which provide fundamental information key to the serial concatenation of building blocks are identified. These concepts are described in the sequel.

2.2.1 Eigen-twist and Eigen-wrench decomposition, and Center of elasticity

In three dimensions, displacements may be represented as twists $\mathbf{T}$, and loads as wrenches $\mathbf{w}$. Twists are a combination of translation vector $\vec{\delta}$ and angular deformation vector $\vec{\gamma}$. Similarly, wrenches are represented as a combination of linear force $\vec{\mathbf{f}}$ and torque $\vec{\tau}$. Lipkin and Patterson characterized the 6×6 compliance matrix by separately normalizing the translation and the rotation degrees-of-freedom (*H. Lipkin* (1992a)).The application of the characterization to 2-D compliant mechanisms can be found in *Kim* (2008). This involved two constrained minimization problems given by

$$\begin{aligned} Minimize: \qquad & PE = \frac{1}{2}\mathbf{w}^T C \mathbf{w} \\ Subject \qquad to: \; & \mathbf{w}^T \tilde{\eta} \mathbf{w} = 1 \end{aligned} \tag{2.1}$$

and

$$\begin{aligned} Minimize: \qquad & PE = \frac{1}{2}\mathbf{T}^T K \mathbf{T} \\ Subject \qquad to: \; & \mathbf{T}^T \tilde{\xi} \mathbf{T} = 1 \end{aligned} \tag{2.2}$$

For 2-D elasticity $\mathbf{w}$ and $\mathbf{T}$ are 3×1 vectors as represented below.

$$\mathbf{T} = \begin{bmatrix} \delta_x \\ \delta_y \\ \gamma \end{bmatrix} \qquad \mathbf{w} = \begin{bmatrix} f_x \\ f_y \\ \tau \end{bmatrix} \tag{2.3}$$

Where, δ_x (f_x) and δ_y (f_y) are translations (forces) and γ (τ) is the rotation (moment) about an axis perpendicular to the plane through the input point. The Compliance matrix $\mathbf{C}$ and the stiffness matrix $\mathbf{K}$ are 3×3 symmetric matrices. The normalizing matrices $\tilde{\eta}$ and $\tilde{\xi}$ are used to separately normalize the translation and the rotation aspects of the wrenches and twists in Eq. 2.1 and Eq. 2.2 respectively.

$$\tilde{\eta} = \begin{bmatrix} 1 & 0 & 0 \\ 0 & 1 & 0 \\ 0 & 0 & 0 \end{bmatrix} \qquad \tilde{\xi} = \begin{bmatrix} 0 & 0 & 0 \\ 0 & 0 & 0 \\ 0 & 0 & 1 \end{bmatrix} \tag{2.4}$$

Eq. 2.1 and Eq. 2.2 can be solved as constrained minimization problems. They lead to two eigen-value problems shown in Eq. 2.5.

$$\mathbf{Cw} = \mathbf{a_f}\tilde{\eta}\mathbf{w} \qquad \mathbf{KT} = \mathbf{k_g}\tilde{\xi}\mathbf{T} \tag{2.5}$$

This makes $\mathbf{a_f}$ (a_{f_1} and a_{f_2}) the eigen translational compliance and k_g the eigen rotational stiffness. The components of the eigen compliance matrix $\mathbf{a_f}$ is given by a_{f_1} and a_{f_2}. The eigen vectors $\mathbf{w_f}$ are given as

$$w_{fi} = \begin{bmatrix} \hat{e}_{fi} \\ \vec{r} \times \hat{e}_{fi} \end{bmatrix} \tag{2.6}$$

The vector $\hat{e}_{fi}$ gives the orientation of the eigen-compliances a_{f_1} and a_{f_2} in a 2-D plane. This is shown in Fig. 4.4 as angle δ. The last term of the above vector describes a

moment that results from the application of a force at a location $\vec{r}_E$ away from the input point. The head of the vector $\vec{r}_E$ is located at the Center of Elasticity (CoE). The CoE is of particular importance in the characterization of planar building blocks because the application of force at this point results in pure translation. Similarly, the application of pure moment at the CoE results in pure rotation.

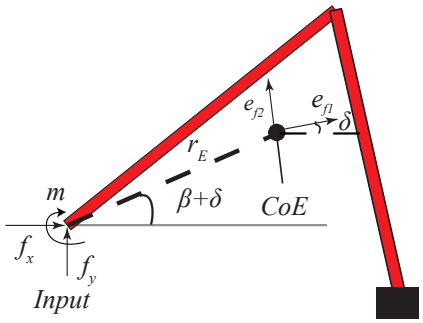

Figure 2.1: Eigen-twist and Eigen-wrench parameters for a particular building block geometry.

The terms in the eigen-twist and eigen-wrench characterization can be summarized with respect to Fig. 4.4 as:

a) *Translational Compliance*: Given by a_{f_1} and a_{f_2}, these eigen-compliance parameters depict the stationary compliance magnitudes and direction for pure translation, at the center of elasticity. The quantity a_{f_1} is the primary compliance direction as observed from the center of elasticity. The ratio of the two eigen-compliances are denoted by $n_p = a_{f_2}/a_{f_1}$. This quantity denotes the cross axis compliance.δ is the orientation of the semi-major axis of the ellipse (a_{f_1}) with respect to the horizontal. This angle can be changed by rotating the dyad about the Z axis.

b) *Eigen-rotational Stiffness* (k_g) : This gives the reaction moment produced by a pure unit rotation at the center of elasticity.

c) *Center of elasticity* ($\vec{r}_E$): Its distance (r_E) and orientation (β) with respect to the point of input represent the coupling between rotational and translational

compliance. It must be noted that β is the orientation of the center of elasticity from the input with respect to the a_{f_1} axis. If the dyad is oriented such that $\delta = 0$, the β is the orientation of r_E with respect to the horizontal.

Each of the above eigentwist/eigenwrench parameters can be obtained from the terms of the stiffness/compliance matrix. This is shown in Section.

2.2.2 Compliance Ellipse and Coupling Vector

In the following section, Compliance Ellipse and the Compliance Coupling Vector are developed to represent the eigentwist/eigenwrench parameters graphically. This representation is of particular importance for concatenation of the building blocks. A similar representation is also developed as the Stiffness Ellipse and the Stiffness Coupling Vector.

The Compliance ellipse has its semi major axes (a_{f_1}) inclined at an angle δ with respect to $X-$ axis. It forms a part of the upper 2×2 portion of the compliance matrix (shown in Fig. 2.2). The other part is a degenerate ellipse with magnitude r_E^2/k_g (matrix with one of its eigen values 0 and the other r_E^2/k_g) inclined at $\beta + \delta$. This signifies that the translational compliance at the input point is the sum of the translational compliances at the CoE and an additional translational compliance caused by applying a moment ($\vec{r}_E \times \vec{f}$) at the CoE. The moment occurs as a result of shifting the unit force from the input to the CoE.

The coupling vector $\vec{c}$ has a magnitude r_E/k_g and is inclined at angle $\beta + \delta$ to the horizontal. The coupling vector signifies the amount of rotation produced at the input point by applying a unit force at the CoE perpendicular to the orientation of $\vec{r}_E$. It must be noted that no rotation is produced by applying a force along the orientation of $\vec{r}_E$. Due to symmetry of the compliance matrix, $\vec{c}$ also represents the amount of translation at the input in a direction perpendicular to $\vec{r}_E$ due to a unit moment at the CoE. There is a total decoupling of forces and moments when the

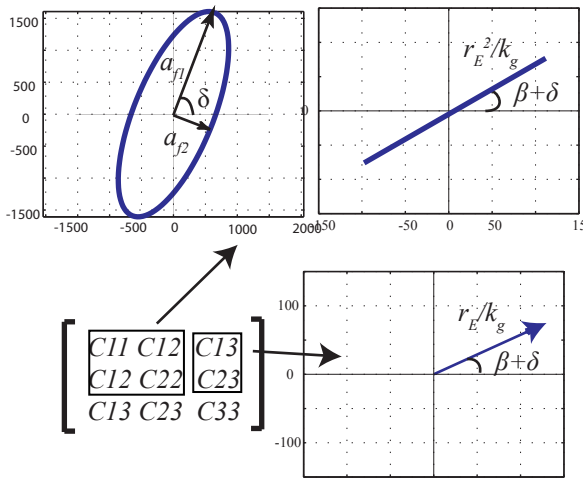

Figure 2.2: Compliance ellipse and Compliance coupling vector (c_v).

magnitude of $\vec{c}$ vanishes. The C_{33} element of the compliance matrix is $1/k_g$.

Similar to the graphical representation of the compliance matrix, stiffness can also be represented by the stiffness ellipse and a stiffness coupling vector, $\vec{s}_c$ (shown in Fig. 2.3). The semi-major and -minor axes of the stiffness ellipse as expected are the reciprocal of the compliance ellipse. The magnitude and the orientation of $\vec{s}_c$ are shown below.

$$|\vec{s_c}| = \frac{2r_E}{a_{f_1}}\left(\frac{1}{n_p^2}\cos\beta^2 + \sin\beta^2\right)$$
$$\gamma = \arctan\frac{1-n_p}{(1-n_p)\cos 2\beta + (1+n_p)} \tag{2.7}$$

These representations show that the compliance and the stiffness matrices can be graphically represented by six parameters a_{f_1}-a_{f_2}, $\vec{r}_E$, r_E, k_g, δ and β. These quantities will be used to characterize and intuitively combine building blocks for given specifications. In the next section, the parametric variation of these parameters for a common building block, i.e. a compliant dyad is investigated.

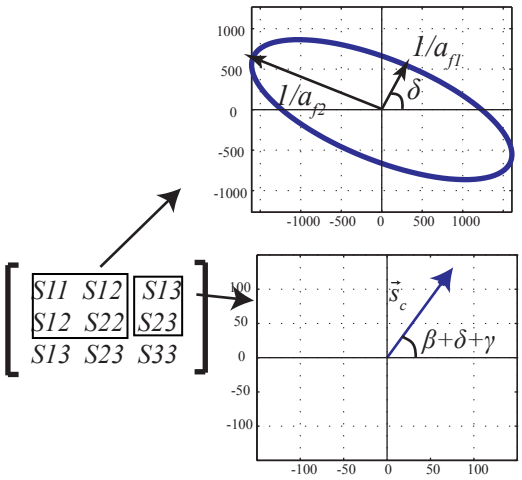

Figure 2.3: Stiffness ellipse and Stiffness coupling vector ($\vec{s}_c$).

2.3 Concatenation of Building Blocks

Building blocks can be combined in series or parallel. Serial concatenation does not change mechanism topology, as the number of fixed points remains constant. Instead serial concatenation modifies mechanism *shape*. A wide range of compliance characteristics can be obtained from serial concatenation of building blocks. Series concatenation for preliminary shape synthesis, which can be further refined to meet specifications are studied. This involves understanding how coupling vectors and the compliance ellipses transform under serial concatenation.

Serial concatenation presents distinct mathematical challenges because the point of interest of one of the building blocks shifts. As shown in Figure 2.4, when $BB2$ adds in series with $BB1$, the input of $BB1$ shifts from I_{p1} to I_{p2}. This shift is given by the vector $\vec{l}_r$. The input point of the mechanism shifts from the input of $BB1$ to the input of $BB2$. The compliance matrices of the two building blocks in series add such that (*Kim* (2005),*Hale* (1999))

$$\mathbf{C}_{resultant} = \mathbf{C}_{BB2} + \mathbf{T}^T \mathbf{C}_{BB1} \mathbf{T} \tag{2.8}$$

where

$$\mathbf{T} = \begin{bmatrix} 1 & 0 & 0 \\ 0 & 1 & 0 \\ l_r \sin\psi & l_r \cos\psi & 1 \end{bmatrix}$$

and l_r and ψ are the orientation of the input of BB2 from the input of BB1, as seen in Fig. 2.4. In the remainder of this section, it is examined how the eigen-twist and the eigen-wrench parameters change graphically due to serial concatenation of building blocks.

2.3.1 Eigen-rotational Stiffness

The eigen-rotational stiffness is not affected by the shift in the input point. This can be seen by expanding terms of Eq. 2.8 and noting that $k_g = \frac{1}{C_{33}}$. The transformation $\mathbf{T}^T\mathbf{C}_{BB1}\mathbf{T}$ leaves the C_{33} term unchanged. Thus, serial concatenation always adds the eigen-rotational stiffness in parallel such that

$$\frac{1}{k_{g_f}} = \frac{1}{k_{g_1}} + \frac{1}{k_{g_2}} \tag{2.9}$$

where k_{g_f} is the eigen-rotational stiffness of the combined mechanism.

2.3.2 Coupling vector

The individual building block coupling vectors ($\vec{c}_1$ and $\vec{c}_2$) add vectorially under serial concatenation with an additional term due to the shift in input for BB1. The shift in the input is given by $\vec{l_r}$. This is shown in Fig. 2.4. The final coupling vector

$\vec{c}_f$ is given as

$$\begin{aligned}
\vec{c}_f &= \left(\vec{c}_1 + \frac{\vec{l}_r}{k_{g_1}}\right) + \vec{c}_2 \\
\vec{c}_f &= \frac{\vec{r}_I}{k_{g_1}} + \frac{\vec{r}_{E_2}}{k_{g_2}} = \vec{c}_n + \vec{c}_2 \\
r_{Ef} &= \frac{|\vec{c}_f|}{k_{g_f}}
\end{aligned} \tag{2.10}$$

The term in the brackets in the above equation adds to give a new vector $\vec{r}_I$, which points from the input of $BB2$ to the CoE of $BB1$. The coupling vector $\vec{r}_I/k_{g_1}$ can be termed as the *modified coupling vector* of $BB1$. Thus during series combination, the modified coupling vector of the grounded beam $BB1$ vectorially adds to the coupling vector of $BB2$. The center of elasticity for the resultant mechanism is given by the last equation in Eq.2.10.

Application to beams

The CoE of a beam is at half its length. Its coupling vector can be given by $\vec{c}_{Beam} = (\frac{\vec{l}_{Beam}}{2})/k_{g_{Beam}}$, where l_{Beam} is the beam length and $k_{g_{Beam}}$ is its eigen-rotation stiffness. When a beam is added in series to a grounded building block such as $BB1$, its shift vector $\vec{l}_r$ equals its length $\vec{l}_{Beam}$. Substituting these simplifications in Eq. 2.10, final coupling vector $\vec{c}_f$ is obtained as

$$\begin{aligned}
\vec{c}_f &= \left(\frac{\vec{r_{E_1}}}{k_{g_1}} + \frac{\vec{l}_{Beam}}{k_{g_1}}\right) + \frac{\vec{l}_{Beam}}{2k_{g_2}} \\
\vec{c}_f &= \frac{\vec{r}_{E_1}}{k_{g_1}} + \vec{l}_{Beam}\left(\frac{1}{k_{g_1}} + \frac{1}{2k_{g_2}}\right)
\end{aligned} \tag{2.11}$$

This understanding is used to show in Appendix B that the center of elasticity for series combination always lies within the footprint of the mechanism.

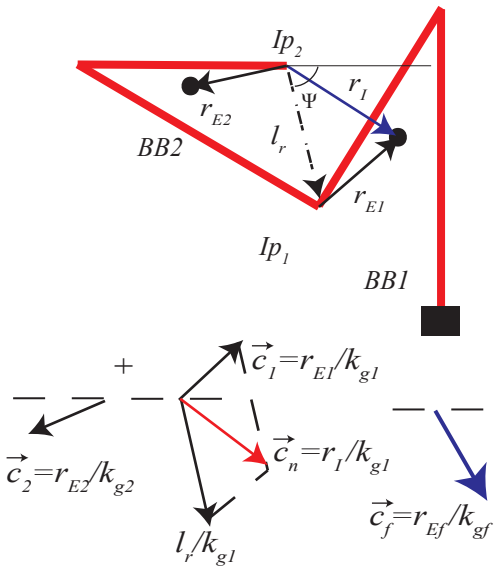

Figure 2.4: Two building blocks BB1 and BB2 in series. The final coupling vector is the vector addition of the *modified coupling vector* of BB1 ($\vec{r}_I/k_{g_1}$) and the coupling vector of BB2 ($\vec{r}_{E_2}/k_{g_2}$)

2.3.3 Compliance Ellipse

Serial concatenation requires more than adding the individual building block compliance ellipses. There is an additional degenerate ellipse (ellipse with one of its axis vanishing) known as the Compliance shift ellipse whose semi-major axis is denoted by a_{shift} that is added to the compliance ellipses of BB1 and BB2. The shift ellipse signifies the shift in the point of interest from the input of BB2 to BB1. The compliance shift ellipse is oriented at an angle δ_{shift}. This is perpendicular to $\vec{r}_m$, which is the orientation of the center of elasticity of the first building block $\vec{r}_{E_2}$ to the center of elasticity of the second building block $\vec{r}_{E_1}$. This is shown in Figure 2.5. These quantities may be calculated as

$$
\begin{aligned}
a_{shift} &= \frac{(|\vec{l_r} - \vec{r}_{E_2} + \vec{r}_{E_1}|)^2}{k_{g_1} + k_{g_2}} \\
\delta_{shift} &= \Omega + \pi/2 \\
\vec{r}_m &= \vec{l_r} - \vec{r}_{E_2} + \vec{r}_{E_1} = \vec{r}_I - \vec{r}_{E_2}
\end{aligned}
\tag{2.12}
$$

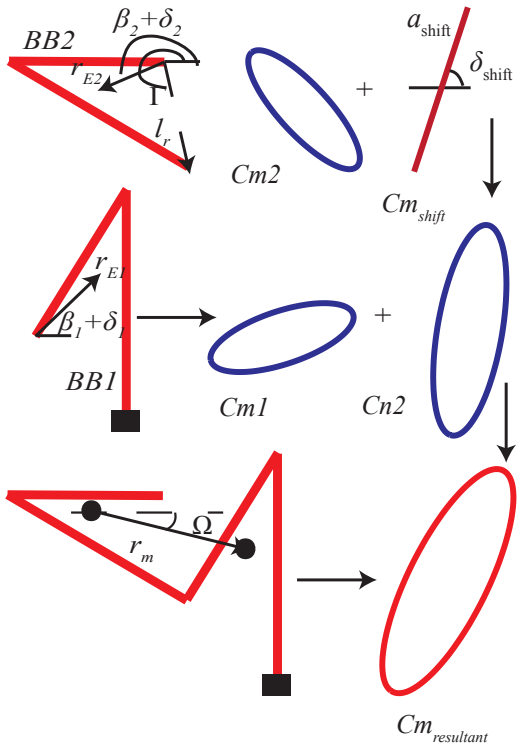

Figure 2.5: The compliance ellipse of BB2 is augmented by a degenerate shift ellipse $r_m^2/(k_{g_1}+k_{g_2})$.

2.3.4 Parallel Concatenation of the building blocks

Parallel concatenation of building blocks was extensively studied by *Kim et al.* (2008). This type of concatenation is necessary to design mechanisms constrained to move in a particular direction. Parallel concatenation is relatively straightforward with the stiffness ellipses and the stiffness coupling vectors of the two building blocks add. This is shown in Fig.2.6.

2.4 Parametric Characterization of a Compliant Dyad Building Block

Most compliant mechanisms are composed of slender, beam-like elements connected in series or parallel.A fundamental building block for such mechanisms is the

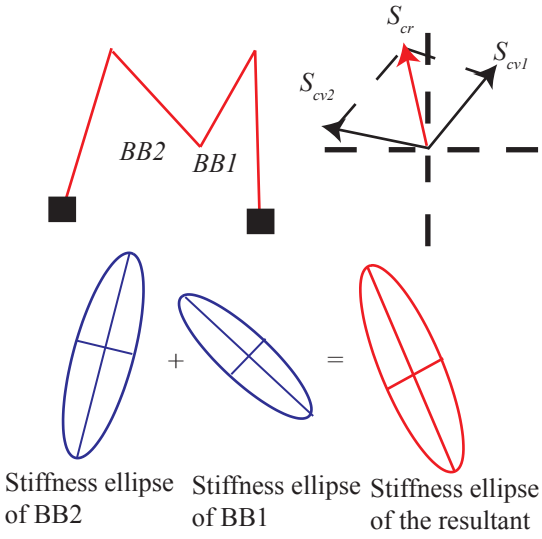

Figure 2.6: Addition of Building blocks in parallel involves addition of the individual stiffness ellipses and the coupling vectors.

compliant dyad. A compliant dyad consists of two beams connected in series as shown in Fig. 4.4 and is versatile in obtaining a wide variety of compliance characteristics (*Kim et al.* (2008), *Kim* (2008)). In this section parametric trends of the compliance quantities introduced in Section 2 are obtained for the compliant dyad. The trends will be utilized subsequently to select building block geometries for given stiffness requirements.

2.4.1 Parametric Trends

The shape of a compliant dyad is captured by the angle between the beams, α, and the ratio of lengths of the two beams, $l_{2_{norm}} = l_2/l_1$ as shown in Fig. 2.7. The total length of the dyad is defined as $l_{dyad} = l_1 + l_2$. For initial characterization, it is assumed that the beams share the same cross-section ($I = \frac{bh^3}{12}$) and material (E). The characteristics developed in Section 2 are presented here for the compliant dyad. When possible, the characteristics have been normalized to highlight dependence on shape alone.

$\mathbf{k_g}$: The eigenrotational stiffness is independent of the dyad shape and is expressed as

$$k_g = \frac{EI}{l_{Dyad}}. \tag{2.13}$$

$\mathbf{n_p}$: The ratio of linear compliances is captured as $n_p = \frac{a_{f_2}}{a_{f_1}}$. Figure 2.7a shows the dependence of n_p with the shape parameters of the dyad. Values of $0.001 < n_p < 1$ can be obtained by adjusting the geometric parameters of the dyad.

$\mathbf{a_{f_{1n}}}$: The linear compliance may be normalized such that

$$a_{f_{1n}} = a_{f_1} \frac{EI}{l^3_{Dyad}}. \tag{2.14}$$

The normalization is valid for beams with slenderness ratios greater than 15. The dependence on the geometry parameters for the normalized compliance is shown in Fig. 2.7b

$\mathbf{r_{E_n}}$: The distance to the center of elasticity may be normalized with respect to l_{Dyad} such that $r_{E_n} = \frac{r_E}{l_{Dyad}}$. The dependence of r_{E_n} is shown in Fig. 2.7c. r_E vanishes only when $\alpha = 0°$, which is not feasible to fabricate. Furthermore, when a dyad tends to a beam (i.e.$\alpha = 180^0$), its center of elasticity is at half its length, i.e. $r_E = l_{Dyad}/2$.

β: Figure 2.7d gives the dependence of the angle β while varying α and l_{2norm}. When $\alpha \to 0°$ and 180°, the direction to the center of elasticity is 90° with respect to the orientation of a_{f_1}. This indicates that a beam's center of elasticity is oriented along its length.

It is possible to size a compliant dyad to obtain desired values for *some* of the parameters. n_p is dependent on the shape alone , whereas both k_g and a_{f_1} depend on shape, cross-section, and material. The shape of a dyad (α and $l_{2_{norm}}$) may be selected based solely on a desired n_p^* using Fig. 2.7a. The selected combination of α and $l_{2_{norm}}$ corresponds to a specific normalized linear compliance, $a_{f_{1n}}$. Subsequently,

the specific length, l_{Dyad}, and cross-section, I, may be ascertained by utilizing Eqns. 2.13 and 2.14.

However, if it is necessary to simultaneously achieve specifications on more than one quantity (e.g. r_E and n_p), a single dyad building block may be insufficient. Serial or parallel combination of more than one building block provides increased capacity to attain various combinations of specified characteristics. Synthesis of building blocks connected in series will be presented in Section 5.

2.4.2 Stress in a dyad

The performance of a mechanism with desired stiffness characteristics largely depends on the magnitude of bending stress induced for a given operating load. The bending stresses are now related to the geometry of the dyad. For a force f_x and f_y in the X and Y direction respectively together with a moment m, the maximum stress is either at the beam junctions or at the grounded end. This maximum stress can be expressed as

$$\begin{aligned}
\sigma &= \frac{max(M_E, M_J)b}{2I} = \frac{max|M_E, M_J|6}{hb^2} \\
M_E &= l_{Dyad}\left(\frac{f_y sin(\alpha) l_{2_{norm}} + f_x(1 - cos(\alpha) l_{2_{norm}})}{1 + l_{2_{norm}}}\right) + m \\
M_J &= l_{Dyad}\left(\frac{f_y sin(\alpha) l_{2_{norm}} - f_x cos(\alpha) l_{2_{norm}}}{1 + l_{2_{norm}}}\right) + m
\end{aligned} \tag{2.15}$$

where M_E and M_J are bending moments at the grounded end and the junctions respectively, I is the second area moment of the cross section, l_{Dyad} is the overall length of the dyad, b is its in-plane thickness and h is the out of plane thickness of

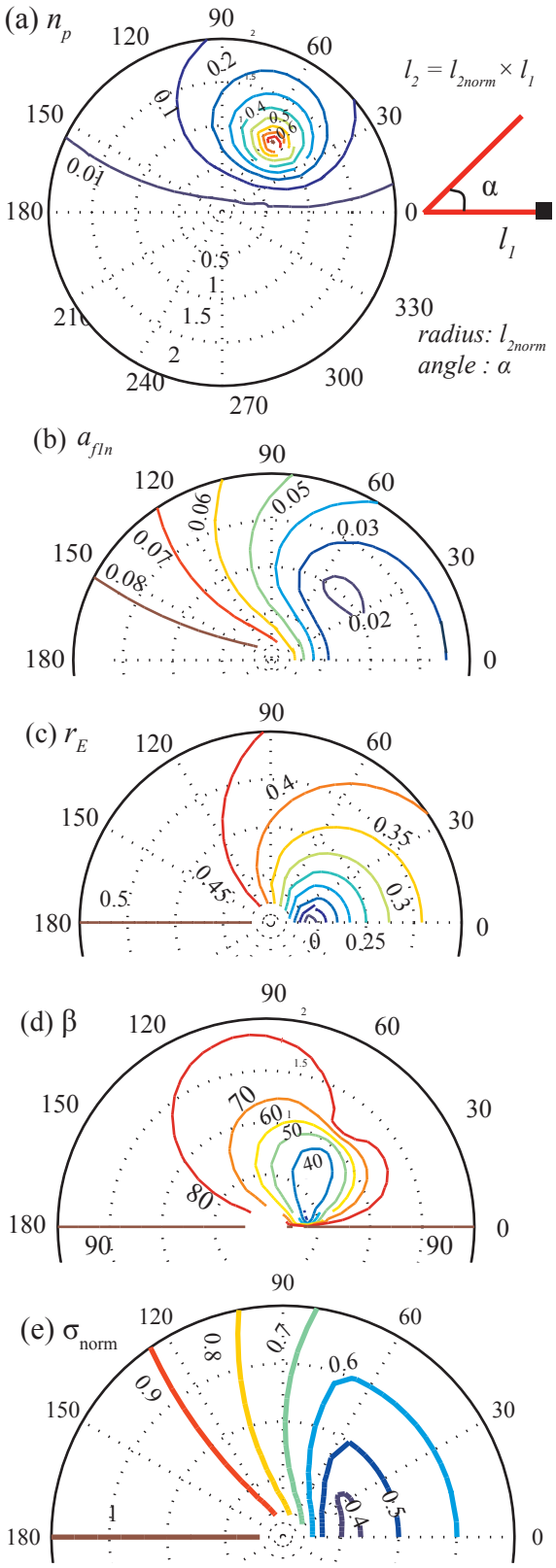

Figure 2.7: (a) A plot of n_p (b) A plot of the normalized value of a_{f_1} and (c) normalized value of r_E (d) angle β, and (e) Normalized stress factor σ_n with respect to the dyad angle and dyad length ratios l_{2norm}.

the beams . The above moments can be written as

$$M_E = \frac{f l_{Dyad} \sqrt{l_{2_{norm}}^2 + 1 - 2cos(\alpha) l_{2_{norm}}} sin(\theta + \omega)}{1 + l_{2_{norm}}} + m$$
$$M_J = \frac{f l_{Dyad} l_{2_{norm}} sin(\theta - \alpha)}{1 + l_{2_{norm}}} + m \tag{2.16}$$

where $\theta = tan^{-1}(f_y/f_x)$, $f = \sqrt{f_x^2 + f_y^2}$ and $\omega = tan^{-1}((1-cos(\alpha) l_{2_{norm}})/(l_{2_{norm}} sin(\alpha)))$. The maximum end moment for a force of magnitude f occurs when $\omega + \theta = 90°$, while the maximum junction moment is at $\theta - \alpha = 90°$. The maximum stress can be expressed as

$$\sigma = (f\sigma_n + m/l_{Dyad}) \frac{6 l_{Dyad}}{b^2 h} \tag{2.17}$$

where σ_n is the normalized maximum stress factor given by

$$\sigma_n = max| \frac{\sqrt{l_{2_{norm}}^2 + 1 - 2cos(\alpha) l_{2_{norm}}}}{1 + l_{2_{norm}}}, \frac{l_{2_{norm}}}{1 + l_{2_{norm}}} | \tag{2.18}$$

This normalized stress factor is plotted in Fig. 2.7e. The maximum stress at the end of the dyad is obtained when $\alpha = 180°$ making $\sigma_n = 1$, indicating that for a given applied load and overall mechanism length, a straight beam experiences the maximum stress. The overall stress is lower for smaller dyad angles but they occur at the junction between the beams.

Another guiding principle can be obtained by a restatement of the above equation using the definition of k_g from Eq.2.13. Substituting the in-plane width b in terms of k_g ($= \frac{Ehb^3}{12 l_{Dyad}}$) in Eq.2.17, the following equation is obtained.

$$\sigma = (f\sigma_n + m/l_{Dyad})(\frac{12 l_{Dyad} E^2}{8 k_g^2})^{1/3} \tag{2.19}$$

In Eq.2.18 that the maximum value for σ_n is 1. Furthermore the maximum moment m can be thought of as the action of force f through a rigid body of length l_{Dyad}

(which is also roughly the footprint of the dyad) separating the point of application from the input of the dyad. Substituting $f\sigma_n + m/l_{Dyad} = 2f$ in the above equation, a safe operating value of k_g can be evaluated knowing the maximum allowable stress in the mechanism (σ_a) as

$$k_g \geq \sqrt{\frac{12 l_{Dyad} E^2 f^3}{h \sigma_a^3}} \tag{2.20}$$

In most design problems, once the material is selected, the out of plane thickness is known either based on the fabrication process or from the thickness of the sheet. Furthermore knowing the maximum force that can be applied and the maximum length of the mechanism, the lower limit of k_g can be estimated such that the stress will always be less than the permissible value from Eq. 2.20.

2.5 Guidelines and Examples for Building Block Concatenation

In this section guidelines are provided for systematically generating conceptual topologies by series, parallel or both series and parallel combinations of compliant dyads. The procedures are based on the mechanics of concatenation described in Section 3 and the parametric behavior of dyads described in Section 4.

2.5.1 Procedure for Serial Concatenation

For a given force, the maximum stress for a dyad always occurs when $\alpha = 180°$, i.e. when it is a beam.

One strategy to lower overall stress levels in a mechanism is to use curved or folded beams. This may be accomplished with a serial concatenation of compliant dyads. To that end, systematic guidelines are proposed for the synthesis of mechanisms composed of two dyads for required compliance behavior and stress constraint. The procedure can be easily extended to synthesis involving multiple building blocks. The

procedure is illustrated in Fig. 2.8 for the synthesis of a mechanism with equal linear compliances ($n_p = 1$) and input at the center of elasticity ($r_E = 0$). The steps are briefly listed here and are utilized in a subsequent example.

Step 1 *Graphical problem specification*: The problem is specified in terms of a compliance ellipse and coupling vector.

Step 2 *Eigen-rotation stiffness estimation*: Determine prudent values of k_g for the two building blocks based on stress considerations as shown in Section 4.2.

Step 3 *Spatial CoE orientation*: For a given footprint choose the CoE positions of the two building blocks so that their combination results in the required coupling vector as given by Eq. 2.10.

Step 4 *Net ellipse evaluation*: When two building blocks are combined in series, their relative CoE separation results in a degenerate shift ellipse given by Eq.2.12. The required net ellipse is the difference between the problem specification and the shift ellipse. The net ellipse must be positive definite.

Step 5 *Net ellipse subdivision*: Subdivide the net ellipse into two smaller ellipses each corresponding to a building block. Different subdivisions lead to different solutions.

Step 6 *Building block design and combination*: Determine building block geometries based on their compliance ellipse specifications.The building blocks are placed such that their CoEs are at the points determined in Step 3. To ensure connectivity between the input of one building block and the fixed port of the other, include rigid connections.

The above synthesis procedures aim at finding feasible values for k_g to ensure that the maximum stress is less than material yield. Subsequently the CoE of the two building blocks are chosen to lie within the prescribed footprint. This is motivated by

the deep co-relation between the CoE, mechanism geometry and the overall footprint (see Appendix B). The net ellipse is then subdivided to avoid overlapping members and further maintain footprint specifications.Overall, the procedure is motivated at simultaneously achieving the coupling vector and ellipse characteristics together with constraining the mechanism within the footprint. It must be noted that there could be alternate procedures to obtain a design for a given problem specification.

2.5.2 Series Concatenation: Example

The synthesis procedure is now explained in detail for a specific example. This example proposes to design a mechanism that has equal compliance in the X and Y direction of magnitude 0.15 mm/N and no coupling between forces and rotation (r_E = 0). The assumed material is spring steel (E = 210 GPa, σ_{yield} = 2000 Mpa) of thickness h = 10 mm. The mechanism needs to withstand a maximum force f of 30 N and must fit within a footprint of 500 mm × 500 mm.

Step 1: The problem specifications can be represented as a circular compliance ellipse of radius 0.15 mm/N and a coupling vector of zero magnitude as shown in Fig. 2.8a.

Step 2: A value for minimum k_g can be obtained by applying values from problem specification into Eq.2.20 , to yield $\sqrt{\frac{12\times500\times(200e3)^2\times30^3}{10\times2000^3}} = 7.5\times10^4 N-mm$. For simplicity, k_g is assumed to be same for the two building blocks, i.e. $k_{g_1} = k_{g_2} = k_g$. Thus Eq. 2.10 reduces

$$\vec{c}_f = \frac{\vec{r}_I + \vec{r}_{E_2}}{k_g} \tag{2.21}$$

As a consequence of this simplification, $\vec{r}_I$ and $\vec{r}_{E_2}$ add as vectors.

Step 3:The two vectors $\vec{r}_I$ and $\vec{r}_{E_2}$ denote the distance of the building block CoEs from the input. To achieve a zero net coupling vector, $\vec{r}_I$ and $\vec{r}_E$ must be equal

and opposite as shown in Fig. 2.8b. Note that these vectors have to be selected to lie within the mechanism footprint. In the present problem, this distance has been selected to be 120 mm (i.e., $r_I = 60\ mm$ and $r_{E_2} = 60\ mm$) to satisfy the footprint constraints.

Step 4: The shift ellipse is given by Eq. 2.12 by substituting $\vec{r}_m = \vec{r}_{E_2} - \vec{r}_I = 2\vec{r}_{E_2}$ as

$$a_{shift} = \frac{2r_{E_2}^2}{k_g} = \frac{2(60mm)^2}{7.5 \times 10^4 N - mm} = 0.09mm/N \tag{2.22}$$

The net required ellipse is then obtained by the difference of the circle of radius 0.15 mm/N and 0.09 mm/N, as shown in Fig. 2.8c. If this difference yields an ellipse with a negative a_{f_1} or a_{f_2}, the relative CoE distances can be adjusted to lower the value of the shift ellipse.

Step 5: The net ellipse can be further subdivided into two smaller ellipses as shown in Fig. 2.8c. To aid in visualization, the two building block ellipses are chosen to be oriented along the same direction. The sub-ellipses that make up the net ellipse must correspond to building block geometry that conforms to the footprint specifications. Furthermore, the members of the building blocks should not overlap with each other. The building block geometry and cross-section parameters are determined in Step 6. Thus, an optimal subdivision can be found by iterating between steps 5 and 6 so that the mechanism geometry is well within the prescribed footprint. In this example, the two sub-ellipses have a_{f_1} = 0.03 mm/N, $a_{f_2} = 0.025\ mm/N$ and $a_{f_1} = 0.12\ mm/N$, $a_{f_2} = 0.035\ mm/N$.

Step 6: The two ellipses obtained by subdividing the net ellipse has n_p of 0.833 and 0.3 respectively. These values are used to determine the geometry variables ($l_{2_{norm}}$ and α) of the dyad from Fig. 2.7a. The dyads were chosen such that their $l_{2_{norm}} = 1$ and α are 57° and 87° respectively. Their cross section and dyad lengths are chosen to match the respective a_{f_1} values based on the parametric

dyad behavior in Section 4. The dyad lengths were found to be 313 mm and 489 mm respectively. The building block geometries are oriented such that their CoEs are placed at $E1$ and $E2$. They were found to fit within the footprint specifications. The input of the first building block is rigidly connected to the fixed port of the second, while the input of the second building block is connected to I_{pm} through a rigid body.

The final mechanism has a circular compliance ellipse ($a_{f_1} = a_{f_2} = 0.15\ mm/N$) and a zero coupling vector.

The presented guidelines are also valid for designing the coupling vector or compliance ellipse separately.

a) *Coupling vector*. To design for a desired coupling vector alone,steps 4 and 5 can be skipped.

b) *Compliance ellipse*. To design for a desired compliance ellipse specification alone, the CoE's of the two building blocks in step 3 can be placed arbitrarily.

Figures 2.9a and b show mechanisms obtained by applying the above guidelines to design for a circular ellipse alone, without any specification on the coupling vector. Figure 2.9 c shows a mechanism with its input at the CoE, without emphasis on its ellipse characteristics.

2.5.3 Parallel Combination of building blocks

In the mechanism in Fig. 2.8, it is seen that the input is surrounded by the mechanism. This makes it difficult to connect it to an actuator for practical applications. Furthermore, it is shown in the Appendix B that CoE for serial concatenations are bound within the footprint of the mechanism. This limits the compliance characteristics that can be obtained by series combination alone. To overcome these limitations it may be advantageous to use parallel combination of building blocks. This leads to

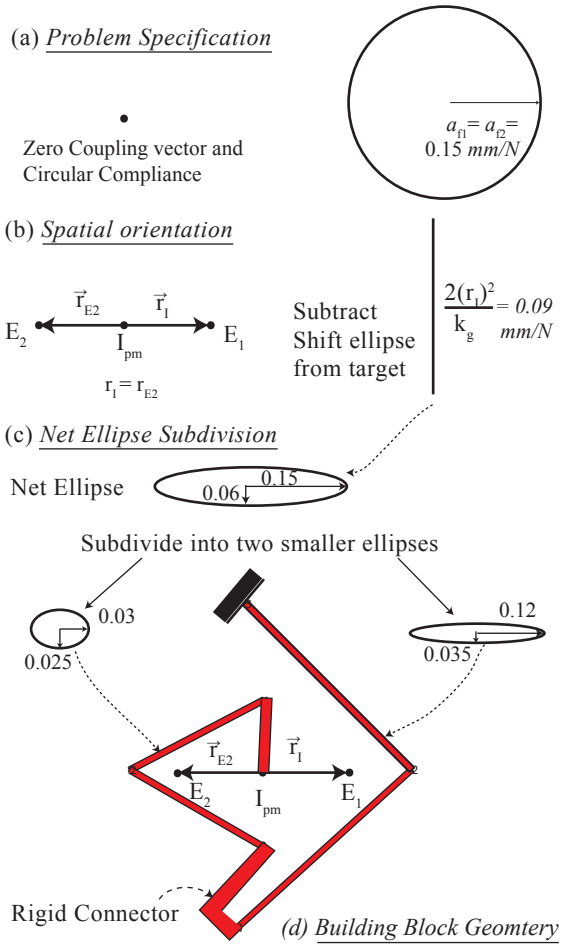

Figure 2.8: Guidelines with an example. (a) Problem Specification in terms of Compliance Ellipse and Coupling vector (b) Choose E1,E2, I_{pm} and evaluate shift ellipse (c) Net ellipse evaluation and subdivision into smaller building block ellipses (d) Design geometry of the two building blocks and their orientation

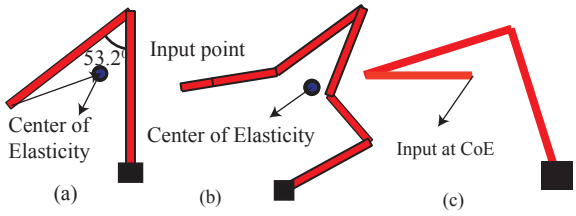

Figure 2.9: Design for a circular compliance ellipse (a and b), and zero coupling vector (c) alone.

robust designs, reducing the sensitivity of the compliance characteristics on geometry and manufacturing errors (*Awtar* (2004)). Furthermore, during parallel combination, the two building block ellipses and coupling vectors combine without the need for shift ellipses and vectors. This makes parallel combination easy to implement.

The input and the COE is desired to be placed at a more accessible position retaining the circular compliance. These specifications stem from the design of a vision-based force sensor for micro-manipulation purposes (*Cappelleri* (2008), *Cappelleri et al.* (2010)). It is further desired to accommodate a rigid probe at the input of the mechanism for manipulation purposes. As shown in Figure 2.6 the stiffness coupling vectors and the compliance ellipses add upon parallel combination. Furthermore, if the symmetric halves have circular compliance, the orientation of the stiffness coupling vectors given by Eq. 2.7 becomes equal to the orientation of the compliance coupling vectors, i.e., $\gamma = 0^\circ$. Thus it is desired to use two symmetric building blocks, each having circular compliance as shown in Fig.2.10 a. These symmetric halves are oriented such that their coupling vectors make an angle with the horizontal. From the addition of coupling vectors shown in Fig. 2.10 b, the resultant coupling vector (and thus the CoE) of the mechanism is at some vertical distance from the input. A rigid pointer can thus be connected from the mechanism to its CoE as shown in Fig. 2.10 d. Note that the net stiffness ellipse of the mechanism will be a sum of the individual building block ellipses.

2.6 Discussion

Characterization of stiffness or compliance at a single point of interest in a compliant mechanism consists of specifying a direction of maximum stiffness (constraint), direction of maximum flexibility (freedom) and quantifying the coupling between translation and rotation for any applied force. The chapter presents a unique graphical characterization to denote the above quantities by representing the force-displacement

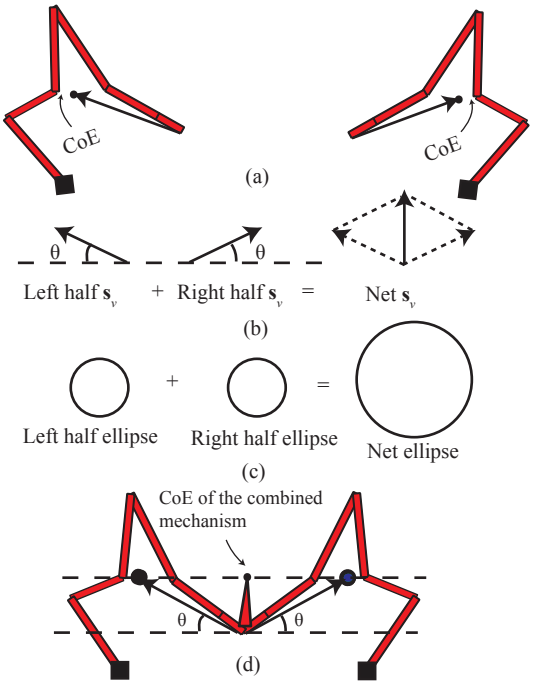

Figure 2.10: Parallel Combination (a) Two symmetric halves (b) Addition of Stiffness Coupling Vectors (c) Addition of Stiffness ellipses (d) Final mechanism with a rigid probe

relationship at a point by a compliance ellipse (specifying constraint and freedom) and a coupling vector (specifying coupling between rotation and translation) obtained from eigen-twist and eigen-wrench characterization of 2-D complaint members. The parameters that are obtained from this characterization form a natural representation of the governing behavior for concatenation. Series and parallel concatenation can be represented by addition of ellipses and vectors, thus providing graphical insight. Furthermore, the graphical approach introduced in this chapter aids in better visualization than 3-D stiffness ellipsoids, as they have a direct co-relation to the building block geometry and eliminate the need for normalizing lengths.

The graphical characterization along with the addition of stress constraints enables realizing practical designs by eliminating topologies unfavorable to the required stress and footprint considerations.These methods enable generation of quick alternate topologies to populate the database of acceptable solutions. This is one of the

greatest advantages of the this method over more computationally intensive techniques. Furthermore the insight obtained on the bounds of the center of elasticity (see Appendix B) for a given topology further enhances the usefulness of this method. The usefulness of this methodology has been demonstrated by a practical vision-based force sensor application having equal stiffness in the X and Y direction with decoupled translation and rotation.

The chapter deals with beam based compliant dyads as building blocks. The parametric analysis of Fig. 2.7 reveals that this simple dyad spans a wide space of eigen-twist and eigen-wrench parameters and is thus an excellent candidate as a building block. Furthermore the design methodology is not building block specific and can be applied to simpler building blocks like beams, and more complex curved building blocks.

2.7 Conclusions

The chapter highlights the use of eigen-twist and eigen-wrench characterization towards series and parallel combination of 2-D compliant building blocks. Some of the important findings of the chapter are summarized below

Main Contributions

1. Representation of 2-D 3×3 compliance(or stiffness) matrix as an ellipse signifying the translational compliance and a coupling vector signifying the coupling between rotational and translational compliances.

2. Emphasis on a unique point known as center of elasticity where translational and rotational compliances are decoupled.

3. Representation of series (or parallel) building block concatenation as addition of individual building block compliance (or stiffness) ellipse and coupling vectors.

4. A bound on the location of the Center of Elasticity within the footprint for a mechanism obtained by a series combination of a number of infinitesimal beams.

5. Ability to obtain a practical topology for a given footprint and stress considerations by following the proposed design guidelines.

2.8 Appendix A

Statement: The Center of elasticity for a 2-D member obtained by a series combination of a number of beams (however small) lies within the foot-print of the mechanism. : Any mechanism as shown in Fig. 2.11a can be divided into a number of straight beams of equal length l. The fixed point of the mechanism, from the point of input can be expressed as a vector sum of all the vectors of length l that make up the mechanism as shown in Fig. 2.11b.

$$L_{mech} = \sum_{k=1}^{N} l e^{i\theta_k} \tag{2.23}$$

Each beam of length l has a coupling vector which has the same orientation as the beam itself. The magnitude of the resultant coupling vector for the m^{th} beam is given by

$$N_m = l(\frac{1}{2k_{gm}} + \sum_{j=1}^{m-1} \frac{1}{k_{gj}})e^{i\theta_m} \tag{2.24}$$

The resultant coupling vector for the m^{th} beam is the vector sum of its actual coupling vector (r_E/k_g or $l/2k_g$) and the change in input point, which in case of a beam is its length l by the rotational stiffness of the building block that it is added into (i.e.$\sum_{j=1..(m-1)} 1/k_{gm}$). To obtain the resultant center of elasticity, the vector sum of all the coupling vectors is divided by the reciprocal of the resultant rotational

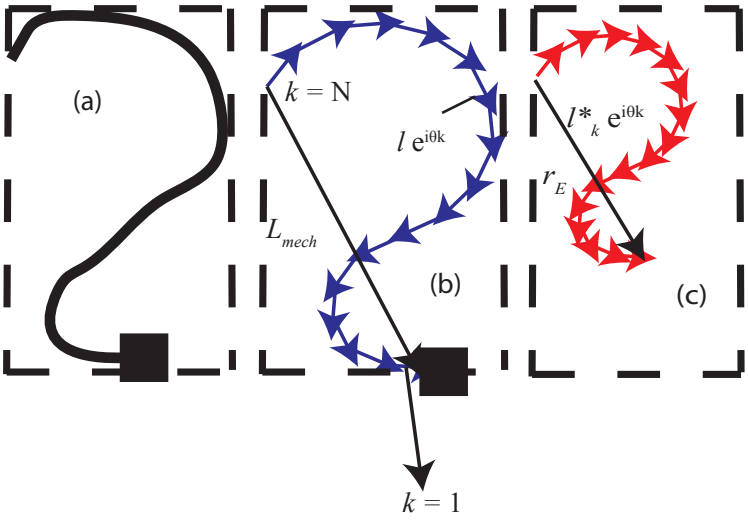

Figure 2.11: The Center of elasticity of any mechanism due to a series combination of building blocks will always lie within its footprint. (a) Entire mechanism (b) Mechanism divided into a number of beams of length l (c) Curve traced by the Coupling vectors, which define the position of the center of elasticity.

stiffness.

$$r_E = \sum_{m=1}^{N} \frac{l(1/2k_{gm} + \sum_{j=1}^{i-1} 1/k_{gj})e^{i\theta_m}}{\sum_{k=1}^{N} 1/k_{gk}} \qquad \Rightarrow \sum_{m=1}^{N} l_m^* e^{i\theta_m} \tag{2.25}$$

Thus the coupling vector traces a curve similar to the actual mechanism, with each elemental length of the mechanism l, mapped to a length l_k^* for k=1...N. It is sufficient for us to prove that for any $1 <= k <= N$, $l_k^* <= l$. This means that the curve traced by the coupling vectors is contained within the geometry. This means that the center of elasticity has to lie within the footprint of the mechanism.

$$\begin{aligned} l_k^* &= \frac{l(1/2k_{gk} + \sum_{j=1}^{k-1} 1/k_{gj})}{\sum_{m=1}^{N} 1/k_{gm}} \\ \sum_{m=1}^{N} \frac{1}{k_{gm}} &= \sum_{m=1}^{k-1} \frac{1}{k_{gm}} + \frac{1}{2k_{gk}} + \frac{1}{2k_{gk}} + \sum_{m=k-1}^{N} \frac{1}{k_{gm}} \\ \sum_{m=1}^{N} \frac{1}{k_{gm}} &\geq (\frac{1}{2k_{gk}} + \sum_{j=1}^{k-1} \frac{1}{k_{gj}}) \end{aligned} \tag{2.26}$$

The above equation means that the numerator is less than the denominator and thus $l_k^* \leq l$. Because each segment length comprising the location of the center of elasticity is shorter than l, the center of elasticity must lie within the footprint of the mechanism.

CHAPTER III

Multi-Port Compliance Representation using Load Flow Visualization

Visualizing load flow aids in conceptual design synthesis of machine components. This chapter presents a mathematical framework to visualize load flow in compliant mechanisms. This framework uses the concept of transferred forces to quantify load flow from input to the output of a compliant mechanism. The key contribution of this chapter is the identification a fundamental building block known as the Load-Transmitter Constraint (LTC) set, which enables load flow in a particular direction. The transferred force in each LTC set is shown to be independent of successive LTC sets that are attached to it. This enables a continuous visualization of load flow from the input to the output. Furthermore, load flow is mathematically related with the deformation behavior of the mechanism. The deformation behavior of a number of compliant mechanisms from literature are explained by identifying its LTC sets to visualize load flow. This understanding inspires a systematic building block based design methodology.

3.1 Introduction

This chapter introduces the concept of load flow visualization to represent compliant mechanism behavior. The hypothesis is that deformation of compliant mechanisms can be comprehended as an action of forces and moments that flow through the mechanism topology. This is motivated by the role of load flow visualization in conceptual design and evaluation of structures and mechanisms (*Skakoon* (2008), *Ullman* (2002; 2003)). Furthermore, it has been argued that computer aided design using topology optimization techniques for stiff structures entails the identification of a path taken by applied forces to flow from the input to the fixed ends (*Suzuki and Kikuchi* (1991)). Just as in structures, compliant mechanisms are also deemed to be dependent on an optimal load path as investigated by **?**. However, until recently the mechanics of load flow in structures were not described mathematically, precluding systematic implementation in design synthesis. This is because unlike stress, load flow is not a physical state of the material. The main aim of this chapter is to evaluate load flow in existing compliant mechanisms and to correlate it with mechanism topology and deformation. The contribution of each member that makes up the overall mechanism can then be comprehended based on load flow.

This chapter is organized into the following sections. In Section 3.2, reviews the mathematical formulations of load flow in literature, and defines the concept of transferred forces as a physical interpretation of load flow. This leads to the definition of Load Transfer Matrix to relate the input and transferred loads. Section 3.3 identifies two explicit members that influence load flow, namely a *Load Transmitter* member that transmits load and a *Constraint* member; together they constitute a *Load-Transmitter Constraint* (LTC) set. One LTC set is proved to be independent of the subsequent sets, thus enabling modular analysis of compliant mechanisms by LTC set decomposition. Section 3.4 derives the elements of the Load Transfer matrix for the simplest LTC set, i.e. a compliant dyad. In Section 3.5, the geometric insight

obtained from examining the dyad LTC set is extended for mechanisms composed of a number of dyad LTC sets, enabling a continuous visualization of load flow. Section 6 examines some compliant mechanisms reported in literature and show that they are made up of a number of LTC sets. Finally, we conclude by summarizing the major contributions of the chapter.

3.2 Quantifying Load Flow in Compliant Mechanisms

In this section we provide a mathematical framework to define and evaluate load flow from the fundamentals of mechanics. Towards this, we review existing formulations in literature that highlight aspects of load flow. The earliest available visualization of load flow in a structure was to follow the trajectory taken by the principal stresses from the point of force application along the continuum topology (*Chong and Boresi* (2000)). However it is argued that the state of stress or internal reaction forces do not accurately represent load transmission (*Harasaki and Arora* (2001a)). Concepts from fluid flow visualization, where the principle of equilibrium was used to balance forces acting along a hypothetical force "stream tube" (*Kelly and Tosh* (2000)) have been used. Another effective method used by *Harasaki and Arora* (2001a) was the concept of transferred and potential transferred forces used to predict the contribution of each element towards load transfer from input to fixed supports in structures. This formulation was used to supplement topology optimization techniques in obtaining feasible solutions (*Harasaki and Arora* (2001b)). Yet another formulation introduced by *Hoshino et al.* (2003) aimed at plotting the change in compliance at each point of the structure by fixing the point under consideration. All the techniques mentioned above have been used only to post-process Finite Element Analysis of designed structures, and not for systematic conceptual design synthesis. *Marhadi and Vekataraman* (2009) in their comparison of these formulations conclude that there is no one formulation that can claim to completely represent load flow.

In this chapter the definition of transferred and potentially transferred forces (*Harasaki and Arora* (2001a)) is adapted for compliant mechanisms, owing to their simplicity and ability to provide insight. Towards this we define the Load Transfer Matrix as shown below.

Load Transfer Matrix

Consider a mechanism shown in Fig. 3.1a with a distinct input and output port. The relationship between the displacements and forces for such a mechanism is captured by the compliance matrix.

$$\begin{bmatrix} \mathbf{u}_{in} \\ \mathbf{u}_{out} \end{bmatrix} = \begin{bmatrix} \mathbf{C}_{in} & \mathbf{C}_{in-out} \\ \mathbf{C}_{in-out}^T & \mathbf{C}_{out} \end{bmatrix} \begin{bmatrix} \mathbf{f}_{in} \\ \mathbf{f}_{out} \end{bmatrix} \tag{3.1}$$

where $\mathbf{u_{in}}$ and $\mathbf{f_{in}}$ are the displacements and applied load respectively at the input, and $\mathbf{u_{out}}$ and $\mathbf{f_{out}}$ are the displacements and applied load respectively at the output. We will define load transfer in two steps

Load Step 1 The input is loaded with $\mathbf{f_{in}}$, while the output is unloaded (i.e. $\mathbf{f_{out}} = 0$). Under these conditions the output displacement can be evaluated from Eq. 3.1 as

$$\mathbf{u}_{out} = \mathbf{C}_{in-out}^T \mathbf{f}_{in} \tag{3.2}$$

Load Step 2 The output displacement $\mathbf{u_{out}}$ from Load Step 1 is enforced at the output and the resultant reaction load is evaluated while the input is unloaded ($\mathbf{f}_{in} = 0$)

$$\begin{aligned} \mathbf{u}_{out} &= \mathbf{C}_{out} \tilde{\mathbf{f}}_{out} \\ \tilde{\mathbf{f}}_{out} &= \mathbf{C}_{out}^{-1} \mathbf{u}_{out} \end{aligned} \tag{3.3}$$

where $\tilde{\mathbf{f}}_{out}$ is the reaction force at the output due to the enforced displacement boundary condition. By substituting for $\mathbf{u}_{out}$ in Eq. 3.2 from Eq. 3.3, we obtain

$$\begin{aligned} \tilde{\mathbf{f}}_{out} &= \mathbf{C}_{out}^{-1}\mathbf{C}_{in-out}^{T}\mathbf{f}_{in} \\ \mathbf{T}_L &= \mathbf{C}_{out}^{-1}\mathbf{C}_{in-out}^{T} \end{aligned} \tag{3.4}$$

where $\mathbf{T}_L$ is the Load Transfer (LT) matrix. Note that the output reaction load $\tilde{\mathbf{f}}_{out}$ in Step 2 is the *transferred load* at the output.

Load transfer can be thus defined as the output load that would cause the same output deformation as an applied input load. This is similar to the notion of transferred forces defined in *Harasaki and Arora* (2001a). The relation between this transferred load and the applied load is given by the LT matrix given by Eq. 4.1.

The dimensions of the LT matrix for frame based topologies is 3×3. For such topologies, each node has three degrees of freedom; $-X$ and $-Y$ translation and in-plane rotation θ_z. Each displacement and force vector has dimensions of 3×1 while each compliance matrix term ($\mathbf{C}_{in}$, $\mathbf{C}_{in-out}$, and $\mathbf{C}_{out}$) has dimensions 3×3. In general the LT matrix is asymmetric and thus not amenable to decomposition by eigen values or eigen-twist and eigen-wrench parameters. However, some physical insight may be drawn from various components of the LT matrix.

$$\mathbf{T}_L = \begin{bmatrix} T_{L_{11}} & T_{L_{12}} & T_{L_{13}} \\ T_{L_{21}} & T_{L_{22}} & T_{L_{23}} \\ T_{L_{31}} & T_{L_{32}} & T_{L_{33}} \end{bmatrix} \tag{3.5}$$

The upper left 2×2 part of the LT matrix relates the transferred and input forces. $T_{L_{13}}$ and $T_{L_{23}}$ relates the transferred forces in the X and Y directions respectively to a unit input moment. $T_{L_{31}}$ and $T_{L_{32}}$ relate the transferred moments due to a unit input force in the X and Y direction respectively. The final diagonal term $T_{L_{33}}$ indicates the

amount of output moment transmitted by a unit input moment. In the next section, we will derive some important results that will enable a continuous visualization of load flow through the LT matrix.

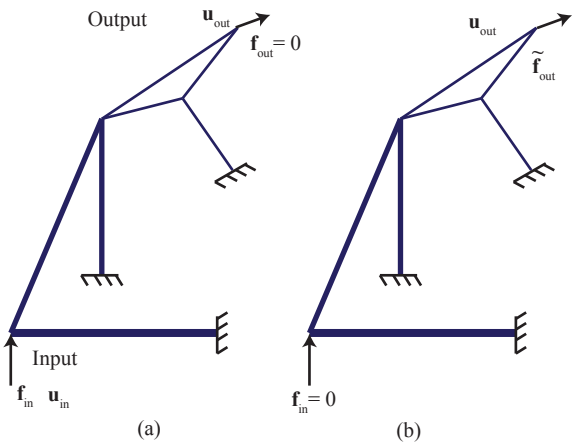

Figure 3.1: Deriving the Load Transfer matrix for Complaint Mechanisms. (a) Output displacement is evaluated for an applied input load (b) Output reaction load is evaluated by enforcing the output displacement from (a) with no input load.

3.3 Load-Transmitter Constraint sets

The LT matrix captures the relationship between the output transferred load and the input applied load. To enable visualization of load flow, we establish an important property of the LT matrix for a simple single-input single-output compliant mechanism. In this chapter, a simple Single input Single output mechanism (*Kim et al.* (2008)) will be decomposed into the three components described below and shown in Fig. 3.2a.

1. *Input Constraint*: This mechanism shown in 3.2b is a single point mechanism that determines the force displacement relationship at the input. Its compliance matrix is given by $\mathbf{C}_i$.

2. *Transmission Mechanism*: This mechanism shown in 3.2c connects the input

port to the output port. The grounded part of the mechanism is connected in series with the input constraint mechanism. Its compliance matrix is denoted by $\mathbf{C}_b$.

3. *Output Constraint*: This (see Fig. 3.2d) determines the stiffness at the output and the direction of motion. Its compliance matrix is denoted by $\mathbf{C}_o$.

It must be noted that all the three compliance matrices $\mathbf{C}_i$, $\mathbf{C}_b$ and $\mathbf{C}_o$ are 3×3 positive definite matrices.

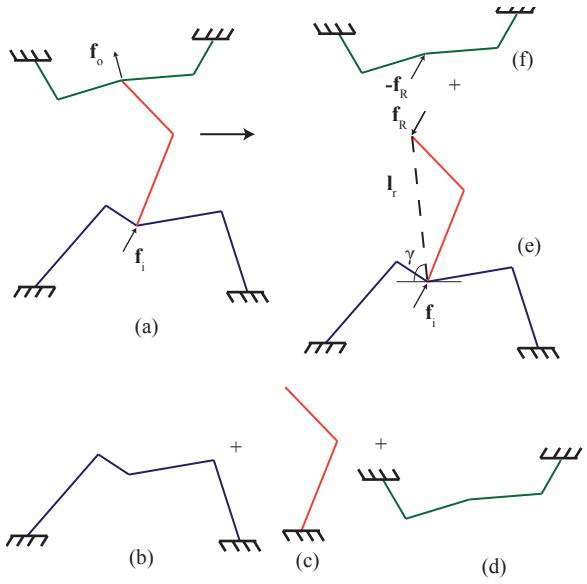

Figure 3.2: (a) A simple single-input single-output compliant mechanism with (b) Input Constraint (c) Intermediate Mechanism and (d) Output Constraint (e) The simple compliant mechanism split into Input constraint together with the intermediate mechanism, and (f) Output Constraint.

We now state and prove an important theorem:

Theorem

The Load Transfer matrix for a simple compliant mechanism is independent of the output constraint $\mathbf{C}_o$.

Consider the simple compliant mechanism shown in Figure 3.2a. An input applied load $\mathbf{f}_i$ produces a displacement at the output. This output displacement can be

evaluated by sectioning the mechanism at the output node as shown in Fig. 3.2e and f. This leads to two mechanisms consisting of

1. Output constraint

2. Input constraint with intermediate mechanism

The internal reaction load $\mathbf{f}_R$ at the output due to sectioning the mechanism can be considered as two equal and opposite applied loads at the output of both the mechanisms. When considering the output constraint mechanism of Fig. 3.2f, the output displacement can be easily evaluated from

$$\mathbf{u}_o = \mathbf{C}_o \mathbf{f}_R \tag{3.6}$$

The mechanisms in Fig. 3.2e and f are connected in parallel at the output and hence have the same displacements. Thus the same output displacement evaluated for the mechanism in Fig. 3.2e involves a linear combination of two terms shown below:

Term 1: Output displacement due to the input force $\mathbf{f}_i$. This can be obtained by the input displacement ($\mathbf{C}_i \mathbf{f}_i$) and a rigid body transformation of this displacement to the output (through the action of l_r and γ).

$$\mathbf{u}_{o1} = \mathbf{Q}^T \mathbf{C}_i \mathbf{f}_i \tag{3.7}$$

$\mathbf{Q}$ is the rigid body transformation matrix as given in Eq. 3.26.

Term 2: Displacement due to the output force $\mathbf{f}_R$. To evaluate this displacement we use the compliance matrix of the output of Fig. 3.2e evaluated in Appendix A.

This matrix is given by Eq. 3.25 as

$$\mathbf{C}_{ib} = \mathbf{C}_b + \mathbf{Q}^T\mathbf{C}_i\mathbf{Q}$$

$$\mathbf{u}_{o2} = \mathbf{C}_{ib}\mathbf{f}_R \tag{3.8}$$

Thus the net output displacement is given by

$$\mathbf{u}_o = \mathbf{Q}^T\mathbf{C}_i\mathbf{f}_i + \mathbf{C}_{ib}\mathbf{f}_R \tag{3.9}$$

From Equations 3.6 and 3.9 we eliminate $\mathbf{f}_R$ to obtain

$$\mathbf{u}_o = \mathbf{Q}^T\mathbf{C}_i\mathbf{f}_i + \mathbf{C}_{ib}\mathbf{C}_o^{-1}\mathbf{u}_o$$

$$\mathbf{u}_o = [\mathbf{I} + \mathbf{C}_{ib}\mathbf{C}_o^{-1}]^{-1}\mathbf{Q}^T\mathbf{C}_i\mathbf{f}_i \tag{3.10}$$

We now invoke Eq. 3.3 where the output transferred load is given in terms of the output compliance of the overall mechanism $\mathbf{C}_{out}$ and the output displacement $\mathbf{u}_o$. Output compliance of the overall mechanism (Fig. 3.2a) is evaluated in Appendix A Eq.3.27 as

$$\mathbf{C}_{out} = [\mathbf{I} + \mathbf{C}_{ib}\mathbf{C}_o^{-1}]^{-1}\mathbf{C}_{ib} \tag{3.11}$$

Thus the final force transformation matrix is given by

$$\mathbf{f}_o = \mathbf{C}_{out}^{-1}\mathbf{u}_o$$

$$\mathbf{f}_o = \mathbf{C}_{ib}^{-1}[\mathbf{I} + \mathbf{C}_{ib}\mathbf{C}_o^{-1}][\mathbf{I} + \mathbf{C}_{ib}\mathbf{C}_o^{-1}]^{-1}\mathbf{Q}^T\mathbf{C}_i\mathbf{f}_i$$

$$\mathbf{f}_o = \mathbf{C}_{ib}^{-1}\mathbf{Q}^T\mathbf{C}_i\mathbf{f}_i \tag{3.12}$$

$$\mathbf{T}_L = \mathbf{C}_{ib}^{-1}\mathbf{Q}^T\mathbf{C}_i \tag{3.13}$$

where $\mathbf{C}_{ib}$ is given by Eq. 3.25. It is seen that Eq.3.13 expresses $\mathbf{T}_L$ in terms inde-

pendent of the output compliance $\mathbf{C}_o$.

QED

From the above theorem, we conclude that the load transfer between the input and the output of a simple compliant mechanism is independent of the output constraints. The only members responsible for transferring load are the input constraint and the intermediate transmitter sub-mechanisms. Together these will be known as *Load-Transmitter Constraint* (LTC) sets. Thus Load-Transmitter Constraint sets can be defined as a series combination of a mechanism that determines the deflection behavior of the input (Constraint) and a mechanism that connects the input to the output such that none of its members are directly grounded (Transmitter). The LTC set is the fundamental building block that transfers load in a simple single-input single-output compliant mechanism. The definition of transferred forces together with the above property of the LT matrix leads to two important observation that aids in visualizing load flow.

- *Observation 1*: An LTC set converts a two-port (input-output) problem into a single port problem at the output. The force applied at the input is transferred to the output by the LTC set. This transferred load can then be considered an applied load at the output. The net stiffness of the mechanism at the output is responsible for determining the value of the output displacement.

- *Observation 2*: Load transfer can potentially take place in a number of stages, each stage representing an LTC set. The transferred force from one stage becomes the input force for the next stage. Load transferred at each stage is independent of the stages that succeed it. This further enables visualization of the load flow path through various stages from the input to the output of the mechanism

Observation 2 can be further explained with respect to Fig. 3.3. Here, the input load

is transferred to the output in two stages, i.e. from point A to point C through point B. In the first stage, load is transferred from A to B. The transferred load at B is independent of beams 3, 4 and 5. For this stage the constraint member is beam 1 and transmitter member is beam 2. The transferred load $\mathbf{f}_B$ now acts as the input load for the next stage. For this stage, the constraint consists of beams 1,2,3 and the transmitter is beam 4. The transferred load at point C is independent of beam 5.

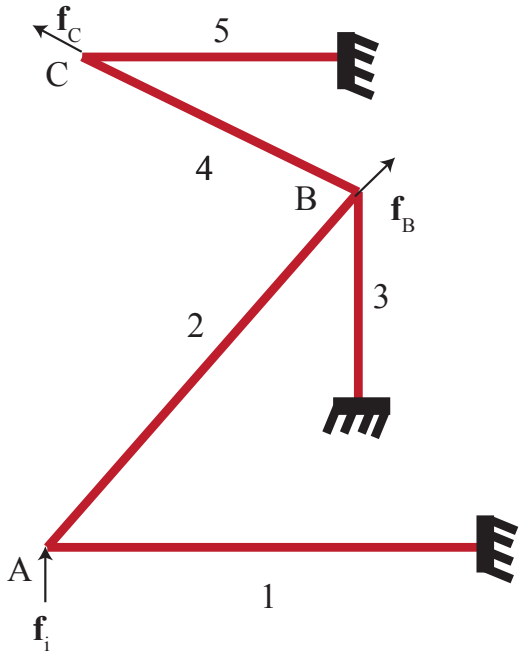

Figure 3.3: A complaint mechanism with two load transfer stages. The input force $\mathbf{f}_i$ is applied at point A. $\mathbf{f}_B$ and $\mathbf{f}_C$ are transferred forces at points B and C respectively

In the above analysis, it has been assumed that the transmitter and constraint sub-mechanisms are composed of compliant members. However, if the transmitter sub-mechanism is rigid, i.e. $\mathbf{C}_b = \mathbf{0}$, then $\mathbf{C}_{ib}$ Eq. 8 becomes

$$\mathbf{C}_{ib} = \mathbf{Q}^T \mathbf{C}_i \mathbf{Q} \tag{3.14}$$

Thus Eq. 3.13 now becomes

$$\mathbf{T}_L = (\mathbf{Q}^T\mathbf{C}_i\mathbf{Q})^{-1}\mathbf{Q}^T\mathbf{C}_i$$
$$\mathbf{T}_L = \mathbf{Q}^{-1} \tag{3.15}$$

Thus, if the transmitter sub-mechanism is rigid, the Load Transfer matrix is independent of the input constraint $\mathbf{C}_i$, and depends only on the geometric orientation of the rigid body.

In the following section, we will look at an elemental LTC set and further consider the above conclusions and their implications.

3.4 A Compliant Dyad as a Load-Transmitter Constraint set

In this section, we will look at the elemental LTC set, i.e. a compliant dyad shown in Fig. 4.2. Its simplicity arises from the fact that constraint and transmitter sub-mechanisms are straight beams. Dyads are well known building blocks for compliant mechanism synthesis (*Kim et al.* (2008),*Krishnan et al.* (2010)). Most mechanism topologies irrespective of their design methodology are observed to be composed of dyads (*Hetrick and Kota* (2003), *Lu and Kota* (2005)). In this section, we will derive analytical expressions for the transferred load of a dyad in terms of its geometry variables. The transferred load will be related to the deformation of the dyad to obtain geometric insight into its behavior.

3.4.1 Evaluating Transferred Load for a Dyad LTC set

The compliant dyad shown in Fig. 4.2, has input at point A and output at point B. As an LTC set, the grounded beam of length l_1 is the constraint, while length l_2 is the transmitter. The ratio of the lengths is $l_{2norm} = l_2/l_1$. The angle between the two beams is α. The ratio between the in-plane thickness for the two beams is given by

$b_r = b_2/b_1$, and the out of plane thickness of the entire dyad is assumed constant. The dyad is modeled using Euler-Bernoulli beams, with its length at least 15 times greater than its thickness. Another valid assumption involves neglecting the compliance of the beams along its axial direction (*Blanding* (1999), *Kim et al.* (2006)). It is thus assumed that any force along the axis of the beam produces no deflection. Energy methods (Castigliano's II theorem) are used to evaluate beam deflections for any applied force. As presented in Section 2, the transferred force can be evaluated in two load steps.

Load Step 1 Force f_{i_y} and m_i is applied at the input and output displacements u_x,u_y and θ are evaluated.

Load Step 2 The above output displacements u_x,u_y and θ is enforced at the output of the dyad, without applying any input force and output reaction forces $\tilde{f}_{o_x}$, $\tilde{f}_{o_y}$ and $\tilde{m}_o$ are evaluated. These reaction forces are the transferred forces at the output.

The obtained expressions are given below

$$\begin{aligned}
\tilde{f}_{o_x} &= cot(\alpha) f_{i_y} - \frac{3(l_{2norm}^2 cos(\alpha) + b_r^3) m_i}{2l_1(l_{2norm} + b_r^3) l_{2norm} sin(\alpha)} \\
\tilde{f}_{o_y} &= f_{i_y} - \frac{3l_{2norm} m_i}{2l_1(b_r^3 + l_{2norm})} \\
\tilde{m}_o &= -\frac{b_r^3 m_i}{2(b_r^3 + l_{2norm})}
\end{aligned} \tag{3.16}$$

The output transferred forces ($\tilde{f}_{o_x}$ and $\tilde{f}_{o_y}$) depends upon the input force and input moment. However, the output transferred moment ($\tilde{m}_o$) is dependent on the input moment alone and its direction is opposite to the input moment. Furthermore, from the above equation, the magnitude of the transferred moment is lower than the applied moment. The direction of the transferred force is given by angle β as shown in

Fig.4.2b.

$$tan(\beta) = \frac{\tilde{f}_{o_y}}{\tilde{f}_{o_x}}$$

$$\beta = \alpha \text{ when } m_i = 0$$

$$\beta = tan^{-1}\left(\frac{tan(\alpha)}{1 + \frac{b_r^3}{l_{2norm}^2 cos(\alpha)}}\right) \text{ when } f_{i_y} = 0 \tag{3.17}$$

When there is no input moment, the output transferred force is along the axial direction of the beam. Furthermore, applied input moments affect the direction of the transferred force. The magnitude of the transferred force when there is no input moment can be given as

$$\tilde{f}_o = \sqrt{cot(\alpha)^2 + 1} f_{i_y} = \frac{f_{i_y}}{sin(\alpha)} \tag{3.18}$$

The magnitude of the transferred output force increases as α decreases. Furthermore, this magnitude is independent of the cross-section or length of each beam, and depends on its orientation alone. All these observations imply that the dyad transfers loads along its stiffest direction, i.e. along the axial direction of the transmitter beam.

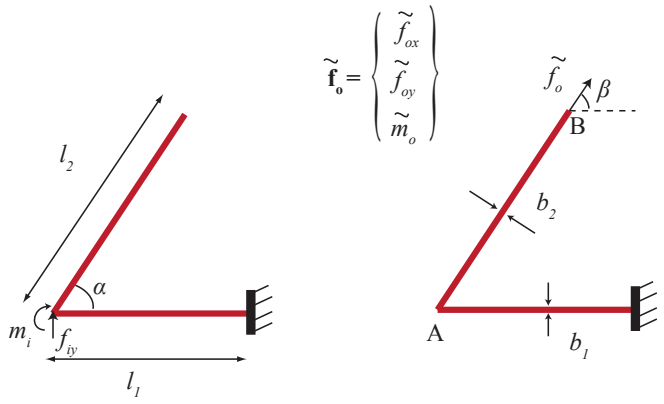

Figure 3.4: (a) Dyad with input force f_{iy} and input moment m_i (b) With output transferred force $\mathbf{f}_o$

The simplicity of dyad LTC sets enables a closed form expression for the transferred load, and provides insight relating it to the dyad geometry. However, if the transmitter sub-mechanism is not a beam, the magnitude and the orientation of the transferred load cannot be determined looking at its geometry. In the next subsection, we will combine the observations of Section 3 together with the derivations of transferred load for a compliant dyad LTC set to reveal geometrical insights about its deformation behavior.

3.4.2 Output Displacement Direction for Dyad LTC sets

In Section 3, transferred load related the input applied load to the output deformation. Output deformation can be evaluated as a single port problem, with the transferred load as an applied load at the output. The magnitude and the direction of the output deformation depends on the stiffness characteristics of the output constraint, which from the conclusions of Section 3 does not affect the transferred load. A natural question is whether any displacement can be obtained at the output by tuning the output constraint. The principles of mechanics dictate that there are only select output displacements that can be obtained. For a dyad, any input force produces a transferred force along the axial direction of the transmitter beam. Treating this as an applied output force and invoking the positive definiteness of the compliance at a point, the possible translation directions lie in a semicircular band $+90^\circ$ - -90° with respect to the direction of the transferred force as shown in Fig. 3.5a. All the possible directions that are contained within this semicircular band is termed as the *Freedom Space*. It is possible to tune the magnitude of the output translation within the directions in the freedom space based on designing a constraint at the output.

The most fundamental single-point constraint frequently seen in mechanisms is a straight beam (see Fig. 3.5b). From the principle of constraint design (**?**) the degree of freedom for a beam is perpendicular to its length for small displacements. The

output displacement of the dyad LTC set is given by the intersection of this degree of freedom line with one of the directions of the semicircular freedom space. This is shown in Fig. 3.5c.

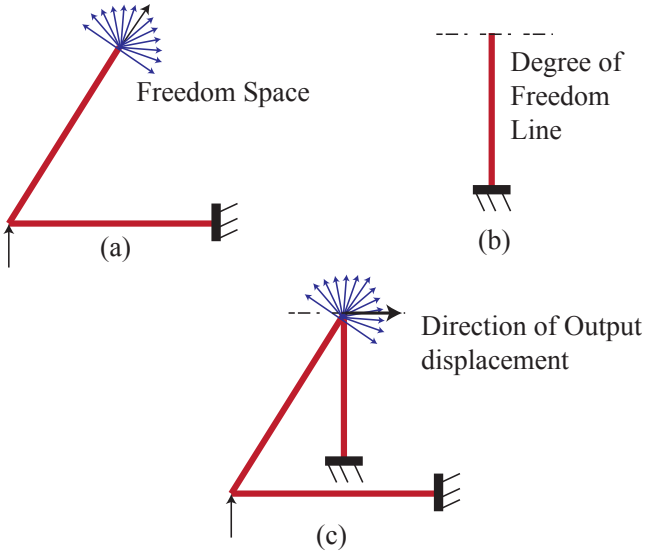

Figure 3.5: (a) The semicircular freedom band denoting the possible directions of output displacements (b) The output beam with its degree of freedom line (c) Direction of output displacement

3.4.3 Output Constraint Beam Orientation: Force Transmission or Motion Amplification

In this section, we will show that the orientation of the output constraints relative to the transmitter beam decides the kinematics of the mechanism. Shown in Fig. 3.6 is an LTC set, with its semicircular band and the output constraint. If the output constraint beam has its freedom line along the direction of the transferred force, the output moves in this direction. This condition shown in Fig. 3.6b is ideal for effectively transmitting force at the output as it has a small deviation angle (*Kim* (2009)). This signifies that the angle between the stiffest direction and the direction of force transmission is small. If the constraint beam has its freedom line close to 90° (or $\zeta \approx 0°$) to the direction of the transferred force, the output translates significantly

relative to the input as shown in Fig. 3.6c. This configuration is used frequently in motion-amplifying stages (*Hetrick and Kota* (2003)). The ratio of the output and input displacement may be given by the method of instant centers (*Kim et al.* (2006)) as shown in Fig. 3.6a.

$$\frac{u_{out}}{u_{in}} = \frac{l_o}{l_i} = \frac{sin(\alpha)}{sin(\zeta)} \tag{3.19}$$

Substituting $\zeta = 90°$ and $\rightarrow 0°$, we get the cases in Figs. 3.6 b and 3.6c respectively for a fixed α.

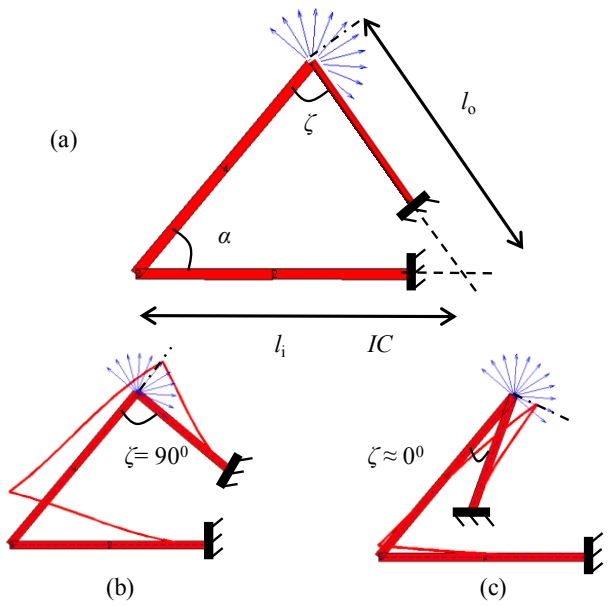

Figure 3.6: (a) An LTC set with an output constraint. The relative displacements between the input and the output can be evaluated using instant centers (b) Configuration that leads to effective force transmission (c) Maximum amplification

3.5 Visualizing Load Flow in Compliant Mechanisms

Geometric insight gained with the dyad LTC sets permits a continuous visualization of load flow within the transmitter beam. A continuous visualization of load flow seen in Fig. 3.7 implies that at each section of the transmitter beam slightly away from point of application of the input force (to avoid local effects), the transferred load is along the direction of transmitter beam and its magnitude is given by Eq. 3.17. In this section, we extend this visualization for a combination of LTC sets.

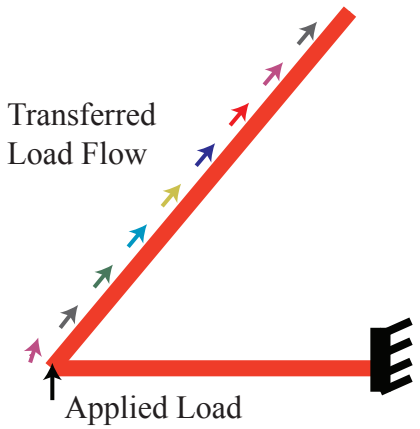

Figure 3.7: Continuous load flow visualization of transferred forces at each section of the transmitter beam.

3.5.1 Combination of LTC sets leads to a load path

One of the chief advantages of representing load flow using transferred forces is that the transferred load at the output of one LTC set becomes the input applied load to the next LTC set as shown in Fig. 3.3. This seamless transition between LTC sets was possible because the transferred load from one LTC set was independent of the successive sub-mechanisms at its output. A similar combination of two LTC sets is shown in Fig. 3.8a, with load flow in the individual LTC sets shown in Fig. 3.8b and c. Load flow in the first LTC set can be visualized along its transmitter beam just as in Figs. 3.7 and 3.8c. The transferred load at its output acts as the applied load at

the input of LTC set 2. Note the constraint for LTC 2 consists of a combination of beams 3 and the entire LTC 1. A simplifying approximation that can ease evaluation of transferred load for LTC 2 is to neglect LTC 1 as a constraint. The approximation is valid as the deformation behavior of LTC 2 is largely dictated by its constraint beam 3, while the stiffness contribution of LTC 1 towards the constraint for LTC 2 can be considered negligible. This approximation can be made when the LTC sets are made of dyads. Thus the transferred load for LTC 2 can be evaluated by Eq. 3.17, and load flow can be visualized along its transmitter beam. The transmitter beams of both the LTC sets together constitutes a load path. Furthermore, the net Load Transfer matrix can be represented as a combination of Load Transfer matrices of the two building blocks as shown

$$\mathbf{T}_{L_{combined}} = \mathbf{T}_{L_1}\mathbf{T}_{L_2} \tag{3.20}$$

where $\mathbf{T}_{L_1}$ and $\mathbf{T}_{L_2}$ are the Load Transfer matrices for LTC 1 and LTC 2 respectively.

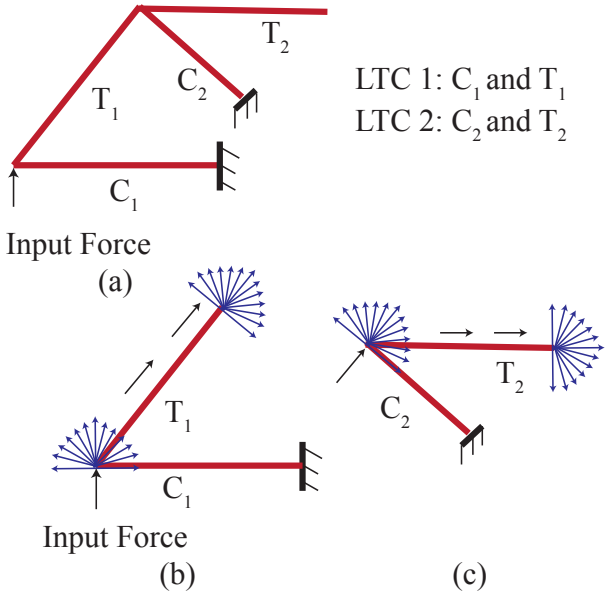

Figure 3.8: (a) Combination of two LTC sets (b) The first LTC set with its constraint band and output freedom band(c) Second LTC set with its constraint band and output freedom band

3.5.2 Bifurcated load paths

A combination of two or more LTC sets connected in series leads to a single load path. A complaint mechanism may consist of two or more independent load paths between the input and output ports. Each of these load paths are comprised of LTC sets. Shown in Fig. 3.9 are simple combination of two load paths. It is possible to derive a relationship between the net transferred load at the output and the input load in terms of the net Load Transfer matrix of individual paths. To enable this we divide the mechanism as shown in Fig. 3.9b and c. The two points along which the input is divided are connected in parallel, which implies that their stiffnesses add and displace by the same amount. The forces acting on these two beams $\mathbf{f}_1$ and $\mathbf{f}_2$ thus readjust so that their combination gives the applied input load $\mathbf{f}_i$.

$$\begin{aligned} \mathbf{f}_1 &= \mathbf{C}_1^{-1}\mathbf{u} \\ \mathbf{f}_2 &= \mathbf{C}_2^{-1}\mathbf{u} \end{aligned} \tag{3.21}$$

Where $\mathbf{C}_1$ and $\mathbf{C}_2$ are the compliance matrices as observed from Figs. 3.9b and c respectively, $\mathbf{u}$ is the displacement of the input. The displacement $\mathbf{u}$ can also be given by

$$\mathbf{u} = \mathbf{C}_I\mathbf{f}_i \tag{3.22}$$

Where $\mathbf{C}_I$ is the combined compliance matrix of the input corresponding to Fig. 3.9a. Combining the above two equations, we obtain

$$\begin{aligned} \mathbf{f}_1 &= \mathbf{C}_1^{-1}\mathbf{C}_I\mathbf{f}_i \\ \mathbf{f}_2 &= \mathbf{C}_2^{-1}\mathbf{C}_I\mathbf{f}_i \end{aligned} \tag{3.23}$$

From the above equation, it is seen that the forces at the input of Figs. 3.9b and c respectively are proportional to their input stiffness. Furthermore from this figure, it

is seen that the two paths from the input to the output can be given as $A - B$ and $C - D$ respectively. Let the LT matrix for path $A - B$ be $\mathbf{T}_{L_1}$ while that for $C - D$ be $\mathbf{T}_{L_2}$. Note that these two paths are independent of each other since each path acts as the output constraint for the other and thus does not affect their respective transferred load. Furthermore from the principle of superposition, the two paths sum up to give the net transferred load at the output given by

$$\begin{aligned} \mathbf{f}_o &= \mathbf{T}_{L_1}\mathbf{f}_1 + \mathbf{T}_{L_2}\mathbf{f}_2 \\ \mathbf{f}_o &= (\mathbf{T}_{L_1}\mathbf{C}_1^{-1} + \mathbf{T}_{L_2}\mathbf{C}_2^{-1})\mathbf{C}_I\mathbf{f}_i \end{aligned} \tag{3.24}$$

Thus, the output transferred load is a linear combination of the loads transferred due to the individual load paths.

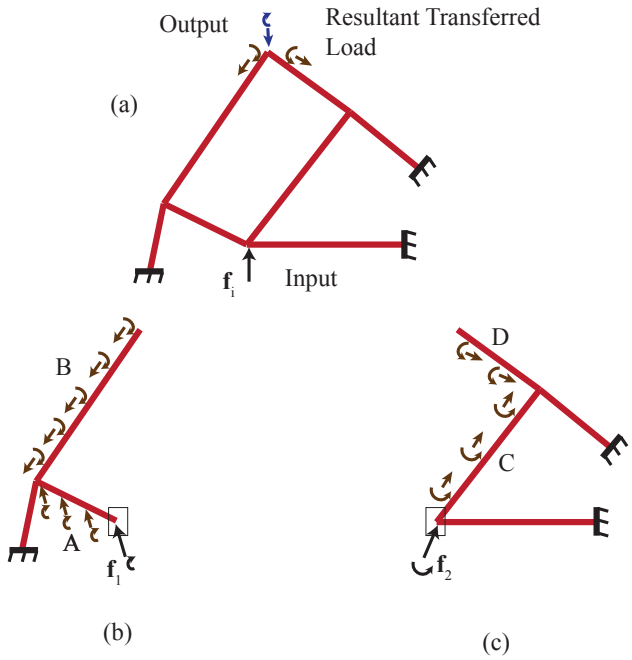

Figure 3.9: Mechanisms with multiple load flow paths (a) Mechanism with input and output. Mechanism is divided to separate two distinct load paths (b) Load flow in one load path (c) Load flow in the other load path.

From this section, it can be concluded that identifying a net load path enables visualization of load flow for both simple and complex topologies. Furthermore, the

deformation behavior of the topology can be understood by analyzing individual LTC sets that make up the net load path. In the next section, we will identify load paths and analyze their deformation behavior for some compliant mechanisms from the literature.

3.6 Identifying LTC sets in existing mechanisms

To identify LTC sets and direction of load flow from input to the output of a mechanism, we follow the guidelines below

1. Identify a net load path: A chain of serially connected line segments that traverses a continuous path from the input to the output is identified as the net load path. These line segments form the transmitters of the LTC sets that make up the mechanism.

2. Identify constraint sub-mechanisms: Along the net load path, constraint sub-mechanisms whose one end is grounded are identified.

3. Group transmitters and constraints into LTC sets and evaluate transferred load for each LTC set: Grouping enables independent analysis of each LTC set. Evaluation of transferred load in each LTC set leads to load flow visualization along its transmitter.

4. Determine deformation behavior for each LTC set: The constraint at the output of each LTC set is identified. This determines the direction of output displacement and the relation between its input and output displacement.

We present some simple examples from the literature whose deformation behavior is explained using the guidelines above.

3.6.1 A Displacement Amplifying Inverter Mechanism I

A displacement amplifying inverter shown in Fig.3.10a is obtained by concatenating a number of dyads in series *Hetrick and Kota* (2003). The mechanism is comprised of two symmetric halves. It is sufficient to analyze one symmetric half to study its deformation behavior. The two halves are connected at the input and the output port.

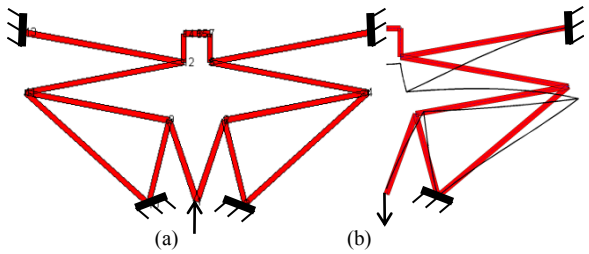

Figure 3.10: (a) The DaCM topology and(c) The deformed profile of the symmetric half

The first stage as indicated earlier is to find a set of continuous line segments from the input to the output. This is the net load path is highlighted in Fig.3.11a by dark lines. The constraints are identified in the same figure as beams from a point in the net load path to the grounded region as $C1$, $C2$, $C3$, $C4$ and $C5$ respectively . Each constraint combines with a transmitter element to form an LTC set (Fig. 3.11c, d, e and f). The first LTC set is constrained by the symmetry boundary condition represented by the vertical roller in Fig. 3.11c. This constraint guides the displacement along the vertical. The direction of the transferred force at the output of LTC set 4 permits displacement within a semicircular band around it shown in Fig. 3.11g. Symmetry constrains the output to move along the vertically downward direction.

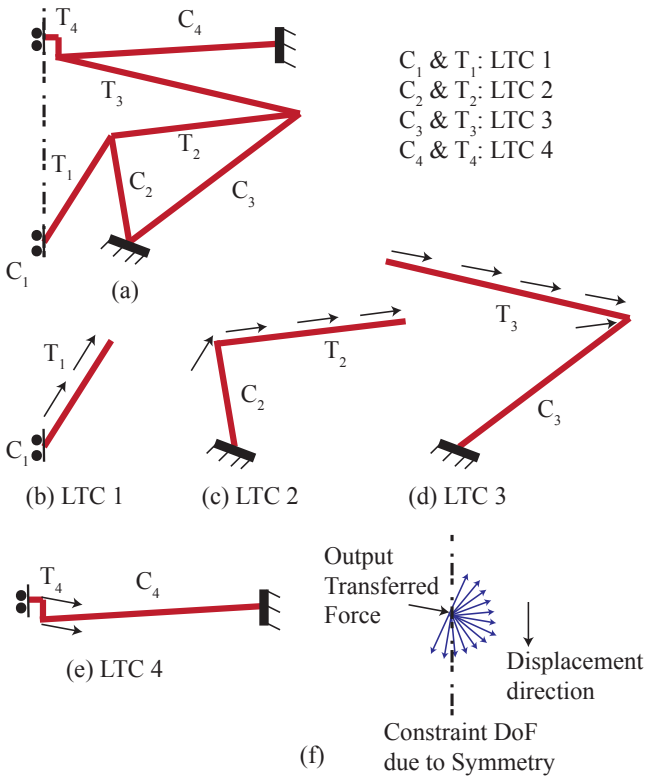

Figure 3.11: Displacement Amplifying Mechanism (*Hetrick and Kota* (2003))(a)Identifying the LTC sets that make up the entire mechanism (b) LTC1, (c) LTC2, (d) LTC3 (e) LTC4 and (g) the direction of the final displacement

3.6.2 A Displacement Amplifying Inverter II

Figure 3.12a shows the topology of a displacement inverter obtained from topology optimization (*Saxena and Ananthasuresh* (2006)). We show that this nontrivial topology is composed of LTC sets. Identifying the net load path and the constraints reveal that the mechanism is composed of three LTC sets shown in Fig. 3.12b, c and d. The overall load flow in the LTC sets is shown in Fig. 3.12e. The output constraint for LTC 3 (i.e. C_4) has its other end connected close to the input. Because the input constraint is stiff, it does not undergo considerable deflection. Thus the other end of C_4 can be considered fixed. Output of LTC set 2 is constrained to move along the vertical while the output of LTC set 3 moves at an angle to the horizontal (see Fig. 3.12f). The motion of the output of LTC set 3 seems to be rotating about the output of LTC set 2. Adding a rigid body (members with larger in-plane thickness) to these two points increases leverage and thus the amplification. The final output is seen in Fig.3.12g.

3.6.3 A Compliant Scissor with flexures

The examples presented above consist of slender beams with dyads as their LTC sets. In the final example we apply the concepts to flexure based mechanisms with lumped compliance. Figure 3.13a shows compliant scissors comprised of rigid links with flexural joints (*http://research.et.byu.edu/llhwww*). For this mechanism, it may not be possible to isolate LTC sets and identify the net load path merely by inspecting its geometry. However, on closer inspection it may be revealed that some of the flexures are constraints while some others are transmitters. Furthermore, the rigid members behave as transmitters. With these guidelines, we isolate LTC sets in the top symmetric half of Fig. 3.13a.

1. LTC 1 consists of rigid link ABC as the transmitter with flexure 1 as the constraint (see Fig. 3.13b). Input load 1 N is applied along the circular hole in

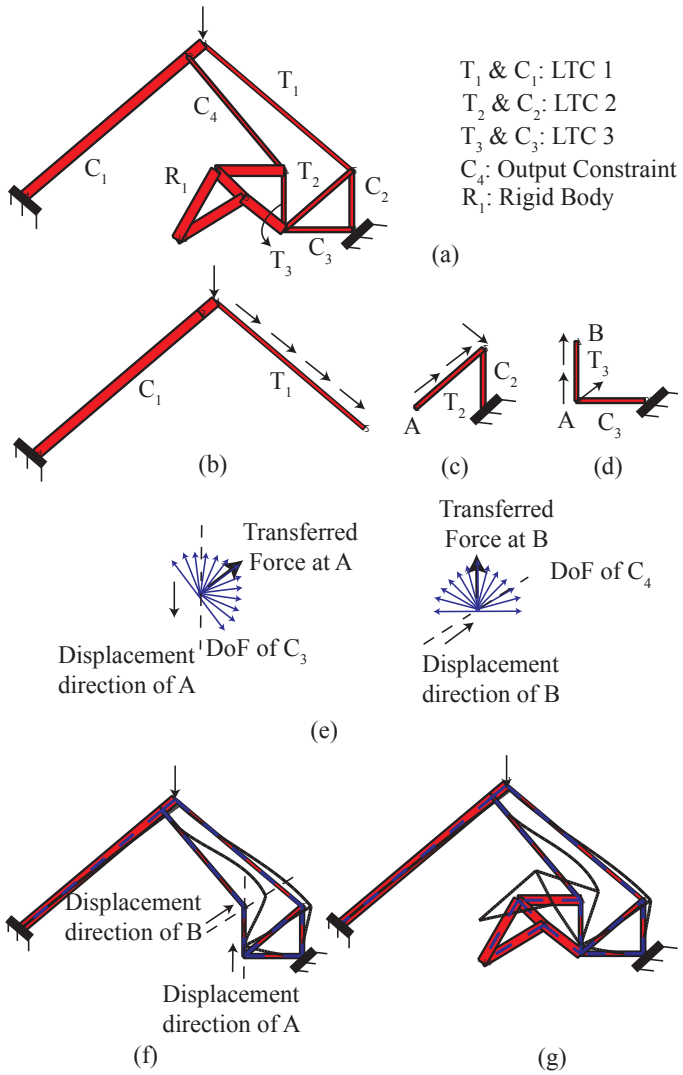

Figure 3.12: (a) A Displacement amplifying compliant mechanism (*Saxena and Ananthasuresh* (2006)) with the LTC sets identified. The direction of load transfer in (b) LTC set 1, (c) LTC set 2 and (d) LTC set 3 (e)direction of displacements at points A and B, (f) deformed profile of the compliant mechanism, (g) rigid leverage amplifies the displacement

the handle. It was seen from Section 3 that load transferred along a rigid transmitter depends upon its geometry and orientation alone. The Load Transfer matrix for such a transmitter was further given by its rigid body transformation matrix $\mathbf{Q}$ given in Eq. 3.26. Thus load transferred at points B and C are

- Point B: $f_{B_x} = 0\ N$, $f_{B_y} = -1\ N$, and $m_B = -1 \times 163 = -163\ N - mm$
- Point C: $f_{C_x} = 0\ N$, $f_{C_y} = -1\ N$, and $m_C = -1 \times 263 = -263\ N - mm$

The rigid body transformation does not change the magnitude and direction of the transferred load, but changes the magnitude of the transferred moment based the distance between the point under consideration and point of application of the moment.

2. LTC 2 consists of the flexure 2 as the transmitter and the entire LTC set 1 as the constraint (see Fig. 3.13c). The direction of motion of the input of this LTC set is dictated by the kinematics of point C. The transferred load at point C now acts as the input load for this LTC set. An ideal flexure would transfer forces along the axial direction alone, without transferring moment. FEA analysis performed to evaluate the transferred loads at point D due to the flexure yielded

   - $f_{D_x} = 1.68\ N$, $f_{D_y} = 0.5\ N$, and $m_D = 3\ N - mm$.

3. LTC 3 (see Fig. 3.13d) consists of the rigid link DEF as the transmitter and flexure 3 with its roller support along with the combinations of LTC 1 and 2 as the constraint. The input load at point D is the transferred load from the previous LTC set. The transferred forces along the entire rigid link, i.e points E and F are the same as point D, while transferred moments depend on the distance between E and F with D. They can thus be evaluated as

- $f_{E_x} = 1.68\ N$, $f_{E_y} = 0.5\ N$, and $m_E = 1.68 \times -60 + 0.5 \times 120 = -40.8\ N - mm$.
- $f_{F_x} = 1.68\ N$, $f_{F_y} = 0.5\ N$, and $m_F = 1.68 \times -30 + 0.5 \times 438 = 168.6\ N - mm$.

The deformed plot for the entire mechanism is shown in Fig. 3.13e.

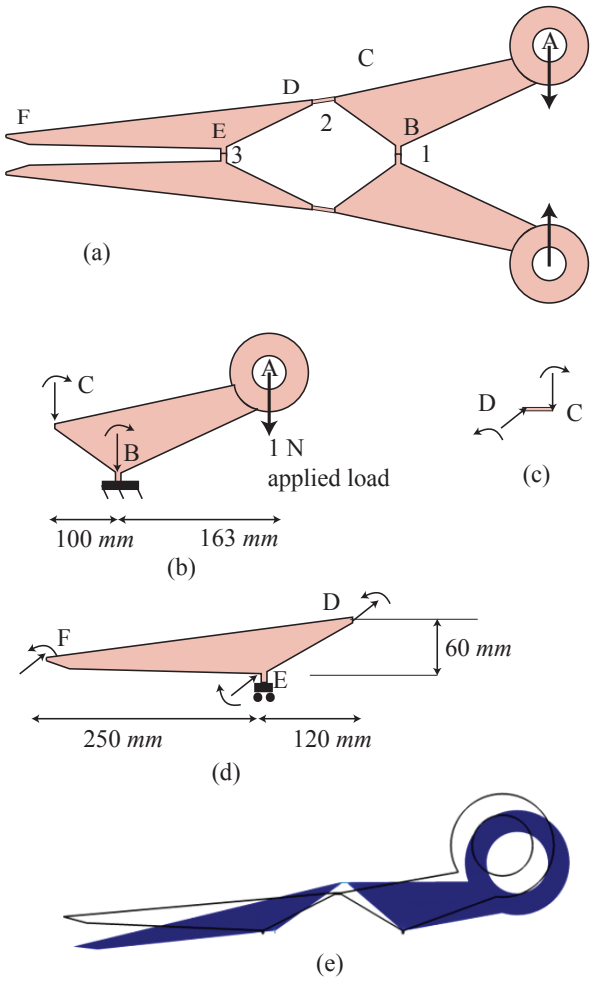

Figure 3.13: (a)Compliant scissors *http://research.et.byu.edu/llhwww*, (b) LTC set 1, (c) LTC set 2, (d) LTC set 3, (e) deformed symmetric half of the mechanism

3.7 Conclusions

In this chapter, we have presented a systematic framework to visualize load flow in compliant mechanisms through the evaluation of transferred forces. Deformation at each point in the mechanism can be evaluated as the effect of this transferred force applied at the point under consideration. Furthermore the transferred force and the deformation produced are deeply rooted in the principle of mechanics without any assumptions. For compliant mechanisms this can be deemed as a natural representation of its deformation behavior just as kinematics represents the behavior of rigid link mechanisms.

To facilitate design it is required to analyze load flow in each sub-mechanism of building block and relate it to the behavior of the overall mechanism. This is enabled by the definition of an LTC set that forms a fundamental building block for load transfer. The load transferred in an LTC set was shown to be independent of the output constraints, and dependent on the input constraints alone. For dyad based LTC sets, this input constraint can be assumed to arise due to its beam constraint alone, neglecting the effects of preceding LTC sets attached at its input. However, this assumption need not be made for mechanisms with flexures and rigid links as the transferred load does not depend on the input or the output constraint (see Eq. 3.15).

Throughout this chapter, we have considered dyad based topologies having distributed compliance and rigid link topologies having lumped compliance due to flexures. In the LTC sets that make up distributed compliance topologies the transmitter element transfers force along its axial direction and does not transfer moments. Rigid link mechanisms however, transfer both forces and moments . This can be seen as a fundamental distinguishing factor seen between transferred forces in distributed and lumped compliance.

Some of the important contributions of the chapter are

1. *Evaluation of Transferred Loads*: A mathematical framework to quantify transferred loads in compliant mechanisms leading to a methodology to evaluate the Load Transfer matrix. This matrix relates the output transferred load to the input applied load.

2. *Insights on Load Transfer Matrix*: The most important among them is the independence of the LT matrix from the output constraints.

3. *Identification of Load-Transmitter constraint sets as fundamental building blocks for load transfer*: This enables a continuous visualization of load flow along the transmitter sub-mechanisms of all LTC sets.

4. *Relating load flow with the mechanism deformation* : Semicircular constraint freedom spaces determine the possible displacement direction at the output, with the actual direction depending on orientation of the constraint.

With the above insights, we were able to explain systematically the mechanism of deformation of compliant mechanisms in literature. Though most of the mechanisms presented had a single net load path made of compliant dyad LTC sets, the method is applicable to a more general building block where the transmitter and constraint elements are not beams. However, we will not be able to intuitively visualize load flow and relate its load path to the topology. At this point, it becomes necessary to evaluate the Load Transfer matrix to obtain the transferred load. Though the entire chapter presents the load flow formulation in a planar 2-D case, all the results are also applicable to generalized 3-D structures and mechanisms.

3.8 Appendix A: Evaluating the compliance matrices for a simple SISO mechanism

In this section, we will derive expressions for the compliance matrices at the input and output of Fig. 3.14, required for the proof in Section 3. These compliance matrices will be expressed in terms of the compliance matrices of the individual sub-mechanisms $\mathbf{C}_i$, $\mathbf{C}_o$, and $\mathbf{C}_b$ shown in Fig. 3.2 b, c and d.

The compliance matrix at the point B in Fig. 3.14a given by $\mathbf{C}_{ib}$ is made up of a series combination of the input ($\mathbf{C}_i$) and intermediate sub-mechanisms ($\mathbf{C}_b$). The resultant compliance matrix is given by

$$\mathbf{C}_{ib} = \mathbf{C}_b + \mathbf{Q}^T \mathbf{C}_i \mathbf{Q} \tag{3.25}$$

where

$$\mathbf{Q} = \begin{bmatrix} 1 & 0 & 0 \\ 0 & 1 & 0 \\ l_r \sin\gamma & l_r \cos\gamma & 1 \end{bmatrix} \tag{3.26}$$

and l_r and γ are the orientation of the point B from the input, as seen in Fig. 3.14a. The compliance matrix at the output point C in Fig.3.14b is formed by a parallel combination of the mechanism in Fig. 3.14a at point B with the output constraint ($\mathbf{C}_o$). In parallel combination, the stiffness matrices add, and thus the resulting compliance at point C is given as

$$\begin{aligned} \mathbf{C}_{out}^{-1} &= \mathbf{C}_o^{-1} + \mathbf{C}_{ib}^{-1} \\ \mathbf{C}_{out}^{-1} &= \mathbf{C}_{ib}^{-1}[\mathbf{I} + \mathbf{C}_{ib}\mathbf{C}_o^{-1}] \\ \mathbf{C}_{out} &= [\mathbf{I} + \mathbf{C}_{ib}\mathbf{C}_o^{-1}]^{-1}\mathbf{C}_{ib} \end{aligned} \tag{3.27}$$

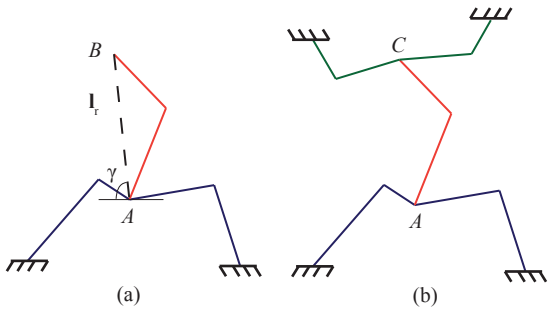

Figure 3.14: Evaluating compliance matrices (a) Compliance matrix at point B is a series combination of the intermediate and input sub-mechanisms (b) Compliance matrix at point C is a parallel combination of mechanism at B and the output sub-mechanism

CHAPTER IV

A Building Block Based Design Methodology for Multi-Port Compliant Mechanism Synthesis

Designers have always conceptualized of load flow as a part of their initial design process for mechanisms and structures. However, the lack of mathematical representation of load flow makes it inappropriate to be included in systematic design processes. Load Transmitter Constraint (LTC) sets provide a mathematical framework for visualizing load paths in compliant mechanisms. In this chapter we propose a systematic design methodology for compliant mechanisms by systematic combination of LTC sets. This enables the designer to conceptualize load flow and choose relevant LTC sets to enforce it. Apart from being intuitive this process gives an understanding of the importance of each member in the mechanism. Furthermore this theory enables accurate and deterministic design for given motion specification without the aid of extensive computation. In this chapter we propose guidelines for the design of mechanisms with a single load flow path and multi load flow path, particularly relevant in shape morphing applications.

4.1 Introduction

Design of mechanisms originate with a conceptual design. This may be the hardest, but is certainly the most creative step in design. Converting the conceptual design to realizable solutions can be systematically accomplished with the aid of analysis tools and optimization softwares. One of the most important tool that aids in conceptual design is the visualization of load path (*Skakoon* (2008), *Ullman* (2002; 2003)). This involves a global, yet simplified view of the path that the applied load takes from the input to the output.In this chapter we seek to obtain guidelines for systematic generation of conceptual compliant mechanism designs using the load path method. Though visualization of the load flow is intuitive for design, there has been no attempt to propose guidelines for systematic synthesis of compliant mechanisms by using this concept. This is because mathematical formulation of load paths have been restricted to post processing of finite element analysis conducted on pre-existing designs (*Marhadi and Vekataraman* (2009)).

The necessity for visualizing load flow and determining optimum load path has been highlighted by *Suzuki and Kikuchi* (1991), and *Lu and Kota* (2005) for structural and compliant mechanism designs, respectively. However there has been very little accomplished towards systematically relating load flow in existing mechanisms and structures to their topologies. In the preceding work (*Krishnan et al.* (2010)), we have taken the first step to systematically visualize load flow in compliant mechanisms from the concept of transferred loads (*Harasaki and Arora* (2001a)). This has beenaccomplished by identifying fundamental building blocks —Load-Transmitter Constraint sets (LTC). The net load path in a compliant mechanism was shown to consist of a number of LTC sets stacked successively.

In this chapter we will propose design guidelines based on characteristics of LTC sets. Key to this method is the conceptualization of load path or the direction along which load is transmitted from the input to output. Geometric guidelines are pro-

vided to indicate all possible orientations of compliant dyad LTC sets that would be applicable towards a given problem specification. The main strength of this methodology is the ability to provide near final designs that have roughly the same stiffness and displacements as the specifications.

In this chapter we propose guidelines for the systematic design of single load path mechanisms and multiple load path mechanisms. Mechanisms with multiple load paths have two or more independent load paths. The findings of this chapter may be used to augment Topology Optimization (*Saxena and Ananthasuresh* (2006), *Ananthasuresh* (1994)) techniques and amenable for analysis using Pseudo-Rigid Body Model (*Howell* (2001)).

The organization of the chapter is as follows. In the next section, we will briefly review the salient features of the Load-Transmitter Constraint sets from (*Krishnan et al.* (2010)). We will then review the eigen-twist and eigen-wrench parameters that provide a basis to describe the overall stiffness behavior of constraints. These are geometrically intrinsic co-ordinate independent parameters that can be used to design the topology of constraints (*Krishnan et al.* (2011)). In Section 3, we will propose systematic guidelines for the design of single load path compliant mechanisms. Section 4 presents systematic guidelines to design multi load path mechanisms with shape-morphing compliant mechanisms as an example. We then conclude with discussions and future work.

4.2 Review of Load Transmitter Constraint Sets

Load Transmitter Constraint sets enable effective visualization of load flow in compliant mechanisms. *Krishnan et al.* (2010) showed with a number of examples that the deformation behavior of existing compliant mechanisms from literature can be explained by the governing principles of LTC sets. In this section, we will review key aspects of these principles that will enable proposing a design methodology for

compliant mechanisms.

4.2.1 transferred load

Consider a mechanism as shown in Fig. 4.1a with two points of interest, i.e. input and output. An input load applied produces an output displacement. The transferred load signifies the load that needs to be applied at the output to obtain the same output displacement. Thus one of the most important aspects of the output transferred load is

- Observation 1: *The transferred load converts an input-output two port problem into a single port problem at the output*

The relation between the output transferred load and input applied load is given in terms of the 6×6 compliance matrix that captures the compliance at the two points as

$$\mathbf{f}_{tr} = \mathbf{C}_{out}^{-1}\mathbf{C}_{in-out}^{T}\mathbf{f}_{in}$$

where $\mathbf{C}_{in}$ and $\mathbf{C}_{out}$ are the compliance matrices at the input and output respectively and $\mathbf{C}_{in-out}$ is the cross diagonal term. An important property of this matrix for a simple compliant mechanism consisting of an input constraint, output constraint and an intermediate mechanism connecting the two is given as follows
"The relationship between the transferred load and input applied load is independent of the output constraints".
Thus in the mechanism shown in Fig. 4.1b the transferred loads are not affected by the output constraint $\mathbf{C}_o$. These lead to two important implications

- Observation 2: *The basic building block the transfers load from input to output consists of two members namely a load transmitter and input constraint collectively known as the Load-Transmitter Constraint (LTC) set.*

- Observation 3: *In mechanisms with a number of LTC sets stacked together, the output transferred load in one LTC set acts as an input load for the other LTC set. This enables a continuous visualization of load flow from the input to the output of the mechanism*

We have shown a number of examples that support the above two statements in DETC 1. Below, we will review the behavior of compliant dyads as Load-Transmitter constraint sets.

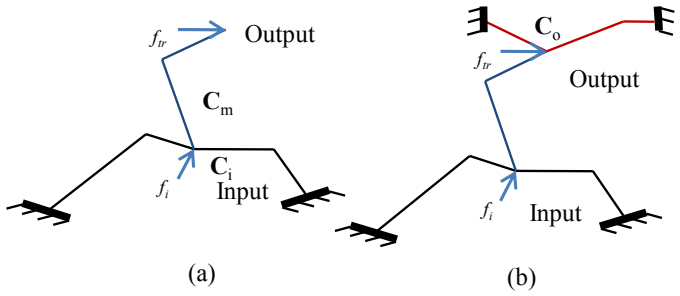

Figure 4.1: (a) A simple compliant mechanism with input and transmitter element (LTC set) (b) with output constraint. It is important to note that f_{tr} is not an applied load but the transferred load at the output.

4.2.2 A Compliant Dyad as an LTC set

The simplest LTC set is a dyad as it contains a single beam as a constraint and yet another beam as a transmitter as shown in Fig.4.2. It is also the most effective and intuitive building block as it transmits load along its axial direction. For an input load having components f_{ix}, f_{iy}, and m_i the output transferred loads are given by

$$\begin{aligned} f_{o_x} &= cot(\alpha) f_{i_y} + \frac{3(l_{2norm}^2 cos(\alpha) + b_r^3) m_i}{2l_1(l_{2norm} + b_r^3) l_{2norm} sin(\alpha)} \\ f_{o_y} &= f_{i_y} + \frac{3l_{2norm} m_i}{2l_1(b_r^3 + l_{2norm})} \\ m_o &= -\frac{b_r^3 m_i}{2(b_r^3 + l_{2norm})} \end{aligned} \tag{4.1}$$

where $l_{2norm} = l_2/l_1$, and $b_r = b_2/b_1$. It is seen from above that when there is no input moment the transferred output force is along the axial orientation of the beam. Furthermore, it is seen that the only components of the force along the $Y-$ direction (the constraint degree of freedom) is transferred as the beam is constrained along the $X-$ direction. With these insights we conclude

- Observation 4: *The dyad LTC takes input forces along its degree of freedom and transmits it along the axial orientation of the transmitter beam*

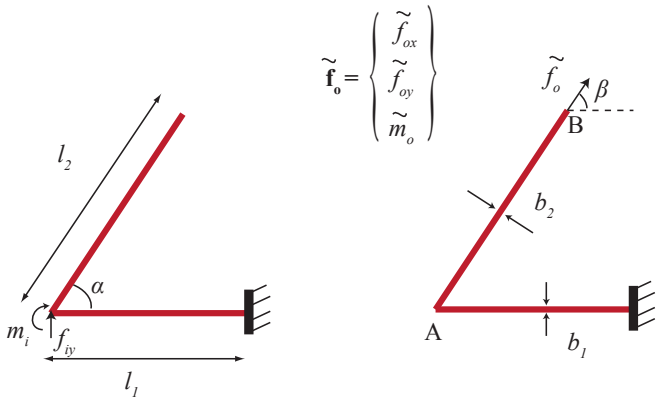

Figure 4.2: (a) Dyad with input force $\mathbf{f}_i$. (b) With output transmitted force $\mathbf{f}_o$

4.2.3 Constraint Bands and Amplification factor

An important aspect of understanding the deformation behavior of compliant mechanisms is relating the load flow to its deformation. At the output of an LTC set where the transferred load acts, the possible displacements that can be achieved is represented by a semicircular band as shown in Fig. 4.3a. This is due to the positive definiteness of the compliance matrix at any single point. The magnitude and direction of displacement are determined by the orientation of the output constraint as seen in Fig. 4.3b. The ratio of the output and input displacements also known as the amplification factor can be expressed in terms of the geometry of the mechanism

as shown below through the instant center method (*Kim et al.* (2006)).

$$\frac{u_{out}}{u_{in}} = \frac{sin(\alpha)}{sin(\zeta)} \tag{4.2}$$

These observations can be summarized as below

- Observation 5: *The possible displacements that can be obtained at the output is determined by a semicircular band centered around the transferred force. The actual output displacement and kinematics is dependent on the output constraint*

We will use all the above italicized observations towards proposing guidelines for synthesis of mechanisms. It was pointed out earlier in the section that the transferred load converted a two-port problem to a single port problem. This means that to obtain a specified translation and rotation at the output, we require to design a single point constraint mechanism that acted against the transferred load to obtain the required displacement. In the next section we present a very brief review of specifying stiffness and compliance as eigen-twist and eigen-wrench parameters.

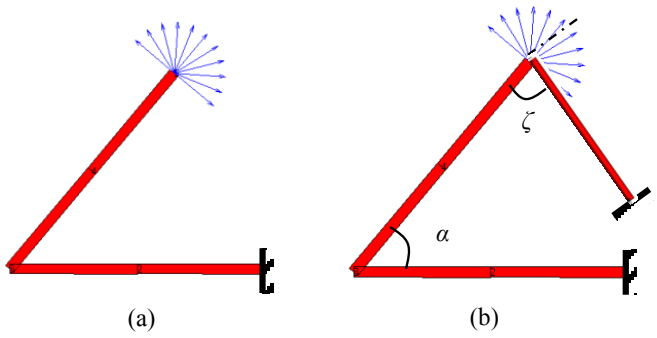

Figure 4.3: (a) Dyad LTC with its semi circular band (b) Output constraint beam defines its output displacement

4.2.4 Expressing Compliance and stiffness as eigen-twist and eigen-wrench parameters

Compliance at a single point in 2-D can be represented as a 3×3 positive definite matrix. This matrix consists of two translational compliances, one rotational compliance and the coupling between translational and rotational compliances. These terms have been successfully represented in a co-ordinate independent geometrically intrinsic framework with the use of eigen-twist and eigen wrench parameters (*Krishnan et al.* (2011)) explained below.

The terms in the eigen-twist and eigen-wrench characterization can be summarized with respect to Fig. 4.4 as:

a) *Translational Compliance*: Given by a_{f_1} and a_{f_2}, these eigen-compliance parameters depict the maximum compliance magnitudes and direction for pure translation, at the center of elasticity. The quantity a_{f_1} is the primary compliance direction as observed from the center of elasticity. We denote $n_p = a_{f_2}/a_{f_1}$. This quantity denotes the cross axis compliance.δ is the orientation of the semi-major axis of the ellipse (a_{f_1}) with respect to the horizontal. This angle can be changed by rotating the dyad about the Z axis.

b) *Eigen-rotational Stiffness* (k_g) : This gives the reaction moment produced by a pure unit rotation at the center of elasticity.

c) *Center of elasticity*: Its distance (r_E) and orientation (β) with respect to the point of input indicates the coupling that exists between rotational and translational parameters. It must be noted that β is the orientation of the center of elasticity from the input with respect to the a_{f_1} axis. If the dyad is oriented such that $\delta = 0$, the β is the orientation of r_E with respect to the horizontal.

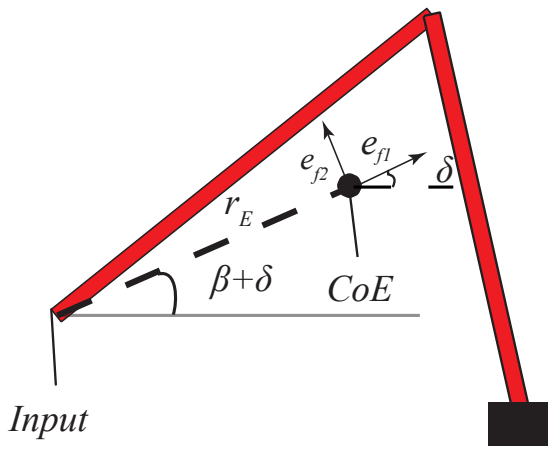

Figure 4.4: Eigen-twist and Eigen-wrench parameters for a particular building block geometry.

4.3 Single Load Path Mechanisms: Guidelines for Synthesis

In this section, we will propose guidelines for systematic synthesis of single load path compliant mechanisms from the observations in the first section. The design methodology stems from a continuous visualization of load flow in the transmission elements of the mechanism. The path taken by the load flow can be related to the topology of the transmission elements. Whenever there is a change in the direction of load flow , there has to be a constraint enforcing it. Furthermore the constraints determine the direction of displacement of each point in the mechanism. Thus each mechanism can be thought of as a combination of Load-Transmitter Constraint sets; its topology determined from a combination of load flow visualization (Transmitter) and displacement specification (Constraints). The guidelines can be summarized by the following steps.

1. *Determine the possible direction of transferred forces at the output and displacement direction at the input.*

2. *Determine the number of LTC building blocks based on required amplification factor.*

3. *Design the topology of transmitter elements connecting the input to the output.*

4. *Conceptualize the direction of load flow in each transmitter beams.*

5. *Determine the acceptable range of constraint orientations to enforce the required load flow directions.*

6. *Design input constraint to obtain the exact input behavior.*

7. *Design the output constraint to match the required value.*

We will now explain the above guidelines based on the observations of Section 2. Figure 4.7-4.9 shows the systematic flow of these guidelines for an example detailed later in the section.

4.3.1 Possible Direction of Transferred Forces

Load path connects the input to the output in such a fashion that the input force is transmitted to the output. The magnitude and the direction of the transmitted load must enable the output to move in the required direction. From Section 3, this implies that the transmitted force must lie within a semicircular band centered on the direction of the required output translation. This is seen in Fig. 4.7a as the band SB2. This figure also shows the semicircular band SB1 about the direction of the input force. This implies that the direction of input displacement has to be within this band.

4.3.2 Number of LTC sets

One of the most common guidelines for the design of stiff structures is to have a direct load path with minimum number of parts in between. This is to prevent the slightest displacement along any of the members within the load path. However if a fixed displacement amplification factor between the input and the output is desired, we

need determine the number of building blocks based on this quantity. In section1, we obtained a relation between the orientation of the LTC set and the output constraint and realized that we can reduce chances of buckling and enable easier fabrication if the angles α and ξ are above 20°, which corresponds to an amplification of 2. If n is the number of building blocks to be chosen, we have a relation

$$N_{amp} = 2^n$$
$$n = log(N_{amp})/log(2) + 1 \tag{4.3}$$

In the above equation an additional building block has been added to distribute the amplification better. The above guideline is valid for displacement amplification problems alone. If force transfer is desired more than displacement amplification, we choose a minimum number of building blocks that transfers the input force to the output. This is usually determined by geometry of the problem specification. For the specification in Fig. 4.7a, a single transmitter between the input and the output is not a feasible solution as the transmitter would not carry load in the directions contained by SB2.

4.3.3 Transmitter Topology

The two factors that decide the orientation of the transmitter beams are

1. Transmitter beams transfer loads along their axial direction.

2. The output transferred load has to lie within the band SB2.

Guided by the above two principles the designer has an infinite number of choices to pick the orientation of the transmitter beams. However, a convenient guideline is determined by the direction of the output applied load. In most compliant mechanisms, the output moves against an external load. This external load counters the

transferred load at the output to produce a resultant deformation. The orientation of the output transmitter beam must be such that the direction of the transferred load at the output must be along the beam's axis. The other transmitter beams can be oriented such that all have equal lengths (see Fig. 4.7b)

4.3.4 Load Flow Directions

Once the transmitter beams have been chosen, we have to determine directions of load flow. This direction is fixed for the input transmitter beam as it corresponds to a direction within its semicircular band. Similarly the output transmitter beam transmits load along the direction that corresponds to its semicircular band. However, the direction of load flow in transmission beams can be chosen arbitrarily. If the direction of loading is unidirectional, it is convenient to orient load flow such that the member experiences tension to avoid buckling (see Fig. 4.7c).

4.3.5 Determining Possible Constraint Orientations

Once we have the orientation of transmitter beams, to complete the LTC sets, we require the orientation of the constraints. It was seen earlier that the constraints are essential to ensure the direction of transmission of the load. We do not aim to design for specific stiffness values but only the constraint directions. It must be noted that the direction of constraint is denoted by the direction of its degree of freedom. This is because the constraint such as a compliant beam is stiff in every other direction and flexible only along its degree of freedom. The orientation of the constraint determines the direction of load transmission along the transmitter beam. To ensure the right direction of load transmission as determined at the end of the previous step, we will determine the possible orientation of constraints. Consider Fig. 4.5 where we show two transmitter beams 1 and 2. The first transmitter has a determined direction of load flow. The second transmitter has a required direction of load flow that will

be imposed by the direction of the constraint at point B. The semicircular band at B gives the possible directions of its displacement. A constraint beam whose DOF intersects with this band will allow the required deformation. However, it must be noted that not all directions in the band would lead to the same direction of load transmission for beam 2. This seen in Fig. 4.5 where the constraint forms an LTC set with beam 2. This LTC set is oriented such that the output transferred load at B leads to the opposite direction of load transmission in beam 2. However, it is seen that the constraints in 4.6 permits load transfer along the required direction. Further investigations reveal that the possible set of directions can be obtained by the intersection of the semicircular band at point C with that at point B. Thus, the semicircular bands drawn at each point needs to be replaced with an intersection of itself with the succeeding constraint band. This is shown in Fig. 4.7d.

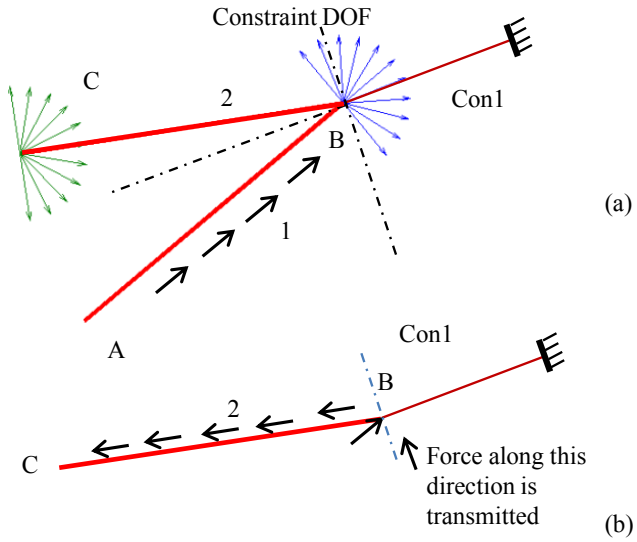

Figure 4.5: Some constraint directions do not transmit load along the required direction (a) Transmitter beams 1 and 2 with a possible constraint Con1 (b) LTC set corresponding to beam 2

Determining the actual constraint orientation depends on the required amplification from each LTC set. Each LTC set along with their output constraints (or the constraint of the successive LTC set) determines its amplification. The net amplification

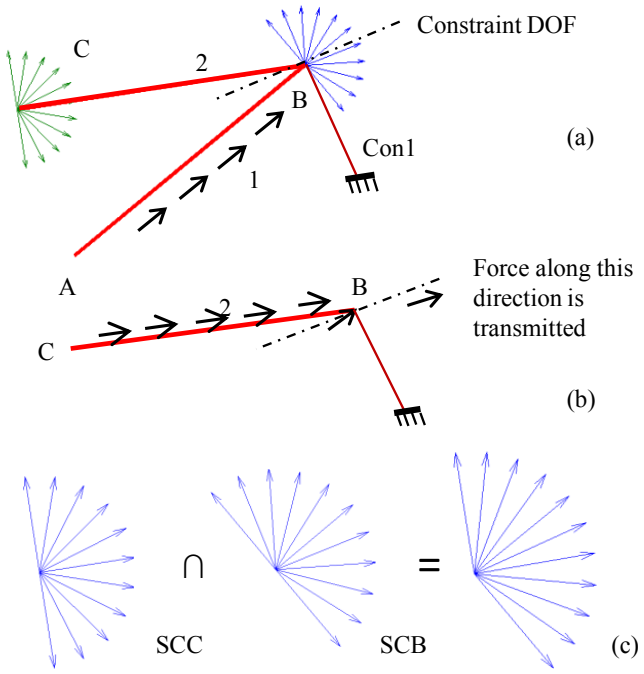

Figure 4.6: Required Constraint orientation (a) Transmitter beams 1 and 2 with a possible constraint Con1 (b) LTC set corresponding to beam 2 showing the transmission direction along beam 2 (c) The constraint DOF must lie within the intersection of the two semicircular bands SCC and SCB

is given by

$$n = \frac{sin(\alpha_1)}{sin(\xi_1)} \times \frac{sin(\alpha_2)}{sin(\xi_2)} \tag{4.4}$$

Furthermore, the input constraint's DOF must coincide with the input displacement direction.

4.3.6 Designing Input constraint

A beam was used as an input constraint to enable the formation of the first LTC set. However further elements need to be added in parallel to this beam in order to obtain the exact displacement characteristics. For example, the input might have to be constrained so that it has no rotation. Towards this it is necessary to add a compliant building block such as a dyad whose stiffness coupling vector cancels out the beam's stiffness coupling vector. This can be seen in Fig. 4.7e.

4.3.7 Determining Dimensions and Designing Output Constraints

So far, we have identified the topology the mechanism that determines its load flow. Furthermore, we have determined the orientation of constraint beams that define the LTC sets. However, the actual dimensions of these beams and an output constraint have to be determined based on the required output displacement. This aspect has been traditionally dealt with as a part of the size and geometry optimization. For a unit input force, we calculate the transferred force at the output. For LTC sets made up of dyads, the transferred force is dependent on the geometry alone. Knowing this force, we can design for the output constraint that gives the desired displacement. The problem specification can now be expressed as a single point synthesis problem, where we design for a required compliance at the output port. A part of the required output stiffness is due to the stiffness of the mechanism as seen at its output. This would correspond to the stiffness of point D in Fig. 4.7d. This stiffness would add in parallel with the stiffness of the constraint to give the net constraint stiffness. To enable design of a constraint, we need to evaluate this stiffness. This is done by associating dimensions and elastic material properties for the whole mechanism. We then evaluate the stiffness at the output in terms of its eigen-twist and eigen-wrench parameters. It is required to obtain the eigen-twist and eigen wrench parameters of an output constraint mechanism that adds with the stiffness at point D to give the

required output displacement. The problem specification can be given by

$$\begin{aligned} \text{Min } v &= (u_x - u_x^*)^2 + (u_y - u_y^*)^2 + (u_\theta - u_\theta^*)^2 \\ \text{w.r.t } \mathbf{X} &= [a_{f_1}, n_p, r_E, k_g, \beta, \delta] \\ \text{s.t.} \begin{Bmatrix} u_x \\ u_y \\ u_\theta \end{Bmatrix} &= (\mathbf{K}_o + \mathbf{K}_c)^{-1}\mathbf{f}_t \\ \mathbf{X}_{lb} &\leq \mathbf{X} \leq \mathbf{X}_{ub} \end{aligned} \tag{4.5}$$

In the above formulation design variable $\mathbf{X}$ is the eigen-twist and eigen-wrench values of the constraint mechanism, $\mathbf{K}_o$ is the stiffness matrix of the output shown in Fig. 4.7e and $\mathbf{K}_c$ is the stiffness matrix of the constraint generated from the design variable $\mathbf{X}$. Optimization in MATLAB was used to obtain the optimum values of the eigen-twist and eigen-wrench characteristics. Infeasible values for the design variables means that the stiffness $\mathbf{K}_o$ is larger than required for to generate the output displacement. In that case, we can decrease the in-plane thickness of the mechanism and evaluate $\mathbf{K}_o$. Once we find the eigen-twist and eigen-wrench parameters for the constraint, we can design it following the instructions laid out in Krishnan et al. (2009). This constraint will now be added in parallel to the output of the mechanism to obtain the final mechanism. Further optimization based refinement can be used to exactly constraint the output and input displacements.

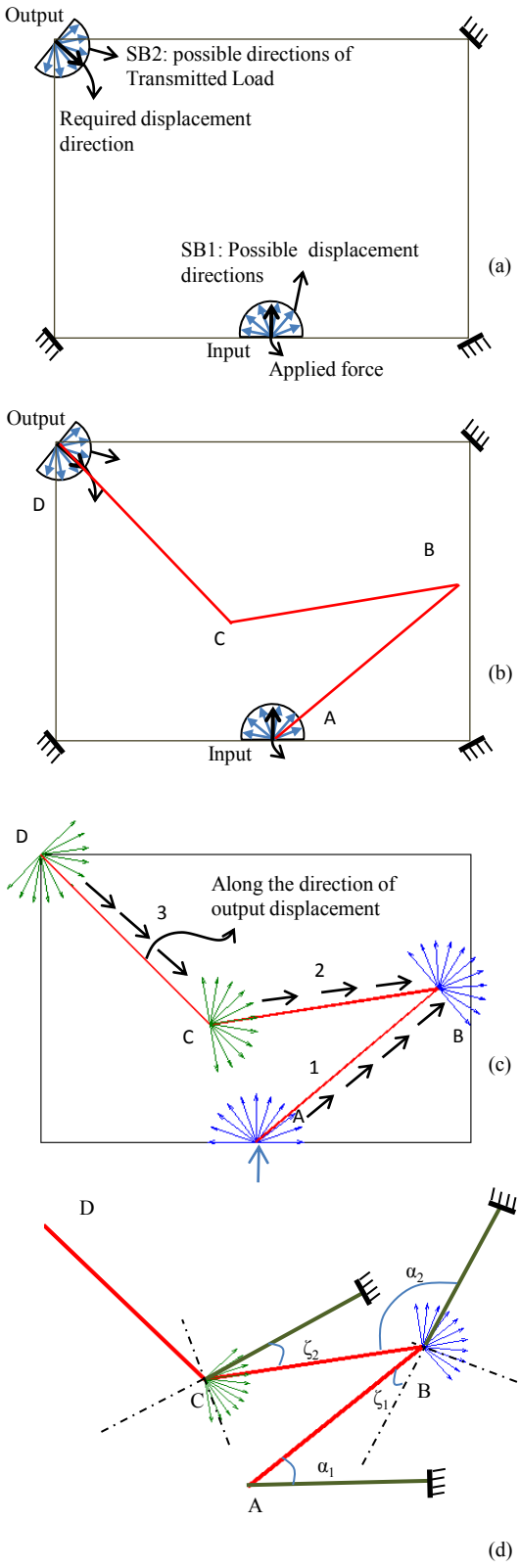

Figure 4.7: Stages in the evolution of the mechanism from specifications to topology (a) Input output specifications with semicircular bands (b) Topology of the transmitter beams (c) Load flow directions in each transmitter beam (d) Truncated bands and constraints that define the LTC sets

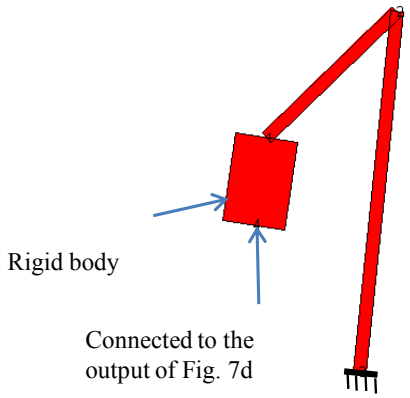

Figure 4.8: Constraint for the output of the mechanism as obtianed from defining the topology to the eigen-twist and eigen-wrench parameters.

4.3.8 Single Load Path: An Example

We will now solve a practical compliant mechanism to demonstrate the utility of the guidelines. The problem can be formulated as

$$\text{Required Output Deformation } \mathbf{u}_{out} = \begin{Bmatrix} 1/\sqrt{(2)}\ mm \\ -1/\sqrt{(2)}\ mm \\ 1^\circ \end{Bmatrix}$$

$$\text{Required Amplification } n = 4$$

$$\text{Required Direction of Input displacement } \mathbf{u}_{in} = 90^\circ$$

$$\text{Required Input Rotation } \theta_{in} = 0$$

$$\text{Direction of the input force } f_{in} = 90^\circ \tag{4.6}$$

One or more of the above specifications need not be specified. In such cases, an arbitrary value or the most intuitive value can be chosen. The specifications are indicated in 4.7a. The transmitter beams that determine the load path is made to lie within the bounding box. Since the amplification required is 4, the number of LTC sets required as given by Eq. 4.3 is 3. The direction of the transmitter beam at

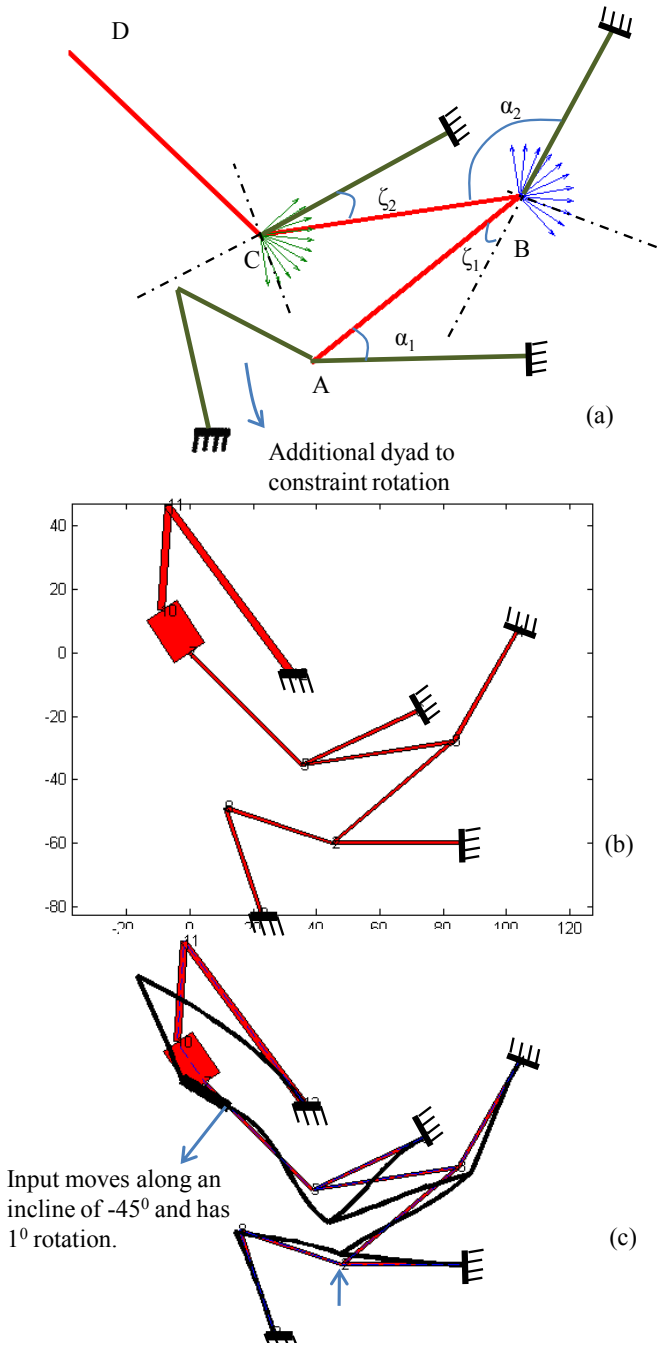

Figure 4.9: Designing input and output constraints (a) Input constraint to prevent input rotation (b) Final mechanism with the output constraints added (c) Deformation under input load

the output can be chosen to be along the same direction as shown in beam 3 in Fig. 4.7b. This maximizes the work done at the output thus maximizing the efficiency. The direction of load flow in the input transmitter beam has to coincide within its semicircular band. Similarly the output transmitter beam transmits load along the direction that corresponds to its semicircular band. This direction of the intermediate beam is chosen such that it is loaded in tension. If the load flow direction indicated is towards the input of the beam, it can be considered to be loaded in tension. This is indicated in Fig. 4.7c. The load path visualization enables choosing constraints that enforce the direction of load flow as explained in the guidelines. They are shown in Fig. 4.7d. The input is further constrained to prevent any rotation under a unit load as shown in Fig. 4.9a. By fixing dimensions and mechanical properties to the mechanism (out of plane thickness =10 mm and Young's Modulus = 200 MPa) we can evaluate the output stiffness and obtain an output constraint by the process explained above. The output constraint obtained is shown in Fig.4.8. When combined in parallel with the designed mechanism we get the final mechanism shown in Fig.4.9b. Its deformed profile is shown in Fig. 4.9c. Preliminary FE analysis using beam elements reveals that the output moved by 0.9 mm (required displacement is 1 mm) at -44° (required value 44°) and output rotation was 0.8° (required 1°). The output was amplified 3.6 times. These results indicate that the methodology was successful in designing a two-port mechanism with the required output displacement. Further shape and geometry refinement can always be used to achieve exact specifications.

4.3.9 A Practical example: An energy storage mechanism for a stapler gun

A stapler gun is a popular consumer product that staples large bundles of paper with minimum user force.This stapler uses a spring and a lever to store the user's gradual input as strain energy, and release it with considerable impact force to perform

the actual stapling operation. The user would be applying a small force over large range, without requiring to provide an impulse during the actual stapling operation (*www.paperpro.com* (2007)). This example aims to design a force transmitting compliant device that can provide mechanical amplification for the stapling operation. The operational stage of this mechanism is as follows

1. In the first step, the input of the mechanism as shown in Fig. 4.10a is deformed by the user applied force. The location of user input from the applied force ensures a force amplification of almost 2.

2. After some prescribed displacement the force handle slips from the input, prompting the entire mechanism to move towards the undeformed configuration. During this step the output hits the staple striker (not shown) with a certain velocity causing the stapling action.

The entire mechanism must fit between a $100mm \times 50mm$ area. A conceptual topology will be first designed for this using the Load Flow techniques. The resulting topology will be associated with practical dimensions in Chapter 5. The steps in conceptual design are illustrated below.

Conceptual Design

Before designing the conceptual topology for this application, the kinematic specifications are laid. Since the problem involves force amplification, the geometric amplification has to be lower than unity. Assuming certain loss in the mechanism due to strain energy (a 70% efficiency), a unit mechanical (or force) amplification can be thought to produce a geometric amplification of at least $n_{amp} = 0.7$. The input force direction is specified in Fig. 4.10a while its displacement direction is left for the user to choose. However, the direction of output displacement is fixed. Input displacement must lie in a semicircular band centered around the input force direction. If the direc-

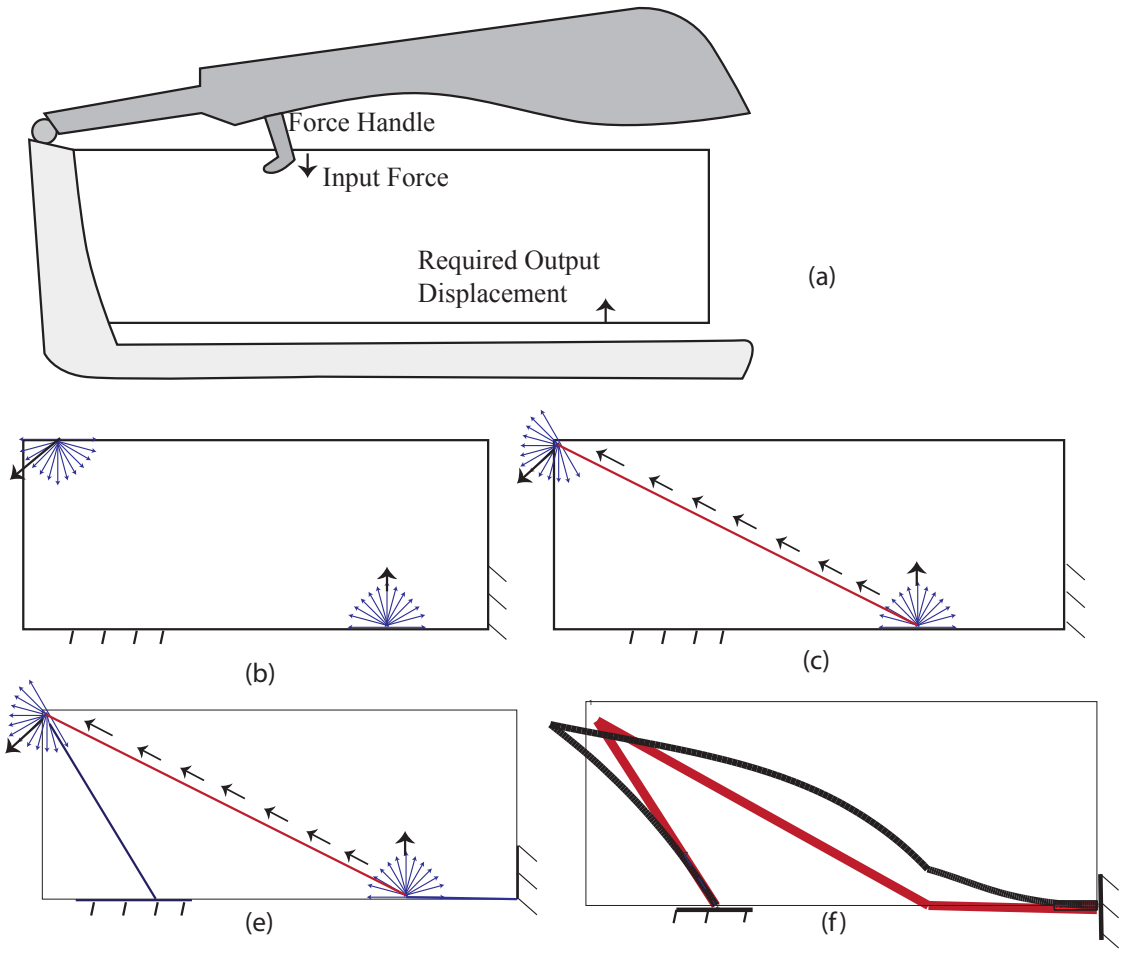

Figure 4.10: Design of a Compliant Force Transmission Mechanism for a stapler gun (a) Stapler gun, actuation lever and footprint within which the mechanism must lie (b) semicircular bands for input and output (c) Input displacement direction and its constraint band (d) Load paths and the corresponding load flow lines (e) Constraints (f) Mechanism with deformed profile.

tion of input displacement and applied force is the same, there is no direct connection possible between the input and the output. Thus the input direction must be chosen such that a semicircular band around it yields the required direct connection between the two ports. It must be noted that this is necessary only for a single load path mechanism.

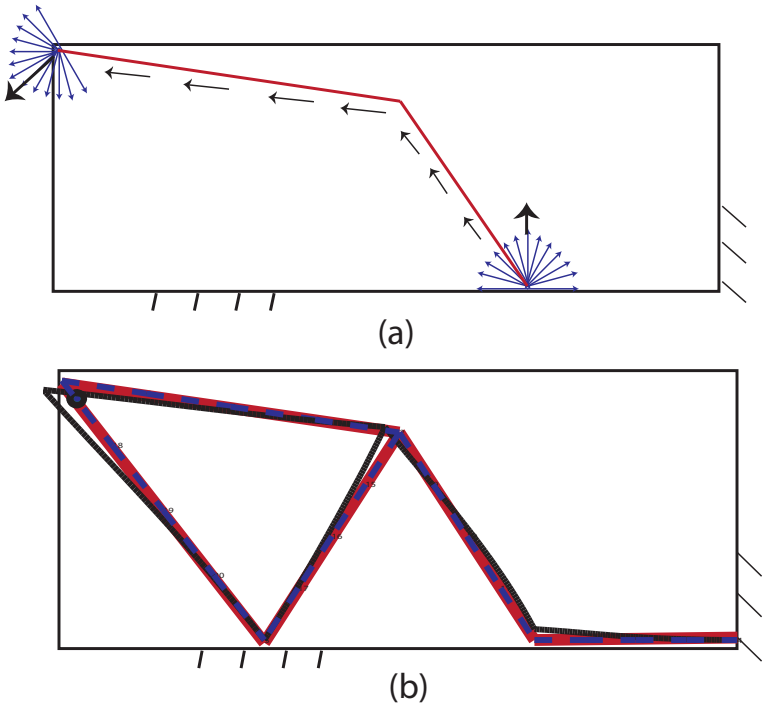

Figure 4.11: Design of a Compliant Force Transmission Mechanism for a stapler gun: Second Design (a) Conceptual topology using load flow(b) mechanism with deformed profile

Choosing an input displacement direction would require a constraint that limits displacement in every other direction. A direct connection between the input and the output would have its load flow in a direction centered around the semicircular band around the input displacement. Note that the load flow lines have to intersect with the output semicircular band. The output constraint must enforce the required output displacement direction as shown in Fig. 4.10e.

Another conceptual design involving two load paths is presented in Fig. 4.11a. In this design it is seen that the load flow direction is more along the direction of the

required output displacement than the first design. These two conceptual designs are

4.4 Design Strategies for Mechanisms with Multiple Load Paths

The net load path can be made up of multiple paths from the input to the output. We showed that the output transferred load is a combination of the load transferred by individual paths. The relative stiffness of the two paths decide which path would be dominant. Consider the mechanism shown in Fig. 4.12. The net load transferred at the output is given by the equation

$$\mathbf{f}_o = (\mathbf{T_{F1}}\mathbf{C}_1^{-1} + \mathbf{T_{F2}}\mathbf{C}_2^{-1})\mathbf{C}_I\mathbf{f}_i \tag{4.7}$$

It can be seen from the above equation that the output transferred load can range between the transferred load due to Load Path 1 and transferred load due to Load path 2. For example if the stiffness associated with Load path 1 is much greater than that of Load path 2 then load path 1 will dominate the output transferred load. Though we cannot intuitively determine which load path predominates, we can determine the range of possible loads transferred at the output. This implies that by tuning the relative stiffness of the load path any vector combination of the two transferred loads can be obtained. This can be achieved through optimization.

In the section below we present an application of using multiple load paths to morph the shape of a semicircular member.

4.4.1 Design of Shape Morphing Compliant Mechanisms

Shape morphing compliant mechanisms (*Lu and Kota* (2005)) have been proposed in the past for a number of applications such as changing aircraft wing profiles during flight. The need for multiple actuators to affect this change in shape is circumvented

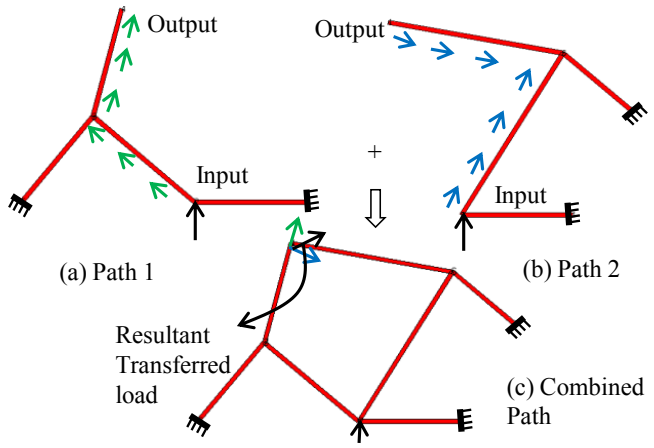

Figure 4.12: A Mechanism consisting of two load paths (a) First load path (b) Second Load path (c) The resultant load path. One of the possible directions of the transferred force at the output is the vector combination of the individual transferred forces

by a compliant mechanism that transfers load from a single input actuator to multiple points in the aircraft wing. To design such a mechanism, topology optimization was used to determine the connectivity of members from the input to various parts in the aircraft wing. The objective function for optimization was minimizing the least square error between the desired shape and the actual deformed shape of the wing.

In this effort, we make the design process more intuitive by conceptualizing load paths. This method converts an input-output two-port problem to a single port stiffness design problem by evaluating the transferred force from the input that is available at the output. To illustrate this, we will consider an example of a semicircular arc as shown in Fig. 4.13a. The deformed profile required is shown. To obtain this deformed profile, we first find out the number of force points, their relative magnitude and direction of application of force. In this example we require two forces of equal magnitude inclined at 135° and -135° to the horizontal. The design domain for the mechanism to fit in is shown in fig. 4.13b. In order to be able to apply these forces the transmitter members at the two force points P1 and P2 should be along the tangent of the mechanism, which is not easy to fabricate. In such cases, we propose

the following guideline

When the transferred force along a required direction cannot be achieved using a single load path, we can decompose it into two or more components whose resultant is in the required direction.

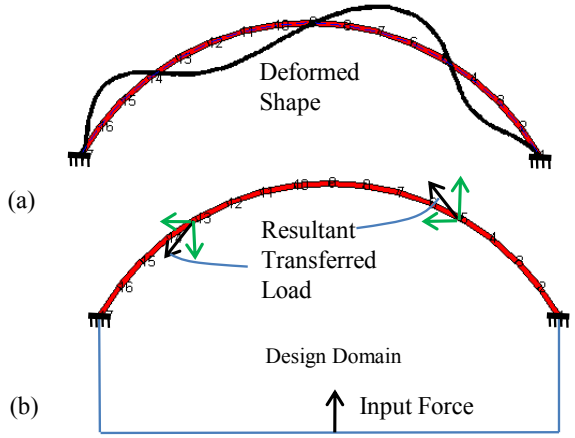

Figure 4.13: Problem Specification for the Shape Morphing Problem. (a) Initial and the required deformed shape (b) Two single point forces of equal magnitude and direction shown in the figure are required to attain the deformed shape. These forces can be decomposed into horizontal and vertical components for simplicity.

Thus, we can decompose the required force at P1 and P2 into two components, i.e. along the horizontal and vertical respectively. This is shown in Fig. 4.13b. The load paths consisting of transmission beams and their desired direction of load transmission is presented in Fig. 4.14a. Using the rules laid out in the earlier section, we can draw truncated bands that enclose the degrees of freedom at the constraint. The force from one of the nodes can be used as the input for a secondary load path that provides the $X-$ direction transferred load at P1 and P2 as shown in Fig. 4.14b . We then place appropriate constraints to complete the mechanism design shown in Fig. 4.15a.

Finally, we need to choose dimensions for these members to make it practical and realizable. It must be noted that arbitrary dimensions are not going to place the output load along the desired direction, as the resultant transferred load depends

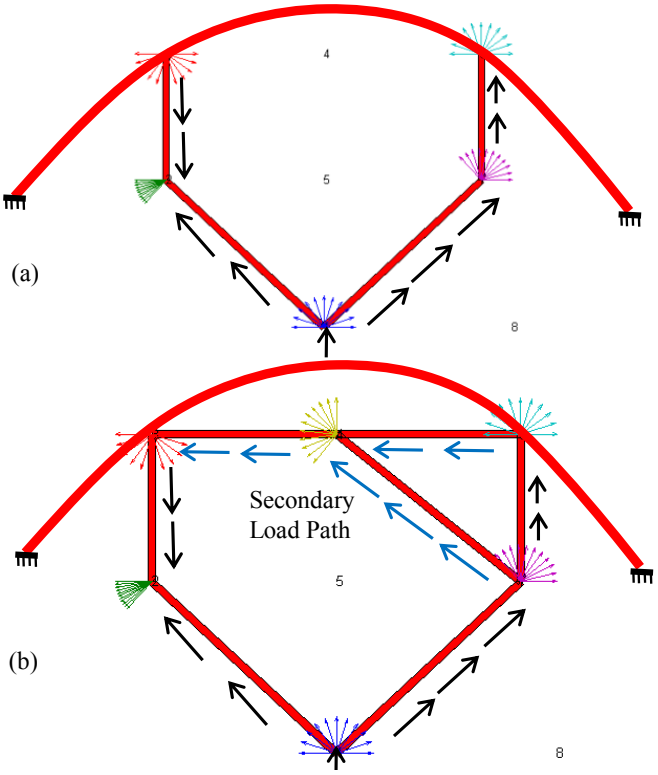

Figure 4.14: Load paths to obtain the required transferred force. (a) Transmitter beams and the direction of load flow in each of them. This arrangement delivers the $Y-$ component of the transferred load. (b) Load path that delivers the $X-$ component of the required transferred load.

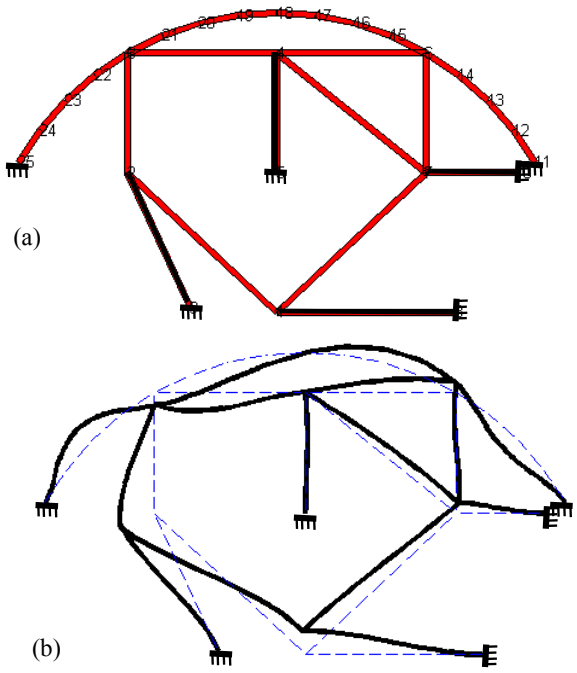

Figure 4.15: (a) Final mechanism with the constraints added (b) Deformed profile.

on the relative stiffness of the individual load paths. However, it is known to us that the desired resultant transferred load can be obtained tuning this stiffness. We thus formulate an optimization problem for the mechanism with the individual beam thickness as the design variable.

$$\begin{aligned} \text{Min } v &= (\mathbf{u}-\mathbf{u}_o)^T(\mathbf{u}-\mathbf{u}_o) \\ \text{w.r.t } \mathbf{X} &= \text{ in-plane thickness of the beams} \\ \text{s.t.} \mathbf{f} &= \mathbf{K}\mathbf{u} \text{ Governing Equation} \\ \mathbf{X}_{lb} &\leq \mathbf{X} \leq \mathbf{X}_{ub} \end{aligned} \tag{4.8}$$

where $\mathbf{u}_o$ is the required deflection profile of the semi circle. The final mechanism and the obtained deflection is shown in Fig. 4.15. It matches closely with the required deformation.

4.5 Conclusion

This chapter presents a systematic methodology to conceptualize compliant mechanism designs utilizing load flow. A mathematical representation of load flow reveals a number of new insights that can be directly adapted to guide designers. It enables visualization of the entire mechanism as a combination of simple fundamental building blocks known as the Load-Transmitter Constraint set. The transmitter elements of all the LTC sets that make up the mechanism are used to visualize load flow. This is more intuitive for LTC sets comprise of compliant dyads as the load is transmitter along the axial direction of the transmitter beam. These transmitter beams can be stacked together along the direction of a load flow path that the designer conceptualizes. Though the guidelines do not propose a unique optimum load path for each problem, it presents general conditions that reveal *all possible load paths*. Each load flow path is associated with a unique set of constraints that enforce directionality in load flow. The design of LTC sets together with appropriate single point constraints at input and output enable attainment of the required displacements at the two ports.

The design of mechanisms involving multiple load paths is more complicated as the load transferred by individual load paths do not directly add according to vector addition. The influence on the resultant transferred load for each individual load path is proportional to its stiffness. However, one can determine the range of output transferred loads attainable from the individual load paths and tune their stiffness using optimization to obtain the desired value. These act as guidelines to decompose the desired transferred load at the output into two tractable load paths comprising of LTC sets. We have implemented these guidelines towards an example involving a shape morphing compliant mechanism.

CHAPTER V

A Strength based Metric for Size Optimization

Conceptual designs for compliant mechanism synthesis were extensively dealt with in the previous chapters. This involved topology generation to satisfy kinematic requirements at single and multiple ports. In this chapter, optimum dimensional embodiments for the conceptual designs will be determined based on enforcing uniform stress distribution throughout the mechanism topology. Uniform stress distribution enables maximum material utilization where each member contributes equally towards the overall function. Furthermore, it reduces the need for excessive material volume making the mechanism stronger and lighter. A non-dimensional performance metric is defined to quantify how evenly stress and thus strain energy is distributed within the mechanism. An optimization based refinement is proposed to tune cross section areas of conceptual designs to maximally distribute stress. Furthermore, an objective comparison of different topologies using this quantity enables identification of some geometries and actuation schemes that better distribute stresses.

5.1 Introduction

An optimum engineering design aims at maximizing performance and minimizing cost, or resources used. In structural design, optimality translates towards obtaining the stiffest structure that has minimum weight. *Michell* (1904) proposed an optimum arrangement of bars in a truss framework (also called Michell structure) as shown in Fig. 5.2. One of the features of this design is that each bar in the framework undergoes equal stress. Bars that are attached at either ends by revolute joints are capable to taking axial internal forces alone, and this force creates stress that is equally distributed throughout the volume of the bar. Thus, each elemental volume in a Michell structure undergoes equal stress. This means that no single member would be inclined to fail before the other, and this leads to maximum utilization of material.

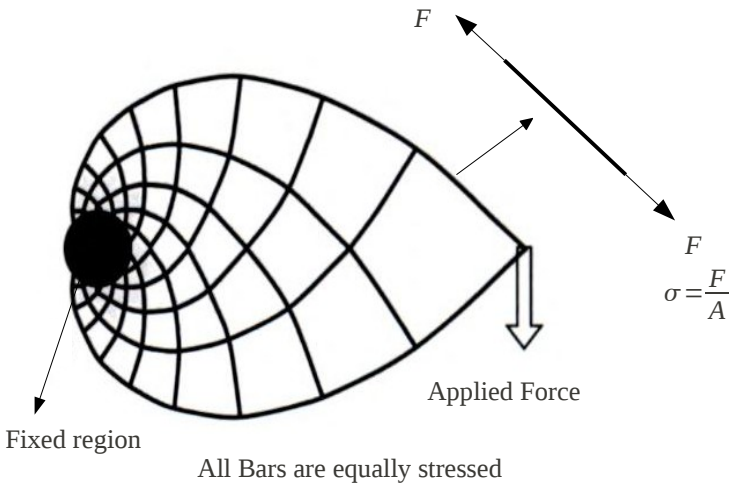

Figure 5.1: Michell structure is the stiffest structure that supports the applied load with minimum volume. All the bars in the truss framework have the same stress.

Nature prefers flexibility or compliance over stiffness, but does not compromise on strength. For example, plants subjected to large wind or water loads undergo significant bending, but rarely fail. Flexibility is preferred because it leads to aerody-

namic configurations in the bent state thus reducing the uprooting moment that wind loads cause [*Vogel* (2003), *Sivanagendra and Ananthasuresh* (2009)]. However, it is subjected to large bending moments that result in bending stresses. These stresses are not equally distributed across the cross section but vary from maximum tension to maximum compression with a central unstressed neutral axis. To distribute the maximum bending stresses evenly throughout the length of a sea anemone or a branch of a tree shown in Fig. 1.2, nature tends to taper the sections from being thick at the fixed end to thin at the free end. For example, consider the end loaded cantilever beam with rectangular cross section and uniform out of plane thickness (h). The end load (F) results in a moment that varies linearly with distance from the point of force application. If stress σ is given by

$$\sigma = \frac{F \times x \times b(x)}{2I(x)} = \frac{6F \times x}{b(x)^2 h} \tag{5.1}$$

where $I(x)$ denotes the second area moment of cross section, and $b(x)$ is the thickness of the cross section. For the above stress to be constant throughout we can find an expression for $b(x)$ as

$$b(x) = \sqrt{\frac{6Fx}{\sigma h}} \tag{5.2}$$

which indicates a parabolic relationship between thickness and distance from the free end. Similarly for a uniformly distributed load, the thickness is linear with respect to distance.

To show that uniform distribution of stress indeed decreases peak bending stress, three beams of equal stiffness and length are compared as shown in Fig. 5.3. The first beam is a flexure with lumped compliance at its joint. The second beam has a uniform cross section, while the third is a parabolic tapered beam that distributes peak bending stresses equally along its length. Figure 5.3d shows the variation of the maximum bending stress with respect to the distance away from the fixed end. It is

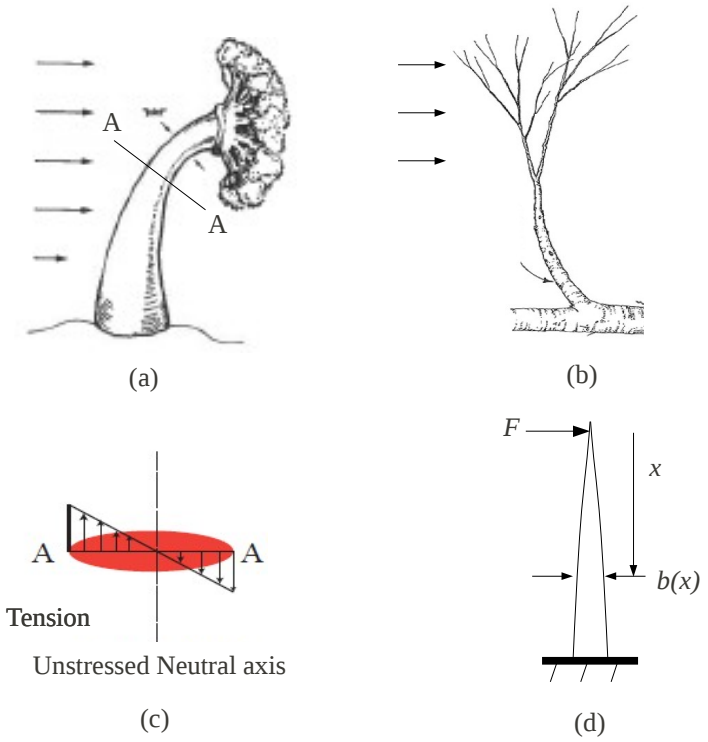

Figure 5.2: Examples in nature with uniform stress distribution (a) A sea-anemone subjected to water currents (*Vogel* (2003)) (b) A tree branch subjected to wind loads (c) bending stress distribution at any given cross-section (d) determining the thickness of the beam with distance from the free end that uniformly distributes stresses along its length.

seen that the the tapered beam has minimum peak stress and this stress is uniformly distributed over the entire beam length. The flexure with lumped compliance has the largest maximum stress.

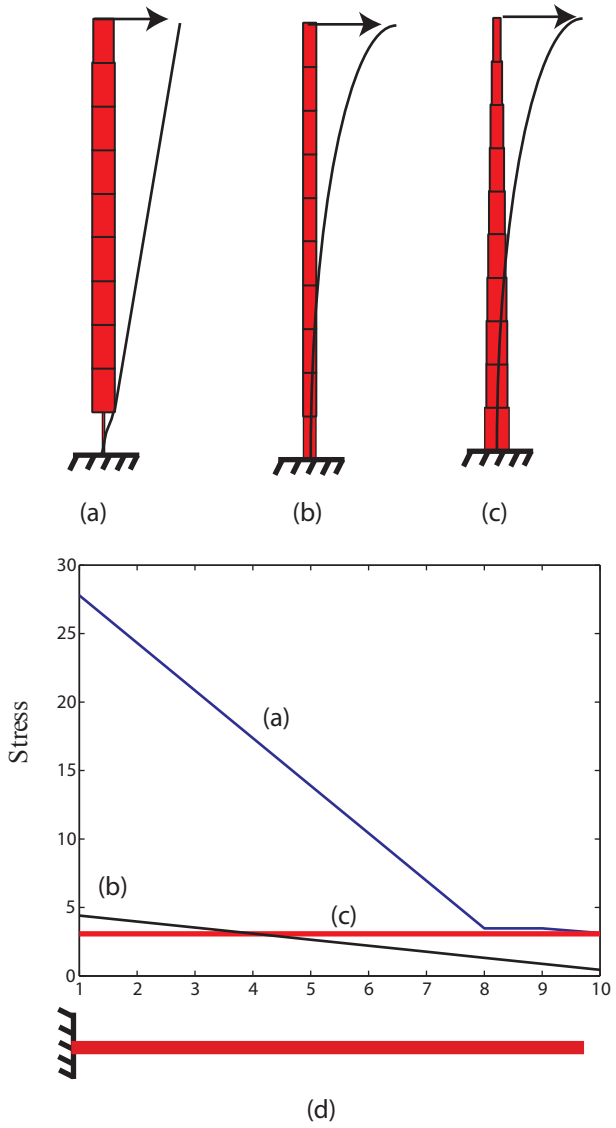

Figure 5.3: Comparison of three beams: (a) flexure with lumped compliance (b) beam with uniform cross section (c) tapered beam with uniform stress distribution, all having the same stiffness (d) comparison of the stress distribution throughout their length

The next section will focus on formulating a metric to evaluate how evenly stresses are distributed in a mechanism.

5.2 Performance Metric: Definition and Physical Interpretation

The previous section motivated the need for evenly distributing stress in a mechanism. For a simple comparison of beams having the same stiffness, this was shown to reduce the peak bending stress. This section will propose a metric that evaluates how evenly stress is distributed within the material volume. For an objective scale-independent evaluation, the metric must be nondimensional and independent of the absolute values of applied force, material properties and cross-section dimensions. This requires the representation of failure stress and output work in terms of known quantities intrinsic to the mechanism topology, and relative cross-section dimensions.

- **Maximum Strain Energy**: The maximum strain energy represents the energy that can be stored in the mechanism if all its members are equally stressed to a given permissible value. This is the maximum value of strain energy that can be stored in a given volume. In most solid bodies subjected to a load, the actual strain energy stored would be less than this quantity. Storing maximum strain energy requires the strain energy density to be constant at every point in the volume. Assuming only uniaxial stresses, as in beams or bars the strain energy density is given by

$$SE_{density} = \int_0^{\epsilon_{max}} \sigma \times d\epsilon \tag{5.3}$$

where σ is the stress at any given point and ϵ is the strain at that point. Assuming linear elastic material with Young's modulus E these two quantities are related as $\sigma = E\epsilon$. Furthermore, if all points in the volume are equally stressed, the maximum strain energy density is given by

$$SE_{density_{max}} = \int_0^{\sigma_{max}} \frac{\sigma \times d\sigma}{E} = \frac{\sigma_{max}^2}{2E} \tag{5.4}$$

The maximum strain energy that the given volume of material can hold before failure is then given by a product of the maximum strain energy density ($SE_{density_{max}}$) and mechanism volume (V)

$$SE_{max} = \frac{\sigma_{max}^2 \times V}{2E} \tag{5.5}$$

Figure 5.4a shows a state where every point in the material volume has the same stress σ_{max}.

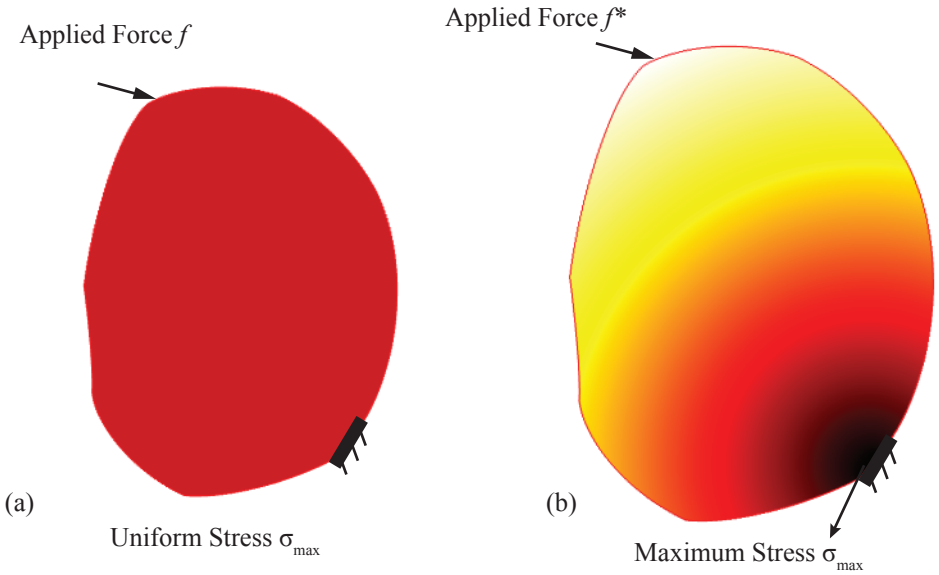

Figure 5.4: Internal stressed state of a material such that (a) each point undergoes the same stress, and (b) a loading case with nonuniform stress distribution

- Work done or Energy Input: From the principle of conservation of energy any input energy supplied or work done into the system is stored in the material as the internal strain energy. For a linear elastic material without considering nonlinearity due to large displacements, input work is given by the area under the force deflection curve as shown in Fig. 5.5 as

$$InputWork = \frac{1}{2}\mathbf{f}^T\mathbf{u} = \int_0^V \frac{\sigma^2}{2E} dV \tag{5.6}$$

where σ is not constant, but depends on the position of the point under consideration similar to Fig. 5.4b.

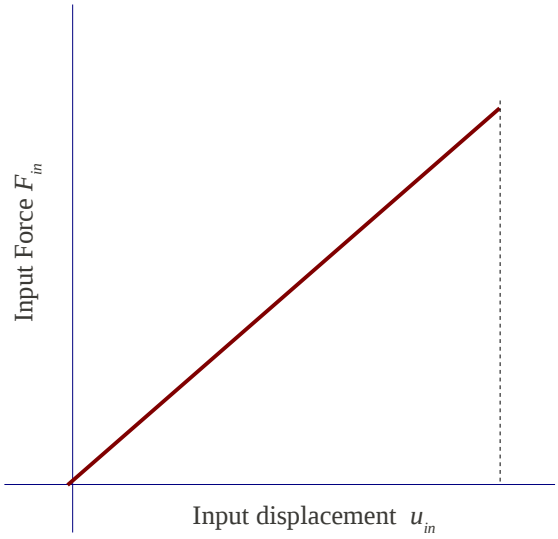

Figure 5.5: Force-displacement relationship at the input when load is gradually applied

- **Performance Factor** n_p: The performance factor is given by the ratio of strain energy stored in the mechanism caused by a certain loading condition given by Eq. 5.6 and the maximum possible strain energy that can be stored in its volume given by Eq. 5.5. In both conditions it is assumed that the maximum stress (σ_{max}) is the same (see fig. 5.4).

$$n_p = \frac{2E \int_0^V \frac{\sigma^2}{2E} dV}{\sigma_{max}^2 \times V} = \frac{E\mathbf{f}^T\mathbf{u}}{\sigma_{max}^2 \times V} \tag{5.7}$$

The performance factor measures the fraction of material volume that uniformly distributes strain energy. Since the strain energy density at a point signifies its contribution to the overall strain energy of the material, a performance factor of value unity implies uniform strain energy density and thus maximum utilization of the material. By laying out the significance of numerator and denominator terms separately, the performance factor indicates the amount of external work that can

be done on the material for a given maximum permissible stress. Furthermore, for a given permissible stress and an applied input force, a higher performance factor indicates larger displacements before failure.

5.2.1 Evaluation of the Performance Factor for simple geometries

The terms used to express the performance factor given in Eq.5.7 can be evaluated for any geometry, simple or complex. However, it is limited to simplified models with only uniaxial stresses such as pure tensile or compressive stress in axial deformation of bars, and a combination of tensile and compressive stresses in bending of beams. For more complex models including the consideration of shear in beams the above terms are insufficient for expressing the performance factor. The thesis thus limits consideration to slender beams and bars, and topologies that can be modeled using an interconnected framework of these elements.

5.2.1.1 A bar in tension or compression

A simple bar in tension or compression, as mentioned earlier distributes stresses evenly along its cross section. For a bar of length L, area of cross-section A and Young's modulus E, any axial force F produces a uniform stress σ_{bar}

$$\sigma_{bar} = \frac{F}{A} \tag{5.8}$$

Since the stress is uniform along its length, σ_{max} in Eq. 5.7 can be considered to be equal to σ_{bar}. Furthermore a force F produces an axial change in length of the bar u given by

$$u = \frac{Fl}{EA} \tag{5.9}$$

Substituting these terms in Eq. 5.7 the performance factor is evaluated by

$$n_p = \frac{E \times F \times \frac{Fl}{EA}}{\frac{F^2}{A^2} \times A \times L} = 1 \tag{5.10}$$

Thus a bar in pure tension or compression utilizes all its material uniformly towards storing the applied input work as strain energy.

5.2.1.2 A beam with uniform cross section under an applied end load

Consider a cantilever beam with an applied end load F(Fig. 5.3b).The end displacement is

$$\delta_{end} = \frac{FL^3}{3EI} \tag{5.11}$$

where E is the Young's Modulus and $I = \frac{b \times h^3}{12}$ is the second area moment of the cross section. Note that 'h' is the in plane thickness and 'b' is the out of plane thickness. The input work done can then be given by

$$Work = F \times \delta_{end}/2 = \frac{F^2 L^3}{6EI} \tag{5.12}$$

The maximum stress developed in the beam is at the fixed end given by

$$Stress = \frac{F \times L \times c}{I} \tag{5.13}$$

where $c = h/2$. The volume of the entire beam is given by $V = bhL$. Substituting these in Eq. 5.7 the performance factor can be expressed as

$$n_p = \frac{4 \times F^2 \times L^3}{\left(\frac{6 \times F \times L \times}{b \times h^2}\right))^2 \times b^2 \times h^4 \times L}$$

$$n_p = 0.11 \tag{5.14}$$

The interpretation of this factor is that a beam with uniform bending utilizes 11% of its total volume into uniformly distributing strain energy. Furthermore, it is interesting to note that this factor is independent of the actual values of the cross section and length of the beam.

5.2.1.3 A beam with uniform cross section under an applied end moment

Consider the beam with the same dimensions as in the previous example with an end moment M applied and no end force. The input work done on the beam can be evaluated as the product of this applied moment and the tip slope or rotation as

$$Work = M \times \theta_{end}/2 = M \times \frac{Ml}{2EI} \tag{5.15}$$

An interesting feature of an applied end moment is that the bending moment at every cross section is constant and equal to the applied moment. This further indicates that the maximum bending stress at any distance along the length of the beam will have the same magnitude.

$$Stress = \frac{M \times c}{I} \tag{5.16}$$

Substituting these in Eq. 5.7 the performance factor can be expressed as

$$n_p = \frac{M \times \frac{Ml}{2EI} \times E}{\frac{M^2 \times c^2}{I^2} bhL}$$

$$n_p = 0.33333 \tag{5.17}$$

The above factor indicates that in pure bending with each cross section under the same bending moment and thus uniform maximum stress, only 33.33% material is uniformly utilized. A similar stress distribution pattern is noticed in an end loaded beam with parabolically varying cross section to distribute the peak bending stress uniformly along its length. Even for such a beam the performance factor can be

shown to be around 0.3333.

While we can derive the performance factors for simple geometries, finite element analysis is required to evaluate the terms of Eq. 5.7 for complicated topologies composed of beams. The main aim of this chapter is to refine topologies such that they attain a higher performance factor, and thus distribute stresses more evenly in their geometries. The next section presents this optimization based refinement strategy for single port compliant mechanisms.

5.3 Size Optimization of Single Port Compliant Mechanisms: Examples

The effectiveness of a single port mechanism as indicated by the performance factor is in capturing as much strain energy as possible before failure. Single port topologies introduced in Chapter 2 can thus be refined towards this end. The basis of the refinement is to distribute material along the beam lengths such that the peak bending stress in each cross section is the same. There may be manufacturing constraints that are imposed on the thickness of the mechanisms that prevent the values of the stresses to be exactly equal everywhere, nonetheless the refinement process guides the mechanism towards maximal material utilization.

5.3.1 A Fixed-Guided Beam

A fixed-guided beam is a fundamental building block in suspensions for precision motion stages [*Awtar and Slocum* (2007)]. The loading conditions subjected to this beam does not distribute the peak stresses uniformly when the cross-section is uniform. The inplane thickness of the beams are varied as shown in Fig. 5.6a such that

stress distribution is uniform. The optimization problem is stated below.

$$\text{Maximize } :n_p(X_i) = \frac{F_{in}u_{in}E}{\sigma_{max}^2 V}$$
$$\text{Such that } :Lb_i \leq X_i \leq Ub_i \tag{5.18}$$

In this problem, the upper and lower bounds were fixed to 5 mm and 1 mm respectively, the Young's modulus of the beam is 200 GPa, out of plane thickness is 10 mm and the length of the beam was 70 mm. The optimized solution shown in Fig. 5.6b tapers towards the center. The optimized objective function value is around 0.28. Figure 5.6c shows a double parallelogram flexure and its deformed profile. The resulting flexure can traverse a longer distance and handle larger input forces than a beam of same stiffness but uniform cross section.

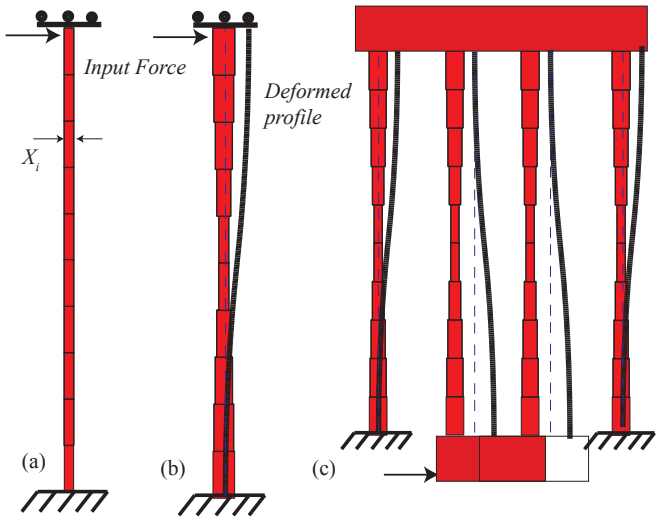

Figure 5.6: Cross-section refinement for a fixed-guided beam (a) Initial beam with uniform cross-section (b) Optimized cross-section (c) Optimized beam used in a double parallelogram flexure

5.3.2 A Compliant Vision based Force Sensor

A compliant vision based force sensor was designed in Chapter 2 using a parallel combination of two single point mechanisms. These single point mechanisms were them-

selves a series combination of two or more beams arranged so that they have equal eigen-compliances in the X and Y direction. In this section, the cross-sections of the beams that make up this topology will be optimized to maximally distribute stresses. However, changing the cross-section alone may alter the relative stiffness in the X and Y direction. Thus, selected end nodes shown in Fig. 5.7a are allowed to vary as design variables within the bounding box. Furthermore, apart from maximizing the performance factor, there must be constraints enforcing equal eigen-compliances. The problem statement is given below.

$$\begin{aligned} &\text{Maximize } : n_p(X_i) = \frac{F_{in} u_{in} E}{\sigma_{max}^2 V} \\ &\text{Such that } : (a_{f_1} - a_{f_2})^2 \leq 0 \\ &\text{And } : Lb_i \leq X_i \leq Ub_i \end{aligned} \tag{5.19}$$

In this problem, the upper and lower bounds were fixed to 5 mm and 1 mm respectively, the Young's modulus of the beam is 200 GPa, out of plane thickness is 10 mm. The optimized solution is shown in Fig. 5.7b. A force applied at 45° to the horizontal displaces the input in the same direction as seen in the deformed profile. The performance factor improved from an initial value of 0.09 to a final value of 0.2. The stresses at all the elements are plotted for both the initial mechanism and the optimized mechanism in Fig. 5.7c. The peak stress in the optimized mechanism is around 50% lower than the initial topology.

5.4 Performance Factor for Multi Port Mechanisms

Multi port mechanisms are characterized by the effectiveness in which the input work done is transmitted to the output. This transmission for compliant mechanisms is through elastic deformation, thus storing significant strain energy within the mechanism. Just as in single-port mechanisms it is desired that this strain energy is evenly

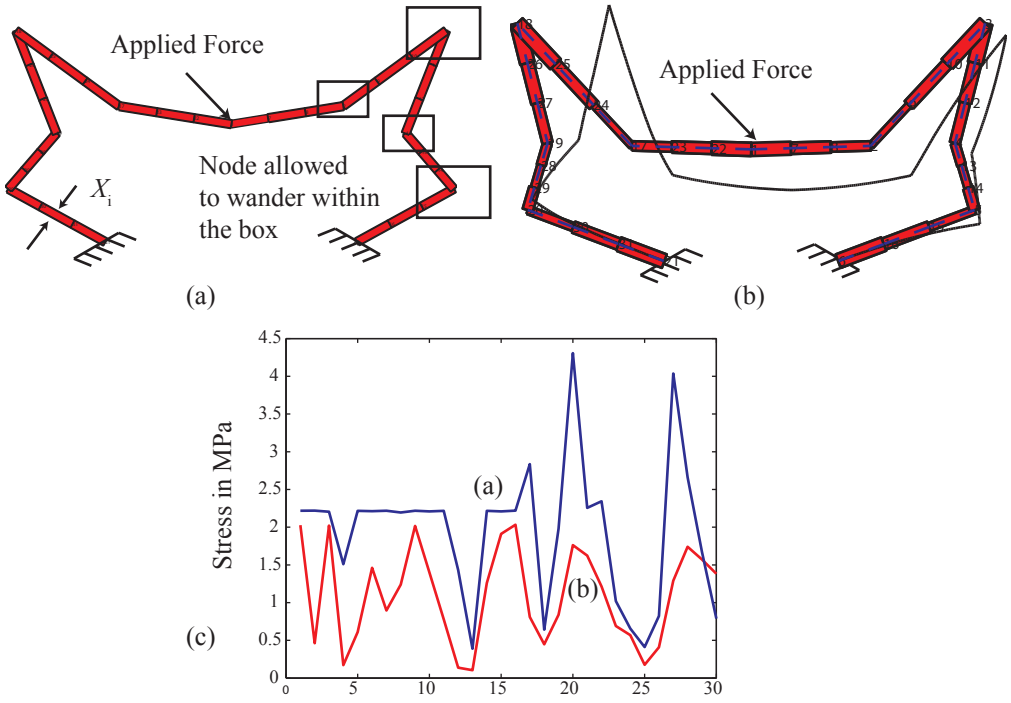

Figure 5.7: Cross-section refinement for a vision based force sensor (a) Initial topology with uniform cross-section (b) Optimized topology with deformed profile(c) Stress distribution along the elements in the initial and optimized topology

distributed throughout the topology. Thus an ideal two port transmission mechanism must efficiently transmit input energy to the output, such that the strain energy is evenly distributed through all members of the mechanism ensuring maximum material utilization.

Efficiency is evaluated using the definition of transferred forces introduced in Chapter 3. Figure 5.8a shows the input force applied to a deformable body. The input work can be evaluated by area under the curve of Fig. 5.5 as

$$InputWork = \frac{1}{2} F_{in} u_{in} \tag{5.20}$$

The transferred force defined in Chapter 3 is an applied output force that causes the same output deformation as a unit input force. Alternatively if a force equal and opposite to the transferred force is applied at the output together with the input force, the output deformation is completely restricted as shown in Fig. 5.8b. Furthermore, if this output force is applied gradually, the force deflection curve at the output will be given by Fig. 5.8c. Thus the output work is given by the area under this curve as

$$OutputWork = \frac{1}{2} F_{tr} u_{out} \tag{5.21}$$

The efficiency η of the mechanism is given by the ratio of the output and input work.

$$\eta = \frac{OutputWork}{InputWork} = \frac{F_{tr} u_{out}}{F_{in} u_{in}} \tag{5.22}$$

The maximum value of η is unity as this indicates a 100% transmission between input and output. Multiplying efficiency with the performance factor for the single port mechanisms yields a modified performance factor (n_{pm}) given below

$$n_{pm} = \frac{\eta \times E \times \mathbf{F}_{in}^T \mathbf{u}_{in}}{\sigma_{max}^2 \times V} \tag{5.23}$$

Combining Eq. 5.22 into Eq. 5.23, we get

$$n_{pm} = \frac{E \times \mathbf{F}_{tr}^{T} \mathbf{u}_{out}}{\sigma_{max}^{2} \times V} = \eta \times n_p \leq 1 \tag{5.24}$$

The performance factor defined for a two port mechanism can be interpreted as the fraction of the overall volume that not only distributes strain energy evenly, but also takes part in completely transferring input energy to the output. It indicates the amount of output work that can be performed for a given failure stress. Furthermore, its maximum value is unity as the single port performance factor and the efficiency have an upper bound of unity.

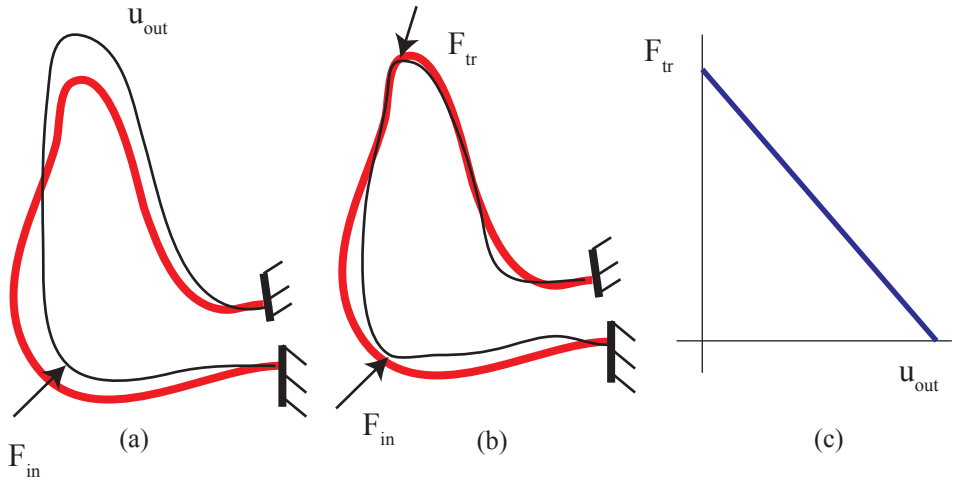

Figure 5.8: Evaluation of output work through transferred forces (a) Input force producing input and output displacements (b) Transferred force applied in the opposite direction at the output restricts its displacement, and (c) Output force vs displacement curve

5.4.1 Evaluation of the Multi Port Performance Metric for Simple Topologies

Consider a beam of length L, area moment I, and Young's Modulus E that is subjected to uniformly distributed load. A uniform loading is expressed as w and has the units of force per unit length (Fig. 5.11 CBD1). The end deflection and end slope

due to such a loading are given by

$$\delta_{end} = \frac{w \times L^4}{8 \times E \times I} \qquad \theta_{end} = \frac{w \times L^3}{6 \times E \times I} \tag{5.25}$$

This uniform load causes an end transferred force and end transferred moment given by

$$F_{end} = \frac{w \times L}{2} \qquad M_{end} = \frac{5 \times w \times L^2}{12} \tag{5.26}$$

These transferred force if applied at the end would produce the same end deflection as the uniform load. The maximum stress experienced at the grounded end is given by

$$\sigma_{end} = \frac{12 \times w \times L^2}{b \times h^2} \tag{5.27}$$

The performance factor can be then obtained by

$$n_{sp} = \frac{F_{end} \times u_{end} \times E}{\sigma^2 \times b \times h \times L} = 0.083 \tag{5.28}$$

The above factor indicates that only 8.3% of the material volume maximally distributes strain energy along with being 100% efficient in transmission. In the next section, this factor will be used to refine two port topologies for maximally distributing stress and increasing efficiency.

5.5 Shape and Geometry Refinement of Two Port Topologies

Chapters 3 and 4 concluded that a two port mechanism could be decomposed into a number of fundamental building blocks known as load-transmitter constraint sets (LTC sets). While transmitters involved in transferring forces and energy from one point to another, constraints provide directionality to the motion. It was further

concluded that the load flow direction along the transmitters were along its axis, while the constraints experienced transverse forces and moments. The examples shown below refine the cross-sections of transmitters and constraints to increase efficiency and evenly distribute stresses within the geometry.

5.5.1 A Displacement Amplifying Inverter

Shown in Fig. 5.9a is the symmetric half of a displacement inverter topology adapted from a patented design by Hetrick and Kota (1999) [*Hetrick and Kota* (2003)]. Its cross-section is optimized to obtain a large performance factor. However, changing cross-sections may reduce the amplification factor or the leverage of the device. Thus a constraint on maintaining a minimum geometrical advantage is imposed. The problem statement is given below.

$$\begin{aligned} &\text{Maximize } : n_{pm}(X_i) = \frac{F_{tr} u_{out} E}{\sigma_{max}^2 V} \\ &\text{Subject to } : n_{amp} = \frac{u_{out}}{u_{in}} \leq 6 \\ &Lb_i \leq X_i \leq Ub_i \end{aligned} \tag{5.29}$$

Figure 5.9 a shows the initial topology with uniform cross-sections and Fig. 5.9 b is the final optimized topology. The transmitters in the optimized topology have almost a uniform cross-section to maximally distribute axial loads, while some of the constraints taper, indicating the presence of transverse loads and moments. Figure 5.9 c shows a topology obtained by just maximizing the energy efficiency given by Eq. 5.22. The tendency for this formulation to result in lumped flexures is noted. Figure 5.9d shows a plot of peak bending stress in each element for the lumped design and the design optimized by using the performance factor. There is a remarkable decrease in stress levels in the optimized design. The performance factor increased from 0.02

in the initial topology to 0.064 in the final topology.

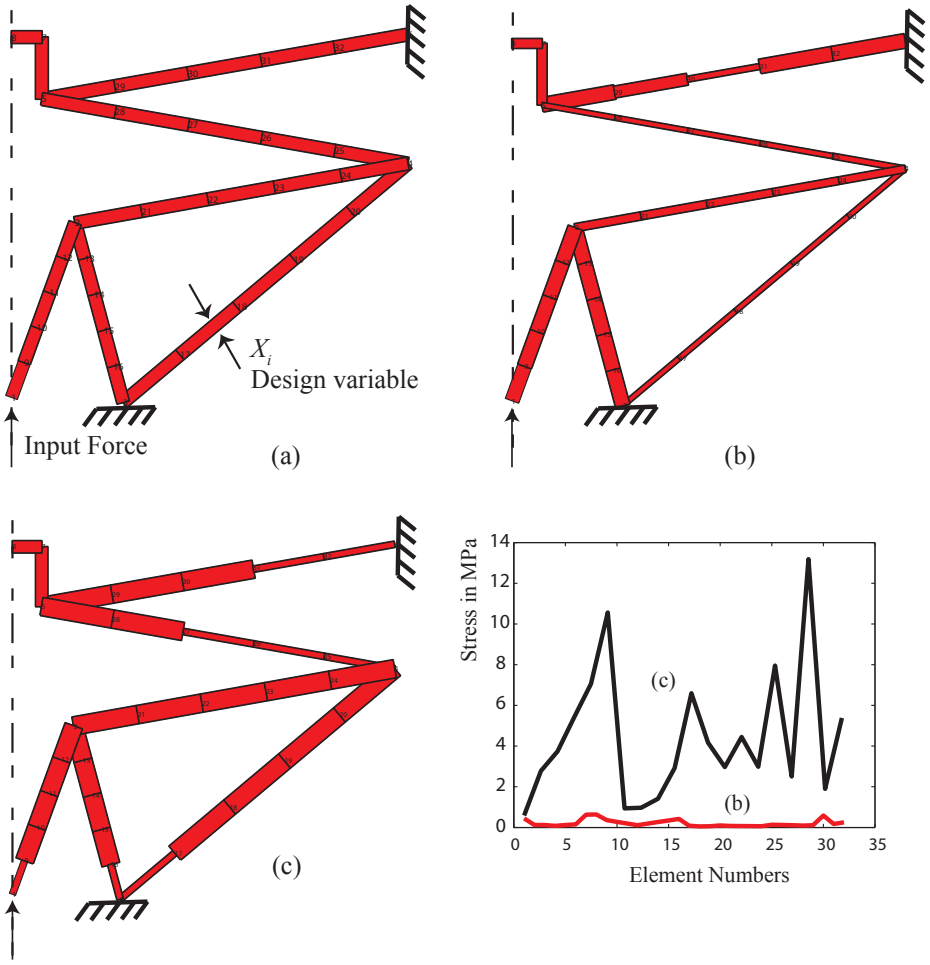

Figure 5.9: Size Optimization of a Displacement inverter [*Hetrick and Kota* (2003)] (a)Intial topology with uniform thickness (b) optimized solution using the performance factor objective function ($\eta = 89\%$, $n_{pm} = 0.064$) (c) solution obtained by optimizing mechanism topology using the energy efficiency formulation without stress constraints ($\eta = 94\%$, $n_{pm} = 0.009$), and (d) comparison of stress distribution between topologies (b) and (c)

5.5.2 A Mechanism for Energy Storage and Release

Two conceptual designs for an energy storage and transmission mechanism were presented in Chapter 4. In this section, both conceptual designs are optimized for having a high performance factor. Some stiffness requirements are imposed in the optimization problem. Kinematic requirements are already met in the conceptual design stage.

The optimization problem can be framed as

$$\begin{aligned} &\text{Maximize } : n_{pm}(X_i) = \frac{F_{tr} u_{out} E}{\sigma_{max}^2 V} \\ &\text{Subject to } : k_{input} = \frac{f_{in}}{u_{in}} \leq 12N/m \\ &1mm \leq X_i \leq 5mm \end{aligned} \tag{5.30}$$

where X_i is the in-plane thickness of the beams to be optimized, and E is the Young's modulus of the material taken to be 2 GPa. The out-of-plane thickness for the material is assumed to be 25.4 mm. The optimized solution for both the conceptual designs are shown in Fig. 5.10b, and Fig. 5.10d respectively. The first design has a performance factor of 0.11, while that of the second design is 0.12. Thus, upon optimization, both designs are equally effective. The mechanisms move by 8 mm at the output with a transferred force of 100 N and maximum stress of 40 MPa.

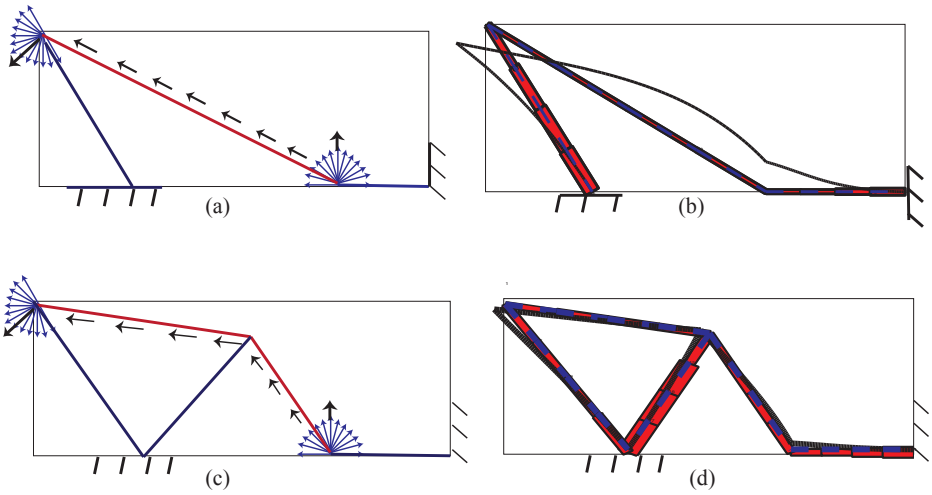

Figure 5.10: Size Optimization of an energy storage and release mechanism: (a)conceptual design 1 from Chapter 4, (b) its optimized solution using the performance factor, (c) conceptual design 2 from Chapter 4, and (d) its optimized design using the performance factor

As seen from the above examples, the performance factor can be successfully used for refinement. While most examples presented here are limited to size or cross-section

refinement, it is equally applicable to refine the parameters that define the geometry of the mechanism. However, both these techniques require a conceptual design that meets the kinematic specifications set forth by the problem. The conceptual designs need not always be generated afresh, but can be chosen from the wealth of literature. Towards this the performance metric will enable comparison of a number of conceptual designs and facilitate creating a database. Such a comparison of conceptual topologies is detailed in the following section

5.6 Global Comparison of Conceptual Designs

Designing a compliant mechanism for practical applications involves a number of steps: (a) designing a topology, (b) choosing an optimum material, and (c) refining the dimensions to suit the selected manufacturing process. These different steps can either be designed separately for simplicity, or concurrently. Rakshit and Ananthasuresh (2008) [*Rakshit and Ananthasuresh* (2008)] used topology optimization to simultaneously determine the optimum structure and choosing the appropriate material for designing stiff structures. For the sake of simplicity this section chooses to design them separately, so that the three distinct steps can be maximally decoupled. This requires separately determining the optimum topology, optimum material and the manufacturing process. Determining an optimum topology can be challenging not only for designing it afresh, but also selection from an existing database. There is a need for a global metric to compare the effectiveness of compliant topologies that is independent of the overall footprint, actual thickness values and material properties. Evaluation of the performance factor for simple topologies like a beam or a bar revealed that its value is independent of the material properties, and absolute cross-section and length dimensions. Thus the performance factor can be used as a metric for global comparison of compliant topologies.

Figure 5.11 plots a number of topologies that have different kinematic behav-

ior, actuation schemes (discrete and distributed actuation), and functional behavior (single port or multi port) under a single global platform. It must be noted that the comparison is of the topology alone and does not depend on how large or thick the mechanism is. The left column of the figure captures the performance factors of beams. Some notable conclusions are that a uniformly loaded beam (CBD1) fares better than a beam loaded discretely (CB2) at half its length. A single point mechanism obtained by a series combination of three beams (FB1) has better performance than an end loaded beam with uniform cross-section. Furthermore, beams with flexures or lumped compliance (CBL1,CBLD,CBL2) have the lowest performance factors and thus need to be avoided in conceptual designs.

The right half of Figure 5.11 compares a number of topologies (SISO1, SISO2, and SISO3) used for transmission, with distinct input and output ports. It can be seen that SISO3 has a better performance factor than the other two because of its rounded edges. Furthermore, it is seen that for the same three topologies the performance factors change by switching to distributed actuation as seen in DISO1, DISO2, and DISO3. The performance of DISO2 and DISO3 increases when compared to SISO2 and SISO3 respectively. However the performance of DISO1 is lower than SISO1. This can be explained by the effect of distributed actuation of the two constraints of the topology producing antagonistic effects. Thus for aptly designed topologies distributed actuation may increase performance factor than having purely discrete actuation.

To further analyze the effectiveness of topologies with distributed actuation, load flow in SISO3 and DISO3 are plotted in Fig. 5.12b and c respectively. While for SISO3 discrete transmitters and constraints are noticed, the distinction between them disappears in DISO3. It is seen that each element of the topology has both transverse and axial loads, with moments flowing in them. Thus in this design transmitters and constraints are distributed along the topology. This may be beneficial in terms of

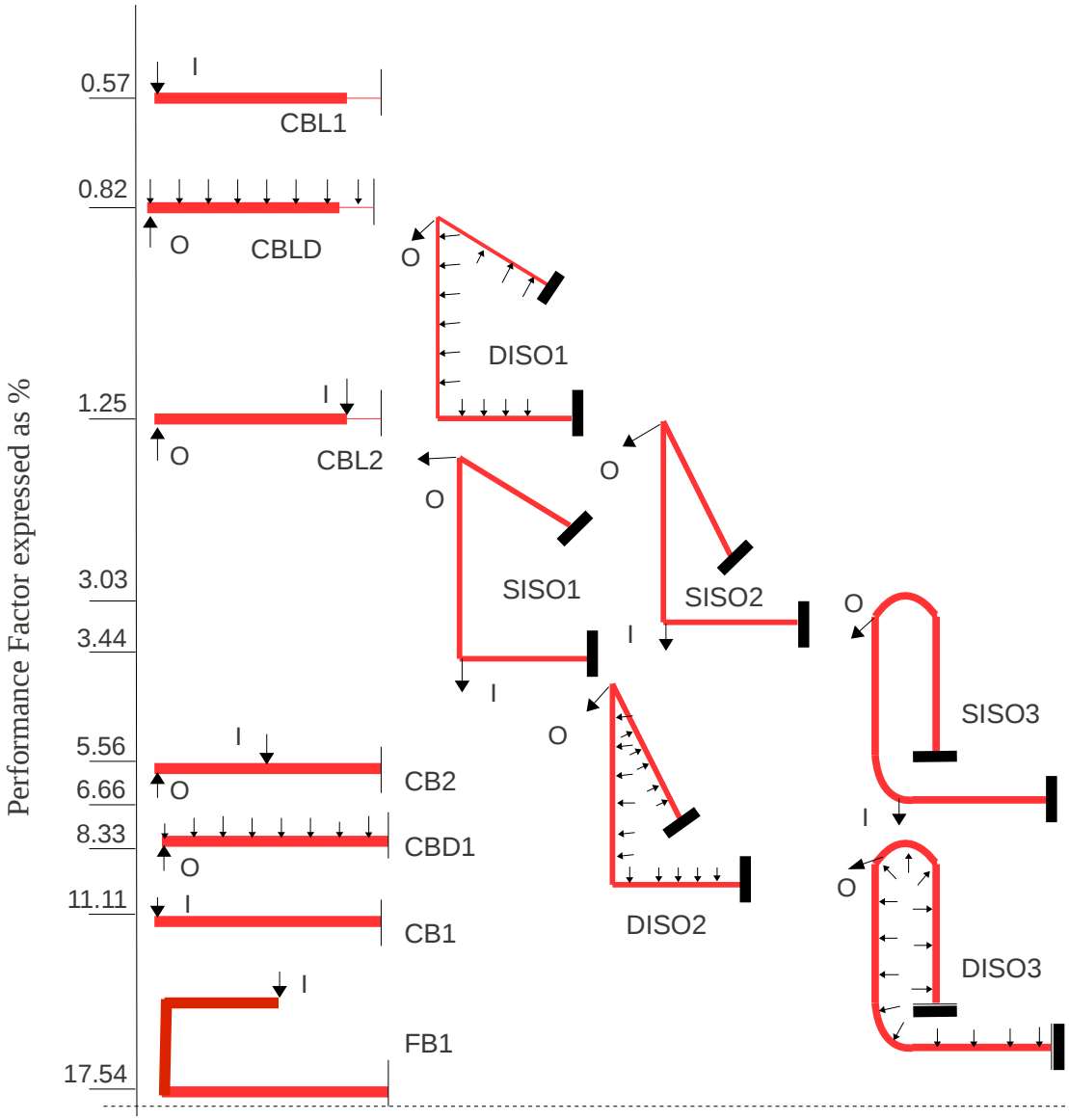

Figure 5.11: performance Factor for various geometries and loading conditions

the performance factor as transmitters with axial load flow components would better distribute stresses along its cross-section than constraints subjected to bending.

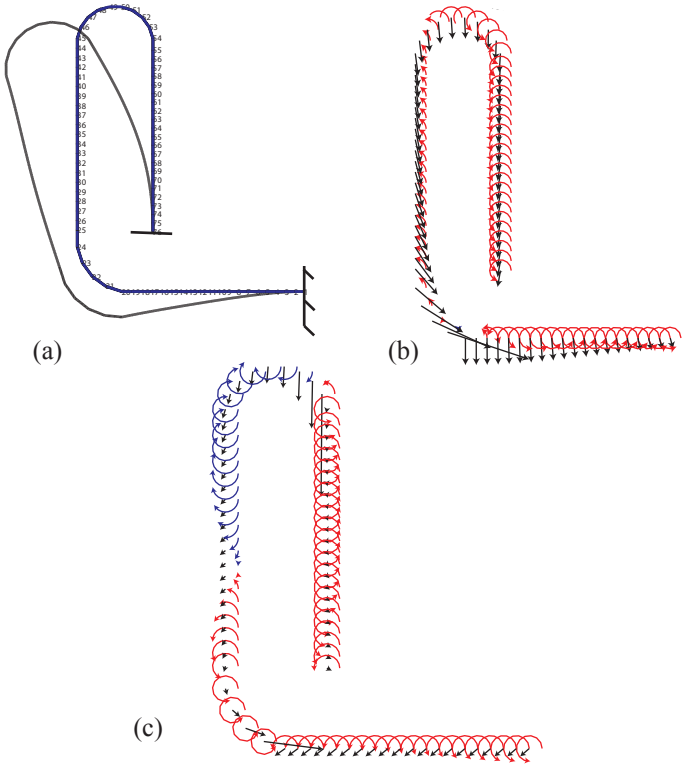

Figure 5.12: Load flow patterns for the topology in SISO3 and DISO3 conditions (a) Deformed Profile (b) Load flow in the topology for discrete actuation and output ports (SISO3) (c) Load Flow in the topology for distributed actuation (DISO2)

Practical implementation of distributed actuation is possible through pressurized fluidic actuation acting against flexible inner walls of the mechanism. These classes of mechanisms are called elasto-fluidic mechanisms. However, two dimensional topologies as shown in the comparison above will not by themselves sustain pressurized fluids. They have to be enclosed within a volume, whose surfaces deform with pressure. The resulting load paths from the enclosures must not act antagonistic to the required deformation of the mechanism. For example, Fig. 5.13 shows ribs that are reinforced into the top and bottom faces of the topology SODI3. These ribs are designed so that it contributes to the net load path of the mechanism. The space be-

tween the ribs can be enclosed by a thin layer of elastomer, so that the entire volume is airtight.

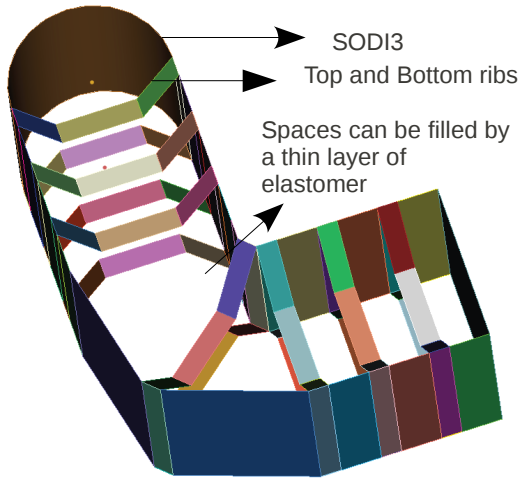

Figure 5.13: The topologies represented by SISO3 or SODI3 in Fig. 5.11. The top and bottom faces can be enclosed with elastomers with reinforced ribs.

5.7 Conclusion

The focus of this chapter was to propose a formulation that evaluates the performance of a compliant mechanism based on how evenly stresses are distributed in its constituent members. It was shown that even stress distribution reduces the net peak stress, thus increasing the amount of strain energy stored or output work performed before failure. The resulting performance factor is a nondimensional metric that can be interpreted as the fraction of the total material volume that takes part in evenly distributing strain energy or stress within the topology. Additionally, for two port topologies this factor signifies the efficiency of transmission between input and the output. The performance factor is used in an optimization procedure to refine cross-section dimensions of conceptual topologies to meet practical specifications. The resulting optimized designs on comparison with the initial topologies show

significant uniformity in stress distribution. Though this chapter presents the refinement procedure for mechanisms undergoing small deflections, it can be extendable to incorporate large deflections with geometric nonlinearity.

Furthermore, the nondimensional nature of the performance factor enables an objective comparison of various topologies and actuation schemes. Effectiveness of topologies with distributed actuation over discrete points of force application were identified for transmission applications. This effectiveness was attributed to a distribution of transmitters and constraints over the entire topology, than at discrete location. This motivates a new class of mechanisms that deform due to forces exerted by pressurized fluids on their surfaces.

CHAPTER VI

Conclusions, Contributions and Future Work

6.1 Conclusions

The purpose of this dissertation is to introduce novel representations of compliance that facilitate analysis and synthesis of distributed compliant mechanisms. Compliant mechanisms are being increasingly used in a number of applications owing to their monolithic structure, and ability to transmit motion and energy through elastic deformation without wear and backlash. Distributed compliant mechanisms make efficient use of each of its constituent members by evenly distributing stresses in them. Traditionally computationally intensive optimization tools that lack user insight have been used to obtain conceptual solutions. The resulting designs leaned towards lumping compliance and localized stresses at these joints. The representations of compliance proposed in this dissertation enables a pragmatic building block based synthesis methodology that seeks to obtain a solution by a systematic combination of simple deformable building blocks. This enables generation of multiple solutions with no additional effort. Furthermore, the representations are derived from the fundamentals of mechanics and thus accurately capture the behavior of mechanisms undergoing small deformation and made of linear elastic material. This accuracy combined with ease of synthesis and analysis deems the formulations to *naturally* represent compliant mechanism behavior. These representations are proposed for single port mechanisms

with one unique point of interest and multi port mechanisms with two or more points of interest.

In addition to conceptual synthesis, the thesis proposes a systematic refinement methodology to distribute stresses evenly in the constituent members of the mechanism, by optimizing their dimensions. These refinement techniques are applicable to single and multi port mechanisms alike, yielding designs combine both flexibility and strength. The metric used for optimization indicates how evenly stress is distributed within the mechanism. Even stress distribution reduces the peak failure stress in the mechanism thus increasing its ability to store more energy and perform more work. The metric is used to compare various topologies and actuation schemes on a global scale. This sheds light on topologies and actuation schemes that are more favorable for evenly distributing stresses. A number of benchmark examples were designed and prototypes fabricated to verify the effectiveness of the proposed methodology.

6.1.1 Summary

The thesis can be summarized into three broad aspects. The first two deal with a building block method for conceptual synthesis of single port and multi port compliant mechanisms respectively, and the third deals with an optimization based refinement technique that determines optimum cross-section dimensions for the conceptual topologies that maximally distribute stress in the mechanism. These are further expanded below.

Single-port Compliance Representation and Synthesis

The first aspect of the thesis presented in Chapter 2 dealt with a building block based synthesis methodology for planar mechanisms that have a specified stiffness behavior along its degrees of freedom. Stiffness (or Compliance) at a single point was represented by the eigen-twist and eigen-wrench characterization. This involved

shifting the point of interest to a new unique location in 2-D space known as the center of elasticity, where translational and rotational compliance were decoupled. At this location, translational compliance was represented as an ellipse and rotational compliance by a scalar. The semi-major axis of the ellipse represented the primary direction of compliance or the direction of least stiffness, where any force applied yielded pure translation along that direction. The perpendicular direction is the secondary, or the stiffest direction. The coupling between translations resulting from a pure applied moment or rotations resulting from a unit force was denoted by a coupling vector that is given by the distance between input and the center of elasticity. These quantities (ellipses and vectors) are independent of the orientation and depend on geometry and dimensions of the mechanism alone.

The variation of the eigen-twist and eigen-wrench parameters for a compliant dyad (series combination of two beams) was studied by varying its geometry parameters. This building block was shown to be versatile as it spans the entire space composed of the eigen-twist and eigen-wrench parameters.Furthermore, the characterization scheme enabled representing series combination of building blocks as addition of individual building block ellipses and coupling vectors respectively. Parallel combination similarly resulted in adding the inverse of compliance ellipses and the coupling vectors with some modification.

The graphical nature of the characterization, and series and parallel combinations enabled a systematic design methodology. A given problem specification expressed in the form of compliance ellipses and coupling vectors were systematically decomposed into a number of smaller sub-problems that were solved by a dyad or beam building block. Guidelines were proposed to obtain designs that minimize stress. Using these guidelines a vision based micro-Newton force sensor for micro assembly and cell manipulation that has equal stiffness in the X and Y directions with decoupled translational and rotational compliance was presented.

Multi Port Compliance Representation and Synthesis

The second aspect of the thesis involved a building block based synthesis of transmission mechanisms where energy applied at an input drives an external load at distinct output points. A holistic representation of this relative compliance between two geometrically distinct locations was presented in Chapter 3 in terms of load flow between input and output(s). The physical interpretation of load flow and its mathematical characterization was explained through transferred forces. In a two port system with an input and output, transferred forces can be defined as the abstract force acting on the output producing the same displacement as a unit input force at the input.

The magnitude and direction of load flow in every member within the topology was mapped to its function in the overall mechanism. Two fundamental functions identified were (a)transmission of energy or forces, and (b)constraint to provide directionality for the mechanism deformation. This further led to the identification of a building block that combines a transmitter and a constraint element, known as the Load-Transmitter Constraint (LTC) set. In a complex geometry composed of a combination of LTC sets, it was shown from the principles of mechanics that each LTC could be can be analyzed independently. This is significant because it permits modularity in the analysis and design of individual building blocks. A fundamental LTC set, namely a compliant dyad, whose transmitter and constraints are straight beams are characterized for load flow. For this building block, it is observed that load flow in the transmitter is always along its axial direction. A number of examples from literature are demonstrated to be composed of dyad LTC sets, whose identification permits load flow visualization.

The functional independence of LTC sets was shown to facilitate a building block based synthesis of compliant mechanisms in Chapter 4. Guidelines were proposed to determine a feasible load path based on problem specifications. The load flow paths were decomposed into several simple linear paths.The entire mechanism topology is

constructed by combining a number of dyad LTC sets, with its transmitters aligned along the load paths, and constraints oriented to enforce the required load flow direction. These guidelines were used in the design of a benchmark example, i.e. a single-input single-output mechanism and a continuous shape morphing mechanism. The synthesis methodology provides user insight into the function of each member that makes up the topology, and generates practical results that can be directly manufactured.

Size and Geometry Refinement for Even Stress Distribution

The final aspect of the thesis deals with refinement of the conceptual topologies towards generating practical designs with minimal failure stress. Synthesis of conceptual mechanism topologies as summarized above met the kinematic specifications alone. To obtain practical designs with the required stiffness for a given material, with minimal peak stress, and ensure manufacturability, the conceptual designs are refined for the parameters that define their cross-sections. This was accomplished previously by maximizing efficiency between the input and output ports.

A performance metric that evaluates the mechanism's tendency to fail for a unit strain energy stored or transmitted was proposed in Chapter 5. This metric is non-dimensional and independent of the magnitude of the loading, and the length scales and dimensions of the mechanism. It depends only on the topology and the nature of loading. It was further shown that the performance metric maximally distributes stress in all the members that make up the mechanism topology. Furthermore, it was shown that an even distribution of stress decreases the overall maximum stress of a mechanism without changing other aspects of its performance. Conceptual designs generated by building block methods were optimized using the metric, and resulted in designs that maximally distribute stress. Furthermore, the resulting designs could perform more output work before failure, when compared with designs obtained from

conventional energy efficiency formulation.

The non-dimensional performance metric was used to compare different topologies and their actuation techniques on a global scale. For transmission based problems, distributed actuation was shown to be preferred as it effectively utilizes all the constituent members of the mechanism.

6.2 Contributions

The main contribution of the thesis is the formulation of compliance representation that enables insightful synthesis of compliant mechanisms with evenly distributed stress along its members. While the principles governing the behavior of compliant mechanisms are the same, all representations that model their behavior are not equally favorable towards systematic synthesis. For building block methods that facilitate user insight the fundamental contribution of the thesis is proposing a holistic geometrical representation of compliance that enables a direct mapping of function to topology. The specific contributions are

- *A graphical representation of single port compliance in two dimensions*: The unique contribution of this work is the graphical characterization of compliance for planar two-dimensional topologies that is intrinsic to the geometry. The variables that define compliance are dependent on the topology alone and not its orientation. This is a significant improvement over previous attempts to obtain the same characterization that required arbitrary normalizing lengths, and thus a dependence on length scales. The importance of the characterization proposed in the thesis lies in representing compliance as graphically insightful quantities such as ellipses and vectors. Series and parallel combinations were explained graphically as additions of ellipses and vectors.

- *A load flow formulation to represent multi port compliance*: A load flow for-

mulation is proposed to characterize relative compliance between two ports in a deformable body. The physical interpretation of load flow is developed from the fundamentals of mechanics in terms of this transferred load. This is the first known effort to provide a physical interpretation to an otherwise abstract concept of load flow in compliant mechanisms. The thesis formulates a Load Transfer matrix to mathematically evaluate load flow between two points.

- *Identifying a fundamental building block for multi port compliance*: The mechanics of load flow visualization permits functional characterization of each member that makes up the mechanism. The most important contribution of the thesis lies in identifying a fundamental building block known as the load-transmitter constraint set (LTC). The functional independence of one LTC set over the others permit modularity in analysis and sets the frame-work for a building block based synthesis.

- *A building block based conceptual compliance synthesis*: The representations of compliance at single and multiple ports were geared towards enabling a building-block based systematic synthesis methodology wherein (i) A given problem specification is expressed in terms of eigen-twist and eigen-wrench characterization for single port, and the required input and output displacements and forces for multi port problems (ii) The specifications are decomposed into a number of sub-problems such as multiple compliance ellipses and coupling vectors for single port synthesis, or a network of load flow paths for multi port synthesis, (iii) finding appropriate building blocks that correspond to sub-problem ellipses, or individual load paths, and (iv) combination of subproblem solutions to obtain the required topology.

- *A performance metric for size and geometry refinement*: The performance factor formulated in the thesis yields designs that maximally distribute stresses in

the constituent members of the mechanism upon size and geometry refinement. This is by far the first attempt at obtaining designs with even stress distribution and purely distributed compliance. Furthermore, the thesis presents a first attempt towards an objective nondimensional and scale independent comparison of various topologies that enables identifying topologies and actuation schemes that can perform more output work for a given failure stress.

Some other contributions of the thesis are listed below

1. Design of a micro-Newton vision based force sensor for micromanipulation operations. The sensor is a single-port mechanism with equal bi-axial stiffness and maximally decoupled translational and rotational compliance.

2. A load flow based visualization tool that plots the transferred load at various sections of members that make up the topology. This tool requires the topology to be modeled by beam elements.

3. A global comparison of topologies and actuation schemes identified mechanisms with distributed actuation to be more effective than discrete input force. This motivates the need for elasto-fluidic mechanisms that combine the effectiveness of fluidic actuation with the advantages of compliant mechanisms.

6.3 Future Work

Single Port Compliance in Three Dimensions

While compliance behavior for two dimensional topologies were studied in this thesis, a more general three dimensional characterization is required. Eigen-twist and eigen-wrench characterization is in general defined for a three dimensional topology, but a complete decoupling between translational and rotational compliance may not be possible. Furthermore, the center of elasticity that was uniquely defined for a

two dimensional topology may not correspond to a spatial location in three dimensions. This loss in graphical intuition and increase in the number of parameters that are required for characterization poses a significant challenge for synthesis in three dimensions.

Characterizing Large Deformations

Compliance characterization was limited to small deformations compared to the overall mechanism geometry. The stiffness or compliance matrix that denotes the force displacement relationship at a point is positive definite for small deformations. This permits eigen-twist and eigen-wrench characterization providing graphical intuition in terms of ellipse and vectors. However the positive definiteness of the compliance matrix is lost for large deflection analysis thus necessitating the need for a different approach to provide graphical intuition and synthesis. Such a methodology will be useful for conceptual synthesis of nonlinear springs that meet a predetermined force displacement relation.

Extension of Load Flow based Characterization and Synthesis

Characterization of relative compliance and its physical interpretation using transferred forces and load flow are general principles. However, in this thesis their evaluation is limited to small deformations compared to the overall geometry. Extension of load flow to account for large deformations will enables synthesis of mechanisms that traverses a prescribed path. Furthermore, stress specifications in conceptual designs have been ignored. Its inclusion would eliminate topologies that are inherently unfavorable for minimizing stress.

The thesis uses reduced order beams to analyze and synthesize conceptual and refined topologies. Though accurate and convenient, continuum models are required to predict the exact stiffness and stress. For example, there is a considerable material

build up at the corners where two beams meet leading to additional stiffness and significant stress concentration at sharp corners. Integrating continuum modeling with the design methodology will provide new practical insights on synthesis.

Size-Geometry Optimization

The performance factor proposed in this thesis is a general metric to characterize the net usefulness of any compliant mechanism in terms of strain energy stored or transmitted before failure. This factor needs to be extended to capture the performance of springs with a prescribed nonlinear behavior. This can be direct extension of the framework proposed in chapter 5 where the strain energy stored in the mechanism given as the area under the force deflection curve is nonlinear.

Elasto-Fluidic Systems

The performance benefits of distributed actuation as seen from the global comparison of topologies with different actuation schemes necessitate the need for extending the load flow based synthesis methodology to a class of fully enclosed shells that deform when pressurized with fluid. Different aspects of how fluidic actuation coupled with constraints imposed by structural stiffness can be used to design devices such as robotic grippers, locomotion devices and other medical devices need to be investigated.

BIBLIOGRAPHY

BIBLIOGRAPHY

Ananthasuresh, G. K. (1994), A new design paradigm in microelectromechanical systems and investigations on compliant mechanisms, Ph.D. thesis, Ann Arbor, MI, USA.

Awtar, S. (2004), Analysis and synthesis of planer kinematic xy mechanisms, Ph.D. thesis, Cambridge, MA, USA.

Awtar, S., and S. Sen (2010), A generalized constraint model for two-dimensional beam flexures: Nonlinear load-displacement formulation, *Journal of Mechanical Design*, *132*(8), 081008, doi:10.1115/1.4002005.

Awtar, S., and A. H. Slocum (2007), Constraint-based design of parallel kinematic xy flexure mechanisms, *Journal of Mechanical Design*, *129*(8), 816–830, doi:10.1115/1.2735342.

Awtar, S., A. H. Slocum, and E. Sevincer (2007), Characteristics of beam-based flexure modules, *Journal of Mechanical Design*, *129*(6), 625–639, doi:10.1115/1.2717231.

Bendsoe, M. P., and N. Kikuchi (1988), Generating optimal topologies in structural design using a homogenization method, *Computer Methods in Applied Mechanics and Engineering*, *71*(2), 197–224.

Blanding, D. K. (1999), *Exact Constraint: Machine Design Using Kinematic Principles*, ASME Press, New York.

Cappelleri, D. (2008), Flexible automation of micro and meso-scale manipulation tasks with applications to manufacturing and biotechnology, Ph.D. thesis, Philadelphia, PA, USA.

Cappelleri, D. J., G. Krishnan, C. Kim, V. Kumar, and S. Kota (2010), Toward the design of a decoupled, two-dimensional, vision-based mu n force sensor, *Journal of Mechanisms and Robotics*, *2*(2), 021010, doi:10.1115/1.4001093.

Cherry, M. S. (2009), Design and evaluation of elastic exoskeletons for human running, Ph.D. thesis, Ann Arbor, MI, USA.

Chiou, S.-J., and S. Kota (1999), Automated conceptual design of mechanisms, *Mechanism and Machine Theory*, *34*(3), 467 – 495, doi:DOI: 10.1016/S0094-114X(98)00037-8.

Chong, K. P., and A. Boresi (2000), *Elasticity in Engineering Mechanics*, John Wiley and Sons, New York.

Ciblak, N., and H. Lipkin (1996), Remote center of compliance reconsidered, *Proceedings of the ASME International Design Engineering Technical Conferences and Computers and Information in Engineering Conference*.

Corporation, A. S. (1964), *Handbook of Mechanical Spring Design*, Associated Spring Corporation, Bristol, CT.

Deepak, S. R., M. Dinesh, D. K. Sahu, and G. K. Ananthasuresh (2009), A comparative study of the formulations and benchmark problems for the topology optimization of compliant mechanisms, *Journal of Mechanisms and Robotics*, *1*(1), 011003, doi:10.1115/1.2959094.

Dohrn-van Rossum, G. (1997), *History of the Hour: Clocks and Modern Temporal Orders*, University of Chicago Press, Chicago, IL.

Erdman, A., G. Sandor, and S. Kota (2001), *Mechanism Design: Analysis and Synthesis Volume I*, Prentice Hall, Upper Saddle River, New Jersey.

Frecker, M., and S. Canfield (2000), Optimal design and experimental validation of compliant mechanical amplifiers for piezoceramic stack actuators, *Journal of Intelligent Material Systems and Structures*, *11*(5), 360–369, doi: http://dx.doi.org/10.1106/D6UJ-0FBT-P1W0-U1WX.

Frecker, M. I., G. K. Ananthasuresh, S. Nishiwaki, N. Kikuchi, and S. Kota (1997), Topological synthesis of compliant mechanisms using multi-criteria optimization, *Journal of Mechanical Design*, *119*(2), 238–245, doi:10.1115/1.2826242.

French, M. J. (1988), *Invention And Evolution: Design In Nature And Engineering*, Cambridge University Press, Cambridgeshire.

H. Lipkin, T. P. (1992a), Geometrical properties of modeled robot elasticity: Part i-decomposition, *ASME Design Tech. Conf. and Computers in Engineering Conf*, *45*, 179–185.

H. Lipkin, T. P. (1992b), Geometrical properties of modelled robot elasticity: Part ii-center-of-elasticity, *ASME Design Tech. Conf. and Computers in Engineering Conf*, *45*, 187–193.

Hale, L. C. (1999), Principles and techniques for designing precision machines, Ph.D. thesis, Cambridge, MA, USA.

Harasaki, H., and J. S. Arora (2001a), New concepts of transferred and potential transferred forces in structures, *Computer Methods in Applied Mechanics and Engineering*, *191*(3-5), 385–406.

Harasaki, H., and J. S. Arora (2001b), Topology design based on transferred and potential transferred forces, *Structural and Multidisciplinary Optimization*, *23*(5), 165–171.

Hegde, S., and G. K. Ananthasuresh (2010), Design of single-input-single-output compliant mechanisms for practical applications using selection maps, *Journal of Mechanical Design*, *132*(8), 081007, doi:10.1115/1.4001877.

Hetrick, J., and S. Kota (2003), Displacement amplification structure and device, patent no.: Us 6557436 b1.

Hetrick, J. A., and S. Kota (1999), An energy formulation for parametric size and shape optimization of compliant mechanisms, *Journal of Mechanical Design*, *121*(2), 229–234.

Hopkins, J. B., and M. L. Culpepper (2010a), Synthesis of multi-degree of freedom, parallel flexure system concepts via freedom and constraint topology (fact) - part i: Principles, *Precision Engineering*, *34*(2), 259 – 270, doi:DOI: 10.1016/j.precisioneng.2009.06.008.

Hopkins, J. B., and M. L. Culpepper (2010b), Synthesis of multi-degree of freedom, parallel flexure system concepts via freedom and constraint topology (fact). part ii: Practice, *Precision Engineering*, *34*(2), 271 – 278, doi:DOI: 10.1016/j.precisioneng.2009.06.007.

Hoshino, H., T. Sakurai, and K. Takahashi (2003), Vibration reduction in the cabin of heavy-duty trucks using the theory of load transfer paths, *Society of Automotive Engineers of Japan Review*, *24*, 165–171.

Howell, L. L. (Ed.) (2001), *Compliant Mechanisms*, John-Wiley.

Howell, L. L., and A. Midha (1996), A loop-closure theory for the analysis and synthesis of compliant mechanisms, *Journal of Mechanical Design*, *118*(1), 121–125, doi:10.1115/1.2826842.

Howell, L. L., A. Midha, and T. W. Norton (1996), Evaluation of Equivalent Spring Stiffness for Use in a Pseudo-Rigid-Body Model of Large-Deflection Compliant Mechanisms, *Journal of Mechanical Design*, *118*(1), 126–131, doi: 10.1115/1.2826843.

http://research.et.byu.edu/llhwww (), Compliant Mechanism Research group at BMU, Provo, UT, "http://research.et.byu.edu/llhwww" "/gallery/Grippers/index.html".

http://www.flxsys.com (), Flexsys inc., ann arbor mi: "http://www.flxsys.com/aerospace.shtml".

Huang, S., and J. Schimmels (1998a), The bounds and realization of spatial stiffnesses achieved with simple springs connected in parallel, *Robotics and Automation, IEEE Transactions on*, *14*(3), 466–475, doi:10.1109/70.678455.

Huang, S., and J. M. Schimmels (1998b), Achieving an arbitrary spatial stiffness with springs connected in parallel, *Journal of Mechanical Design*, *120*(4), 520–526.

Huang, S., and J. M. Schimmels (2000), The eigenscrew decomposition of spatial stiffness matrices, *Robotics and Automation, IEEE Transactions on*, *16*(2), 146–156, doi:http://dx.doi.org/10.1109/70.843170.

Huang, S., and J. M. Schimmels (2001), Minimal realizations of spatial stiffnesses with parallel or serial mechanisms having concurrent axes, *Journal of Robotic Systems*, *18*(3), 135–146, doi:http://dx.doi.org/10.1002/rob.1011.

Joo, J. (2001), Nonlinear synthesis of compliant mechanisms: Topology and size and shape design, Ph.D. thesis, Ann Arbor, MI, USA.

Kelly, D. W., and M. W. Tosh (2000), Interpreting load paths and stress trajectories in elasticity, *Engineering Computations*, *17*(2), 117–135.

Kim, C. (2008), Functional characterization of a compliant building block utilizing eigentwists and eigenwrenches, *Proceedings of the ASME International Design Engineering Technical Conferences and Computers and Information in Engineering Conference*.

Kim, C. (2009), Design strategies for the topology synthesis of dual input-single output compliant mechanisms, *Journal of Mechanisms and Robotics*, *1*(4), 041002, doi:10.1115/1.3204252.

Kim, C. J. (2005), A conceptual approach to the computational synthesis of compliant mechanisms, Ph.D. thesis, Ann Arbor, MI, USA.

Kim, C. J., S. Kota, and Y. M. Moon (2006), An instant center approach toward the conceptual design of compliant mechanisms, *Journal of Mechanical Design*, *128*(3), 542–550.

Kim, C. J., Y. M. Moon, and S. Kota (2008), A building block approach to the conceptual synthesis of compliant mechanisms utilizing compliance and stiffness ellipsoids, *Journal of Mechanical Design*, *130*(2).

Kota, S., and S.-J. Chiou (1992), Conceptual design of mechanisms based on computational synthesis and simulation of kinematic building blocks, *Research in Engineering Design*, *4*, 75–87, 10.1007/BF01580146.

Kota, S., and J. Hetrick (2008), Compliant windshield wiper systems, patent no. us 7360272 b2.

Kota, S., J. Hetrick, Z. Li, and L. Saggere (1999), Tailoring unconventional actuators with compliant transmissions: Design methods and applications, *IEEE/ASME Transactions on Mechatronics*, *4*(4), 396–408.

Krishnan, G. (2006), Displacement-amplifying compliant mechanisms for sensor applications, Master's thesis, Bangalore, India.

Krishnan, G., and G. K. Ananthasuresh (2008), Evaluation and design of displacement-amplifying compliant mechanisms for sensor applications, *Journal of Mechanical Design*, *130*(10).

Krishnan, G., C. Kim, and S. Kota (2010), Load-transmitter constraint sets: Part i-an effective tool to visualize load flow in compliant mechanisms and structures, in *Proceedings of 2010 ASME International Design Engineering Technical Conferences and, Computers and Information in Engineering Conferences*, ASME.

Krishnan, G., C. Kim, and S. Kota (2011), An intrinsic geometric framework for the building block synthesis of single point compliant mechanisms, *Journal of Mechanisms and Robotics*, *3*(1), 011001, doi:10.1115/1.4002513.

Li, Y., and Q. Xu (2010), Development and assesment of a novel decoupled xy parallel micropositioning platform, *IEEE/ASME Transactions on Mechatronics*, *15*(1), 121 – 135.

Liaw, H. C., and B. Shirinzadeh (2010), Constrained motion tracking control of piezo-actuated flexure-based four bar mechanisms for micro/nano manipulation, *IEEE Transactions on Automation Science and Engineering*, *7*(3), 699 – 705.

Lipkin, H., and T. Patterson (1992), Generalized center of compliance and stiffness, *1992 Proceedings on the IEEE International Conference on Robotics and Automation*, pp. 1251–1256 vol.2, doi:10.1109/ROBOT.1992.220077.

Lobontiu, N. (2003), *compliant Mechanisms: Design of flexure Hinges*, CRC Press, Boca Raton.

Loncaric, J. (1985), Geometrical analysis of compliant mechanisms in robotics (euclidean group, elastic systems, generalized springs, Ph.D. thesis, Cambridge, MA, USA.

Lu, K.-J. (2004), Synthesis of shape-morphing compliant mechanisms, Ph.D. thesis, Ann Arbor, MI, USA.

Lu, K.-J., and S. Kota (2005), An effective method of synthesizing compliant adaptive structures using load path representation, *Journal of Intelligent Material Systems and Structures*, *16*(4), 307–317.

Lu, K. J., and S. Kota (2006), Topology and dimensional synthesis of compliant mechanisms using discrete optimization, *Journal of Mechanical Design*, *128*(5), 1080–1091.

Luzhong Yin, G. K. A. (2003), Design of distributed compliant mechanisms, *Mechanics based design of structures and machines*.

Marhadi, K., and S. Vekataraman (2009), Comparison of quantitative and qualitative information provided by different structural load path definitions, *International Journal of Simulation and Multidisciplinary Design Optimization*, *3*, 384–400.

Michell, A. G. M. (1904), The limits of economy of material in frame-structures, *Philosophical Magazine Series*, *6*.

Midha, A., L. L. Howell, and T. W. Norton (2000), Limit positions of compliant mechanisms using the pseudo-rigid-body model concept, *Mechanism and Machine Theory*, *35*(1), 99 – 115, doi:DOI: 10.1016/S0094-114X(98)00093-7.

Nevins, J. L., and D. E. Whitney (1985), Computer controlled assembly, *Scientific American*, *238*.

Oh, Y.-S. (2008), Synthesis of multistable equilibrium compliant mechanisms, Ph.D. thesis, Ann Arbor, MI, USA.

Parcel, J. I., and R. B. Moorman (1955), *Analysis of Statically Indeterminate Structures*, John wiley and Sons.

Paros, J. M., and L. Weisbord (1965), How to design flexure hinges (design equations and curves for calculating critical spring rates of single-axis and two-axis flexure hinges), *Machine Design*, *37*, 151–156.

Rakshit, S., and G. Ananthasuresh (2008), Simultaneous material selection and geometry design of statically determinate trusses using continuous optimization, *Structural and Multidisciplinary Optimization*, *35*, 55–68, 10.1007/s00158-007-0116-4.

Roberts, R. G. (1999), Minimal realization of a spatial stiffness matrix with simple springs connected in parallel, *Robotics and Automation, IEEE Transactions on*, *15*(5), 953–958, doi:http://dx.doi.org/10.1109/70.795799.

Ryu, J. W., D.-G. Gweon, and K. S. Moon (1997), Optimal design of a flexure hinge based xy[phi] wafer stage, *Precision Engineering*, *21*(1), 18 – 28, doi:DOI: 10.1016/S0141-6359(97)00064-0.

Saxena, A., and G. K. Ananthasuresh (2006), On an optimal property of compliant topologies, *Structural and Multidisciplinary Optimization*, *19*, 36–49.

Sivanagendra, P., and G. Ananthasuresh (2009), Size optimization of a cantilever beam under deformation-dependent loads with application to wheat stalks, *Structural and Multidisciplinary Optimization*, *39*(3), 327–336, doi:10.1007/s00158-008-0342-4.

Skakoon, J. G. (2008), *The elements of mechanical design*, ASME, New York, NY.

Slocum, A. H. (1992), *Precision machine design*, Prentice Hall, Englewood Cliffs, New Jersey.

Smith, S. T. (2000), *Flexure: Elements of Elastic Mechanisms*, Gordon and Breach Science Publishers, Amsterdam.

Su, H.-J., D. V. Dorozhkin, and J. M. Vance (2009), A screw theory approach for the conceptual design of flexible joints for compliant mechanisms, *Journal of Mechanisms and Robotics*, *1*(4), 041009, doi:10.1115/1.3211024.

Suzuki, K., and N. Kikuchi (1991), A homogenization method for shape and topology optimization, *Computer Methods in Applied Mechanics and Engineering*, *93*(3), 291–318.

Trease, B. P., Y.-M. Moon, and S. Kota (2005), Design of large-displacement compliant joints, *Journal of Mechanical Design*, *127*(4), 788–798, doi:10.1115/1.1900149.

Ullman, D. G. (2002; 2003), *The mechanical design process*, xv, 415 p. pp., McGraw-Hill, Boston, Massachusetts, iD: 004271693; Includes index.

Vehar-Jutte, C. (2008), Generalized synthesis methodology of nonlinear springs for prescribed load-displacement functions, Ph.D. thesis, Ann Arbor, MI, USA.

Vogel, S. (1988), *Life's Devices: The Physical World of Animals and Plants*, Princeton Press, Princeton, NJ.

Vogel, S. (1998), *Cats' Paws And Catapults: Mechanical Worlds of Nature and People*, Norton, New York.

Vogel, S. (2003), *Comparative Biomechanics*, Princeton University Press, Princeton, New Jersey.

Wang, M. Y. (2009), A kinetoelastic formulation of compliant mechanism optimization, *Journal of Mechanisms and Robotics*, *1*(2).

www.paperpro.com (2007).

Xu, D., and G. K. Ananthasuresh (2003), Freeform skeletal shape optimization of compliant mechanisms, *Journal of Mechanical Design*, *125*(2), 253–261, doi: 10.1115/1.1563634.